University of New Mexico
UNM Digital Repository

Electrical and Computer Engineering ETDs | Engineering ETDs

Fall 11-13-2016

# NEW APPROACHES FOR ESTIMATING HEMISPHERIC LATERALIZATION FROM RESTING STATE FMRI DATA WITH RELATIONSHIP TO AGE, GENDER AND MENTAL DISORDERS

Oktay Agcaoglu
*University of New Mexico*

Follow this and additional works at: https://digitalrepository.unm.edu/ece_etds

 Part of the Signal Processing Commons

Recommended Citation
Agcaoglu, Oktay. "NEW APPROACHES FOR ESTIMATING HEMISPHERIC LATERALIZATION FROM RESTING STATE FMRI DATA WITH RELATIONSHIP TO AGE, GENDER AND MENTAL DISORDERS." (2016).
https://digitalrepository.unm.edu/ece_etds/306

This Dissertation is brought to you for free and open access by the Engineering ETDs at UNM Digital Repository. It has been accepted for inclusion in Electrical and Computer Engineering ETDs by an authorized administrator of UNM Digital Repository. For more information, please contact disc@unm.edu.

Oktay Agcaoglu
*Candidate*

Electrical and Computer Engineering
*Department*

This dissertation is approved, and it is acceptable in quality and form for publication:

*Approved by the Dissertation Committee:*

Vince D. Calhoun , Chairperson

Marios Pattichis

Arvind Caprihan

Erik Erhardt

# NEW APPROACHES FOR ESTIMATING HEMISPHERIC LATERALIZATION FROM RESTING STATE FMRI DATA WITH RELATIONSHIP TO AGE, GENDER AND MENTAL DISORDERS

**by**

**OKTAY AGCAOGLU**

B.S., Electrical and Electronic Engineering, Bogazici University, 2011
M.S., Electrical Engineering, University of New Mexico, 2014

DISSERTATION

Submitted in Partial Fulfillment of the
Requirements for the Degree of

**Doctor of Philosophy**
**Engineering**

The University of New Mexico
Albuquerque, New Mexico

**Dec, 2016**

## DEDICATION

*To my family for their great supports and devotion, and inspiring encouragement.*

## ACKNOWLEDGEMENTS

I heartily acknowledge Dr. Vince Calhoun, my advisor and dissertation chair, for his patience, support and guidance throughout this doctoral work. He has been a great mentor to me.

I would like to sincerely thank to my committee members, Dr. Marios Pattichis, Dr. Arvind Caprihan and Dr. Erik Erhardt for their valuable recommendations pertaining to this study.

I would like to thank all my colleagues at the Medical Imaging Analysis Laboratory, especially to Dr. Robyn Miller, Eswar Damaraju, Rogers F. Silva and Barnaly Rashid for their help and contributions.

Finally, I would like to thank my beloved family for their love and support.

**NEW APPROACHES FOR ESTIMATING HEMISPHERIC LATERALIZATION FROM RESTING STATE FMRI DATA WITH RELATIONSHIP TO AGE, GENDER AND MENTAL DISORDERS**

**by**
**OKTAY AGCAOGLU**

B.S., Electrical and Electronic Engineering, Bogazici University, 2011
M.S., Electrical Engineering, University of New Mexico, 2014
PhD, Engineering, University of New Mexico, 2016

## ABSTRACT

Lateralization is specialization of the brain hemispheres in certain tasks, such as language, mathematics, cognition and motor skills. It is one of the most queried topics related to the human brain. After the invention of modern medical imaging techniques including functional magnetic resonance imaging (fMRI), scientific research about the human brain, including lateralization, gained huge momentum. There have been a remarkable numbers of studies about lateralization and most of these studies focused on investigating which part of the brain dominates in which tasks. However, there have been very few lateralization studies on brain intrinsic activity, i.e., resting state activity where subjects are asked to stay awake while resting without performing any specific tasks.

Independent component analysis (ICA), a data-driven blind source separation method, has become one of the conventional data analysis tools for brain imaging data. ICA can separate the brain imaging data into functional regions that are temporally

coherent, and functional network connectivity (FNC) of these regions can be computed. FNC is a measure that captures the temporal covariance of the brain networks.

In this dissertation, we focus on the lateralization during the resting state and assess hemispheric differences during the resting state. The lateralization of the resting state networks and their association with age and gender is presented using a large resting state fMRI dataset. A novel approach for generating hemisphere specific time-courses and computing FNC inside the hemispheres and between hemispheres is proposed and the relationship of these FNC values with age, gender and mental illness, schizophrenia is reported. Finally, a new framework to estimate power spectral density of 4D brain imaging data and a dimension reduction method to reduce dimensionality from 4D frequency domain to 2D frequency domain has been proposed. This framework helps us to reveal spatiotemporal organization differences between hemispheres. In summary, our work has made several contributions to advance lateralization analysis and has improved our understanding of various aspects of hemispheric differences during the resting state.

# Table of Contents

**List of Figures** ..... **xi**

**List of Tables** ..... **xix**

**Chapter 1 : Introduction** ..... **1**

**1.1 Motivation** ..... **1**

**1.2 Thesis Statement** ..... **2**

**1.3 Innovations and Contributions** ..... **2**

**1.4 Organization of the Dissertation** ..... **3**

**Chapter 2 : Background and Literature Review** ..... **5**

**2.1 Basics of fMRI** ..... **5**

**2.2 Independent Component Analysis** ..... **7**

**2.3 ICA of fMRI data** ..... **8**

**2.4 Functional Network Connectivity** ..... **10**

**2.5 Schizophrenia** ..... **11**

**2.6 Lateralization** ..... **12**

**Chapter 3 : Lateralization of Resting State Networks and Relationship to Age and Gender** ..... **16**

**3.1 Motivation** ..... **16**

**3.2 Methods and Materials** ..... **17**

3.2.1 Participants ..... 17

3.2.2 Data Acquisition ..... 18

3.2.3 Data Preprocessing ..... 19

3.2.4 Group Independent Component Analysis ..... 22
3.2.5 Lateralization maps ..... 22
3.2.6 Global Effects: Laterality cofactor ..... 27
3.2.7 Local Effects: Voxel-vise Modeling of Age and Gender Effects ..... 27
**3.3 Results ..... 29**
3.3.1 Global laterality effects (laterality cofactors ..... 30
3.3.2 Voxel-wise effects of age ..... 35
3.3.3 Voxel-wise effects of gender ..... 37
3.3.4 Gender laterality cofactor effects ..... 39
3.3.5 Age laterality cofactor effects ..... 40
3.3.6 Effects of the sample size on the laterality ..... 40
**3.4 Discussion ..... 42**
3.4.1 Limitations ..... 46
**3.5 Conclusion ..... 47**
**Chapter 4 : Decreased Asymmetry of Intra Hemisphere and Inter Hemisphere Functional Network Connectivity at Rest in Schizophrenia ..... 48**
**4.1 Motivation ..... 48**
**4.2 Methods and Materials ..... 49**
4.2.1 Participants ..... 49
4.2.2 Data Acquisition ..... 51
4.2.3 Preprocessing ..... 51
4.2.4 Group Independent Component Analysis ..... 52
4.2.5 Generating Templates and Hemisphere Specific Time-courses ..... 52
4.2.6 Functional Network Connectivity Calculation ..... 54

4.2.7 Calculating Group Averages ..... 56
4.2.8 Comparing Strength of lateralized FNC types in Patients and Healthy Control..... 56
4.2.9 Modeling Age, Gender, Schizophrenia and Handedness Effects in Intra FNC Differences ..... 57
4.2.10 Modeling Age, Gender, Schizophrenia and Handedness Effects in Intra Hemisphere and Inter Hemisphere FNC ..... 58
4.2.11 Modeling Effects of Cognitive Scores, Symptom Scores and Mean Antipsychotic Dose 58
**4.3 Results..... 58**
4.3.1 Results of Group Averages ..... 58
4.3.2 Results of Connectivity Strength ..... 62
4.3.3 Results of Regression Analysis ..... 65
**4.4 Discussion..... 74**
4.4.1 Limitation ..... 76
**4.5 Conclusion ..... 76**
**Chapter 5 : Increased spatial granularity of left brain activation and unique age/gender signatures: A 4D Frequency Domain Approach to Cerebral Lateralization at Rest ..... 78**
**5.1 Motivation..... 78**
**5.2 Introduction ..... 78**
**5.3 Methods and Materials ..... 81**
5.3.1 Dataset ..... 81
5.3.2 Extracting Hemispheres ..... 81
5.3.3 Transforming to Frequency Domain ..... 83
5.3.4 Spatial Spherical Band Profiles (SSBPs) ..... 83

5.3.5 Paired t-test ..... 84
5.3.6 Modeling Age and Gender Effects ..... 85
5.3.7 Age Effects on Subjects Movement ..... 86
**5.4 Results ..... 86**
5.4.1 Hemispheric Differences ..... 87
5.4.2 Age Effects ..... 88
5.4.3 Gender Effects ..... 91
**5.5 Discussion ..... 92**
5.5.1 Limitations ..... 97
**5.6 Conclusion ..... 98**
**Chapter 6 : Conclusion and Future Works ..... 99**
**6.1 Summary ..... 99**
**6.2 Future Work ..... 100**
**A. Appendix ..... 102**
**Age and Gender Effects in Age Subgroups ..... 102**
a. Age effect in age subgroup 12 to 29 ..... 103
b. Age effect in age subgroup 30 to 71 ..... 106
c. Gender effect in age subgroups ..... 107
**Bibliography ..... 109**

## List of Figures

Figure 2.1: Matrix representation of the tICA and sICA of the fMRI data, matrixes consist of 3D structure of the voxels are flattened into 1D and the other dimension has the temporal information. tICA tries to find temporally independent time-courses and corresponding spatial maps, while sICA attempts to find spatially independent component and corresponding time-courses. Figure used with permission from Calhoun et al. (2001b). ..... 9

Figure 2.2: Illustration of the temporally concatenation of fMRI data and gICA, following by back-reconstruction to generate subject specific time-courses and spatial maps, by projecting the subject data onto corresponding part of the mixing matrix. Figure used with permission from (Calhoun et al., 2009b) ..... 10

Figure 3.1: Flowchart of the data processing, see Section 3.2 for details (Figure adapted from Allen et al. (2011)). ..... 21

Figure 3.2: Spatial maps of the 28 components that are identified as RSNs, plotted as one sample t-statistics, thresholded with $tc>3\sigma c$, and are displayed at the three most informative slices. RSNs are divided into groups based on their anatomical and functional properties and include basal ganglia (BG), auditory (AUD), sensorimotor (MOT), visual (VIS), default-mode (DMN), attentional (ATTN), and frontal (FRONT) networks. We refer to (Allen et al., 2011) for the details of grouping. ..... 25

Figure 3.3: One sample t-statistics of the laterality component masked with the RSN activation mask, and thresholded with $tb> \sigma b$. RSNs are displayed at the same coordinates with the spatial maps and grouped with a similar matter with Figure 3.2 RSNs are divided into groups based on their anatomical and functional properties and

include basal ganglia (BG), auditory (AUD), sensorimotor (MOT), visual (VIS), default-mode (DMN), attentional (ATTN), and frontal (FRONT) networks. We refer to Allen et al. (2011) for the details of grouping. ..... 28

Figure 3.4: Laterality cofactors for each component over 600 subjects that are ranging from age 12 to 71. The cofactors that have absolute value above the 0.75 (red line) are called highly lateralized and the cofactors that have absolute value above 0.2 are called lateralized. ..... 30

Figure 3.5: Probability distribution of the absolute laterality cofactors on synthetic dataset ..... 33

Figure 3.6: Age effects on each voxel and each component, voxels that survives FDR correction shown in color, are displayed at the same coordinates with the spatial maps and grouped with a similar matter with Figure 3.2. RSNs are divided into groups based on their anatomical and functional properties and include basal ganglia (BG), auditory (AUD), sensorimotor (MOT), visual (VIS), default-mode (DMN), attentional (ATTN), and frontal (FRONT) networks. We refer to Allen et al. (2011) for the details of grouping. ..... 34

Figure 3.7: Gender effects on each voxel and each component, voxels that survives FDR correction shown in color, are displayed at the same coordinates with the spatial maps and grouped with a similar matter with Figure 3.2. RSNs are divided into groups based on their anatomical and functional properties and include basal ganglia (BG), auditory (AUD), sensorimotor (MOT), visual (VIS), default-mode (DMN), attentional (ATTN), and frontal (FRONT) networks. We refer to Allen et al. (2011) for the details of grouping. ..... 36

Figure 3.8: Laterality Cofactors for gender subgroups. Visible blue bars shows the components that are more lateralized for males, visible red bars shows the components that are more lateralized for females..... 38

Figure 3.9: Beta values for Gender effects on laterality cofactors. Blue bars show the components that are more lateralized for males, Red bars shows the components that are more lateralized for females. No components survive from 0.05 levels FDR correction. Component 46 is more lateralized for females ($P<0.05$) and component 55 is more lateralized for males ($P<0.05$)..... 38

Figure 3.10: Beta values for Age effects on laterality cofactors. Blue bars show the components that are more lateralized as age goes from 12 to 71. Red bars show the components that are less lateralized as age goes from 12 to 71. Components 38 and 67 (dashed circulated) survive 0.05 levels FDR correction, and are getting less lateralized as age goes from 12 to 71. No other component has p-value smaller than 0.05, besides the ones that also survive FDR correction. ..... 40

Figure 4.1: Symmetrized aggregated spatial maps of the 43 RSNs, are displayed at the three most informative slices. RSNs are divided into groups based on their anatomical and functional properties, and include sub-cortical (SC), sensorimotor (SM), auditory (AUD), visual (VIS), attention/cognitive control (CC), default-mode (DMN), and cerebellar (CB) networks. ..... 53

Figure 4.2: Averages of L_FNC (top left), R_FNC matrix (top right) and Cross_FNC (bottom) are displayed as t-statistics thresholded with 0.01 levels FDR. Homotopic FNCs are also plotted as bar plot for visualization purposes. Connectivity pattern look very similar in all FNC types, indicating that in general communication in brain do not differ

much in hemispheres, though the strength of communication may differ. Homotopic regions have the highest connectivity strength. ..... 60

Figure 4.3 Averages of Patients (left column) and Healthy Control (right column) subgroups for all FNC types (R_FNC, L_FNC and Cross_FNC from top to bottom respectively) are displayed as t-statistics thresholded with 0.01 levels FDR. Homotopic FNCs are also displayed in bar plots for visualization purposes and they have the highest connectivity strength. In all FNC types, we observe diminished connectivity strength in patients. ..... 61

Figure 4.4: Comparing strength of connectivity in different FNC types for patients and healthy control groups. LL is the L_FNC, RR is the R_FNC, LR is the lower triangular of Cross_FNC, and RL is the upper triangular of Cross_FNC. Dark blue shows the number of regions significant in both of the corresponding FNCs, light blue shows the significant regions with same sign, yellow shows the number of regions having greater connectivity strength in FNC written in first, while red shows the number of regions having greater connectivity strength in FNC written in the second..... 63

Figure 4.5: Paired t-test (L_FNC minus R_FNC) results in – *log10(p-value)*sign(beta)* format to compare left and right FNC, corrected with 0.05 levels FDR. A lot of networks pairs exhibit significant differences, mostly suggesting right hemisphere having more connectivity strength. ..... 65

Figure 4.6: Regression results of age, gender and diagnosis effects on L_FNC and intra R_FNC, presented in – *log10(p-value)*sign(beta)* format. With a cross check with on the mean L_FNC and R_FNC differences (Figure 4.5) lads the observation that patients have diminished left and right connectivity differences, consistent with our findings in

comparing connectivity strength. Age and gender seems to affecting both FNCs in similar ways. ..... 68

Figure 4.7: Schizophrenia effect on all FNC types, displayed as – *log10(p-value)*sign(beta)* format (at left column); after 0.05 levels FDR correction (at right column). General patterns look similar, for almost all pairs patients have weaker connectivity. Especially, highly positively connected regions auditory, visual, sensorimotor networks show less connectivity in patients. ..... 69

Figure 4.8: Age effect on all FNC types, displayed as – *log10(p-value)*sign(beta)* format (at left column); after 0.05 levels FDR correction (at right column). General patterns look similar, network pairs have weaker connectivity with increasing age. Especially, visual, sensorimotor networks diminished connectivity in elders, homotopic network pairs also show a decrease with increasing age. ..... 72

Figure 4.9: Gender effects on all FNC types, displayed as – *log10(p-value)*sign(beta)* format (at left column); after 0.05 levels FDR correction (at right column). Gender is not a significant factor affecting FNCs, we do not have any significances besides the sensorimotor regions in. ..... 73

Figure 5.1: Flowchart of data processing. ..... 82

Figure 5.2: Subject mean frame displacement versus age is presented, while there are a few more higher mean framewise displacement subjects at the younger ages, repeating the analysis with a subset of 503 subjects whose mean frame displacements less than 0.4 mm, revealed similar results with the full analysis. ..... 86

Figure 5.3: Group averages of hemisphere SSBPs (A & B) and paired t-test result of comparison (C & D) are presented, In each image; left bottom represents the low

temporal and low spatial frequencies; on the x-axis from left to right, temporal frequencies increase from 0 Hz to 0.25 Hz; on the y-axis from bottom to top, spatial frequencies increases from 0 cycles/mm to 0.17 cycles/mm. Left hemisphere (A) and Right hemisphere (B) displayed in log10 format (unit is decibel-Watt). Paired t-test results for hemisphere SSBPs, values are plotted as – *log10(p-value)*sign(t-statistic)* (C) and after 0.01 levels FDR correction (D). Red color represents the spatiotemporal frequencies bands favoring left hemisphere, while blue color represents the frequency bands favoring right hemisphere. Overall, regions favoring right hemisphere occupies a larger area and includes low and middle spatial frequencies, left hemisphere has more power in high spatial frequencies. ..... 88

Figure 5.4: Regression analysis result on subject SSBPs for age effects on Left and Right hemispheres. In each image; left bottom represents the low temporal and low spatial frequencies; on the x-axis from left to right, temporal frequencies increase from 0 Hz to 0.25 Hz; on the y-axis from bottom to top, spatial frequencies increases from 0 cycles/mm to 0.17 cycles/mm. Values are plotted as – *log10(p-value)*sign(beta value)* (A & C) and after 0.01 levels FDR correction (B & D). Generally, the age effects on left hemisphere (A & B) are very similar to the effect on right hemisphere (C & D). Overall, temporal frequencies determine the direction of the age effects, from 0.016 ($3^{rd}$ index) Hz to 0.14 ($19^{th}$ index) Hz and in all spatial frequencies, show a decrease in power with increasing age, while other temporal and spatial frequencies increases in power with aging..... 90

Figure 5.5: Regression analysis result on subject SSBPs for gender effects on Left and Right hemispheres. In each image; left bottom represents the low temporal and low

spatial frequencies; on the x-axis from left to right, temporal frequencies increase from 0 Hz to 0.25 Hz; on the y-axis from bottom to top, spatial frequencies increases from 0 cycles/mm to 0.17 cycles/mm. Values are plotted as *-log10(p-value)*sign(beta value)* (A & C) and after 0.01 levels FDR correction (B &D).Blue color shows the region favors males while red color shows the region favors females. Overall, the gender effects on left hemisphere (A & B) are very similar to the effect on left hemisphere (C & D). Gender patterns are complicated and dependent on both spatial and temporal frequencies. ..... 92

Figure A.1: Laterality cofactors for different subgroups. Yellow bar shows components that are more lateralized for the age group 12 to 29 and green bars show the components that are more lateralized for age group 30 to 71. ..... 102

Figure A.2: Beta values for Age effects on laterality cofactors for the subgrouped data between 12 to 29. Blue bars show the components that are more lateralized as age goes from 12 to 29, Red bars show the components that are less lateralized as age goes from 12 to 29. Component 17, 29 and 47 (dashed circulated) survive 0.05 FDR correction, components 17 and 29 are getting less lateralized and component 47 is getting more lateralized as age goes from 12 to 29. Component 38, 64, 67 (green circulated) do not survive FDR correction, but they have p-values smaller than 0.05, and are getting less lateralized as age goes from 12 to 29. ..... 104

Figure A.3: Beta values for Age effects on laterality cofactors for the subgrouped data between 30 to 71. Blue bars show the components that are more lateralized as age goes from 30 to 71, Red bars show the components that are less lateralized as age goes from 30 to 71. No component survives 0.05 FDR correction. Component 23 (outlined in green

) does not survive FDR correction, but it has a p-value smaller than 0.05, and is getting more lateralized as age goes from 30 to 71..... 105
Figure A.4: Gender effects on the data age subgroup ranging from 12 to 29. Blue bars show the components that are more lateralized for males, Red bars show the components that are more lateralized for females. No components survive 0.05 levels FDR correction. Component 46 is more lateralized for females (P<0.05). ..... 107
Figure A.5: Gender effects on the data subgroup ranging from 30 to 71. Blue bars show the components that are more lateralized for males, red bars show the components that are more lateralized for females. No components survive 0.05 levels FDR correction. Components 60, 55 and 47 are more lateralized for males (P<0.05)..... 108

## List of Tables

Table 3.1: Demographic information of the subjects. Gender and age distribution. ..... 18

Table 3.2: The talairach table associated with the each selected RSN shown on Figure 3.2, BA = Brodmann area; Vl = number of voxels in each cluster; tmax = maximum t-statistic in each cluster; Coordinate = coordinate (in mm) of tmax in MNI space, following LPI convention. ..... 26

Table 3.3: The talairach table associated with the each t-model of RSN (shown on Figure 3.3), BA = Brodmann area; Vl = number of voxels in each cluster; tmax = maximum t-statistic in each cluster; Coordinate = coordinate (in mm) of tmax in MNI space, following LPI convention. ..... 29

Table 3.4: Statistics of the simulated laterality cofactors. ..... 32

Table 3.5: The talairach table associated with the FDR surviving regions on age effects, that are becoming less lateralized as age goes from 12 to 71, each (shown on Figure 3.6) , BA = Brodmann area; Vl = number of voxels in each cluster; Coords = coordinate (in mm) of tmax in MNI space, following LPI convention..... 35

Table 3.6: a-) The Talairach table associated with the FDR surviving regions on gender effects, that are more lateralized at males, each (shown on Figure 3.7) , BA = Brodmann area; Vl = number of voxels in each cluster; Coords = coordinate (in mm) of tmax in MNI space, following LPI convention. b-) The Talairach table associated with the FDR surviving regions on gender effects, that are more lateralized at females, each (shown on Figure 3.7) , BA = Brodmann area; Vl = number of voxels in each cluster; Coords = coordinate (in mm) of tmax in MNI space, following LPI convention. ..... 37

Table 3.7: Robustness test on the laterality cofactor. ..... 41

Table 3.8: Required number of samples to observe gender effects for each component . 41

Table 3.9: Required number of samples to observe age effects for each component..... 42

Table 4.1: Demographic information of the subjects, age, gender, and diagnosis distribution. ..... 49

Table 4.2: Distribution of Positive and Negative Syndrome Scale and mean antipsychotic dose as CPZ equivalent are presented for schizophrenia patients. 148 patients had PANSS score and 122 patients had mean antipsychotic dose data available. ..... 50

Table 4.3: Distribution of cognitive scores, as CMINDS composite scores, for 276 subjects. ..... 50

Table 4.4: MNI labels associated with the each symmetrized RSN show in Figure 4.1, BA = Brodmann area; Vl = number of voxels in each cluster; Tmax = maximum t-statistics in each cluster; Coordinate of Tmax in MNI space, following LPI convention. 55

Table 4.5: Comparing Strength of different FNC types in patients and healthy control separately. For all pairs, we see a lack of asymmetries in patients comparing to healthy control. Also, right hemisphere interact with itself more comparing to left hemisphere and, also right hemisphere has more strength in communication with itself comparing inter hemispheric interaction..... 64

# Chapter 1 : Introduction

## 1.1 Motivation

The human brain is a very sophisticated and complicated organ that mainly diverges humans from each other. Scientists have been working on revealing its secrets for centuries. In the modern era, with the invention of non-invasive imaging techniques such as functional magnetic resonance images (fMRI) and positron emission tomography (PET), brain studies have gained huge momentum and neuroimaging became a fast growing research field. The existence of two similar but not identical lobes in the human brain raises multiple questions regarding their differences and what roles they play in our thinking or behaviors. Cerebral lateralization involves the brain hemispheres becoming specialized in certain tasks such as cognitive, language or motor tasks. Most previous lateralization studies have been focused on tasks related data where subjects were asked to perform certain cognitive tasks during the scanning (Breier et al., 1999; Cai et al., 2013; Clements et al., 2006; Gobbele et al., 2008; Groen et al., 2012; Powell et al., 2012; Seghier et al., 2011; Smith et al., 1996; Stephan et al., 2003; Thomason et al., 2009), and only a few lateralization studies focused on the brain's intrinsic activities, i.e., resting state data which subjects were asked to stay awake without doing any particular task (Gotts et al., 2013; Liu et al., 2009; Nielsen et al., 2013; Swanson et al., 2011; Zuo et al., 2010b). In this dissertation, we focused on novel methods for assessing cerebral differences during the resting state.

## 1.2 Thesis Statement

This PhD dissertation focuses on estimating lateral differences between cerebral hemispheres from resting state fMRI data. The studies performed are focused on revealing network level differences in the content of lateralization of activated regions and temporal covariance of these networks, and global level differences in the content of spatiotemporal organization of hemispheres. Network level differences between hemispheres are investigated using group independent component analysis (gICA) while global differences are investigated using 4D whole hemispheres frequency domain analysis. The identified differences are investigated from the perspectives of age, gender and a mental illness, schizophrenia.

## 1.3 Innovations and Contributions

A list of the primary innovations and contributions of the dissertation includes:

- Analyzing lateralization of intrinsic networks, regions showing similar patterns of covariation among voxels, in the resting brain using a large dataset that is balanced in gender and investigating age and gender effects on network lateralization.
- The development of independent component analysis (ICA) based algorithms to calculate hemisphere specific time-courses of brain networks and investigating the differences of connectivity in two hemispheres using functional network connectivity (FNC), a measure that summarizes the temporal covariance of the brain networks and effects of age, gender and mental disorder, schizophrenia.

- The development and improvement of algorithms to robustly estimate spectral density of 4D whole brain fMRI by utilizing the Welch method and reducing dimension of data from 4D frequency domain to 2D frequency domain by combining the spatial frequencies to spatial bands. Welch method utilizes sliding window technique on the temporal dimension and calculates the 4D Fourier transform of each window and later averages the magnitudes of the Fourier coefficients among windows to robustly estimate the spectral density. We apply these methods to study the cerebral hemispheres, to investigate the organization differences between hemispheres, and to study the effects of age and gender.

## 1.4 Organization of the Dissertation

The organization of this dissertation is as follows:

Chapter 2 provides some basics concepts of fMRI technique relevant background and provides background on gICA and its implementation using fMRI data and FNC. In addition, it describes and presents general information about one of the severe mental disorder, schizophrenia, and reports what has been found in the literature related to brain lateralization.

Chapter 3 presents the lateralization study on the spatial maps of the resting state networks, and their relationship with age and gender.

Chapter 4 explains the proposed algorithm to calculate hemisphere specific time-courses and FNCs, and presents what abnormalities among schizophrenia patients compared to healthy controls in the content of functional connectivity and lateralization have been

reported in the literature. Finally, this chapter reports our finding on FNC differences between hemispheres in healthy controls and schizophrenia patients, and their relationship with age and gender.

Chapter 5 explains the proposed method to estimate of each hemisphere's 4D power spectral densities, and provides the dimension reduction method based on spherical bands.

Chapter 6 contains the conclusions, final comments and future work.

# Chapter 2: Background and Literature Review

In this chapter, an overview of the fMRI technique and some basics concept of ICA approach that is widely used for processing fMRI data are provided. Also, in this chapter, some information on schizophrenia, a severe chronic mental disorder, is presented, and the history of lateralization research and the focuses of the previous studies are reported.

## 2.1 Basics of fMRI

Since its inception in 1990, fMRI became one of the most popular non-invasive brain imaging techniques and has been used in a significant number of studies in the area of cognitive neuroscience, clinical psychology, clinical psychiatry and pre-surgical planning (Bandettini, 2012; Glover, 2011; Rosen et al., 2012). In PudMed, a search with the keyword, "fMRI" brings over 400,000 articles.

fMRI measures the brain activity indirectly either by measuring the increase of local cerebral blood flood flow (CBF) or the change in the oxygenation concentration (Bandettini, 2012; Glover, 2011; Rosen et al., 2012). The CBF can be detected via MRI with the injection of some contrast agent to the subject. The first CBF based fMRI was demonstrated by Belliveau et al. (1991), a non-invasion version of CBF based fMRI was also demonstrated in rats by Detre et al. (1992) and Williams et al. (1992) who used a technique called anterior spin labeling (ASL), however the ASL based method suffered from problems such as reduced sensitivity, higher sensitivity to motion and, longer acquisition time (Glover, 2011). The blood oxygenation-level dependent (BOLD) fMRI can detect the deoxyhemoglobin concentration due to neural activity. Fully oxygenated hemoglobin, $HbO_2$, has a diamagnetic property which is same with the brain tissue and

therefore unrecognizable. However deoxygenated hemoglobin Hb is highly paramagnetic due to the existence of 4 unpaired electrons. In the influence of magnetic fields, this paramagnetic property causes local gradients with strength depending on the hemoglobin concentration (Glover, 2011; Rosen et al., 2012). The first demonstrations of the BOLD fMRI were on rats by Ogawa et al. (1990a) and Ogawa et al. (1990c) and shortly after that on humans (Bandettini et al., 1992; Kwong et al., 1992; Ogawa et al., 1990b; Ogawa et al., 1993), and it is currently the conventional technique for fMRI (Glover, 2011).

## 2.2 Independent Component Analysis

ICA is a blind source separation method that recovers underlying maximally independent sources from the linear mixtures using higher order statistics (Beckmann et al., 2005; Bell et al., 1995; Calhoun et al., 2001a; Calhoun et al., 2009b; Comon, 1994; McKeown et al., 1998). ICA algorithms were developed to solve the well-known "cocktail party" problem, where independent sources can be considered as the people talking at the same time and ICA algorithm can be used to separate this mixed signal into individual independent voices (Bell et al., 1995; Calhoun et al., 2001b; Calhoun et al., 2009b). The logic behind ICA can be thought as an extension of principle component analysis (PCA), while PCA looks for components that are uncorrelated, i.e., second order statistics which is not same as being independent, ICA algorithm tries to find components that are statistically independent by utilizing higher order statistics (Bell et al., 1995; Calhoun et al., 2001b; Calhoun et al., 2009b; Comon, 1994).

A conventional ICA has the assumptions of unobservable, statistically independence and non-Gaussian sources, as well as an unknown linear mixing process. Mathematically, ICA can be defined as:

$$X = As$$

Where $X$ is the M-dimensional vectors of observed signal that $x = [x_1, x_2, x_3 \dots, x_M]^T$ and $s$ is the N-dimensional vectors of independent sources; $s = [s_1, s_2, s_3 \dots, s_N]^T$. $A$ is the mixing matrix of size MxN, where $M \geq N$, so that in this case the problem is not under determined. The ICA algorithm tries to estimate an unmixing matrix of W of size NxM such that:

$$Y = Wx$$

Where $Y$ is the estimate of true source $s$. ICA makes use of higher orders statistics to maximize independence of the sources (Calhoun et al., 2001a, b; Calhoun et al., 2009b). There are different ICA algorithms based on maximum likelihood estimation, maximization of information transfer, mutual information minimization, and maximization of non-Gaussianity (Calhoun et al., 2009b).

## 2.3 ICA of fMRI data

The first application of ICA to fMRI data was performed by McKeown et al. (1998), since then there has been a numerous number of application to fMRI. ICA is a data-driven approach and unlike the other conventional analysis methods, such as general linear model (GLM), it does not require any prior models for the brain activity, which makes ICA easy to apply on the cases where no prior information of the time-course available (Beckmann et al., 2005; Calhoun et al., 2009b; Guo et al., 2008). ICA has also been applied to other imaging techniques such as electroencephalography (EEG) and magnetoencephalographic (MEG) data (M. Cetin et al., 2016; Houck et al., 2016; Makeig et al., 1997; Vigario et al., 2000) ICA can be applied to fMRI data to reveal its spatial-temporal structure in two ways; separating the data into temporally independent sources via temporal ICA (tICA) or into spatially independent sources via spatial ICA (sICA). sICA seeks components that are maximally independent in space and has dominantly been used in fMRI studies (Calhoun et al., 2009b). For the fMRI data, these independent spatial components are called networks and each network is associated with a corresponding time-course. Erhardt et al. (2011a) suggest that it is incumbent upon authors to provide a meaningful interpretation of networks utilized in their studies. In this

dissertation, we refer to regions that have temporally-coherent time series as "networks", and thus use it interchangeably with the word component.

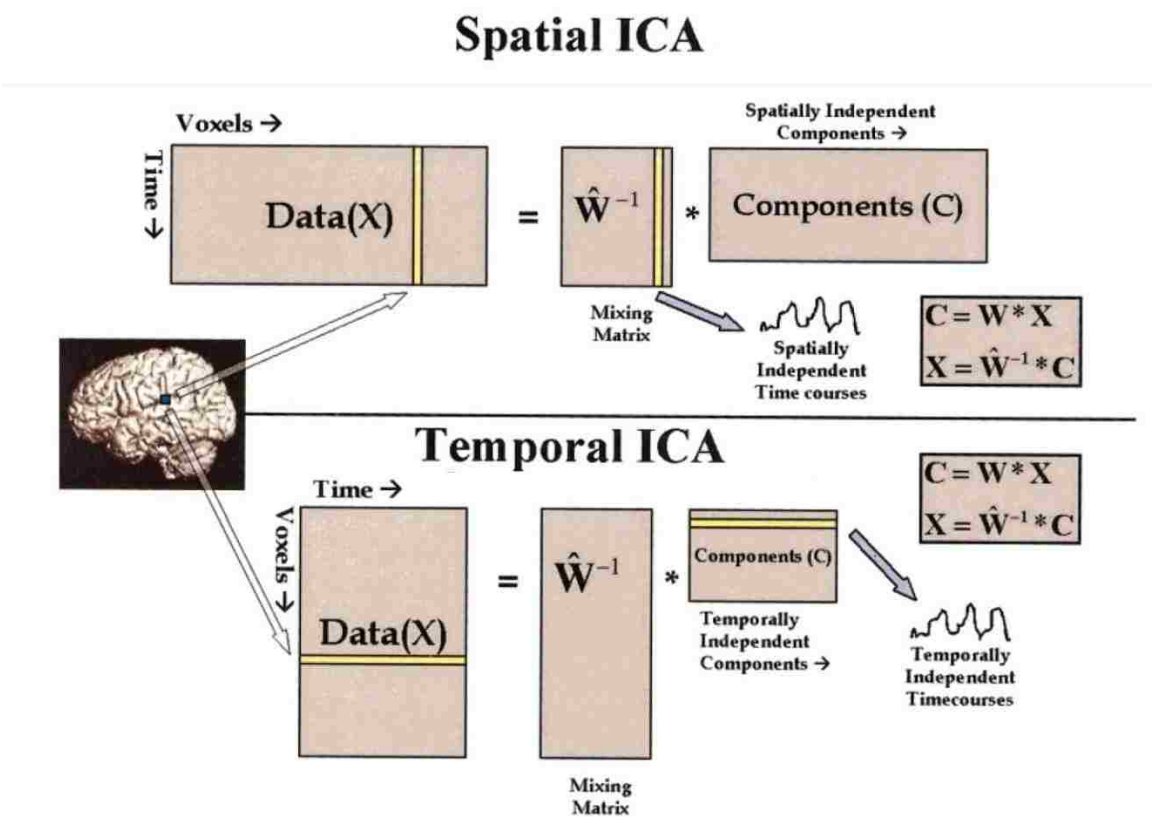


**Figure 2.1: Matrix representation of the tICA and sICA of the fMRI data, matrixes consist of 3D structure of the voxels are flattened into 1D and the other dimension has the temporal information. tICA tries to find temporally independent time-courses and corresponding spatial maps, while sICA attempts to find spatially independent component and corresponding time-courses. Figure used with permission from Calhoun et al. (2001b).**

ICA can be applied to group of subjects using gICA algorithms. In the application to an fMRI dataset, usually gICA is preferred due to the fact that it enables us to compare components and time-courses among subjects. There are several algorithms available to implement gICA, some of these algorithms perform single subject ICA followed by post processing such as component correlation or self-organized clustering to combine the output into group, while other algorithms stack the data in the spatial (spatial concatenation) or temporal (temporal concatenation) domain. Studies report that temporal

concatenation works better for the fMRI data due to the fact that temporal variation of fMRI data is larger than the spatial variation (Calhoun et al., 2009b). A back–reconstruction is performed following the temporal concatenation in gICA to generate subject specific time-courses and spatial maps (Calhoun et al., 2009b). The details of the ICA algorithms and their implementation can be found in (Calhoun et al., 2001a, b; Calhoun et al., 2009b).

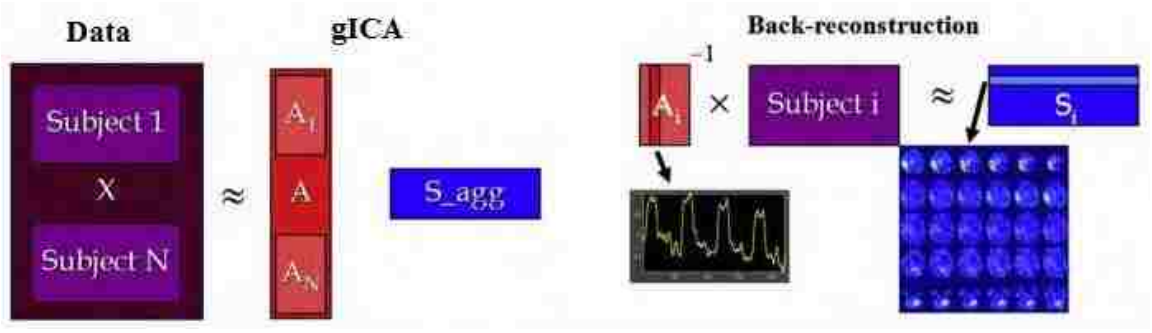


**Figure 2.2: Illustration of the temporally concatenation of fMRI data and gICA, following by back-reconstruction to generate subject specific time-courses and spatial maps, by projecting the subject data onto corresponding part of the mixing matrix. Figure used with permission from (Calhoun et al., 2009b)**

## 2.4 Functional Network Connectivity

FNC is a common way of summarizing functional relationships in the brain. It reports evidence, often based on temporal correlation, of connectivity between functionally-coherent distributed brain networks obtained by data-driven methods such as ICA (Arbabshirani et al., 2013; Jafri et al., 2008). Subject specific time-courses generated from gICA, go through various post-processing steps, usually including detrending and despiking, and band-pass filtering. FNC between two components can be calculated by using a Pearson's correlation (Jafri et al., 2008) as follows:

$$Corr_{(C_x,C_y)} = \frac{TC_{Cx} * TC_{Cy}}{\|TC_{Cx}\| * \|TC_{Cx}\|} = \frac{\sum_{i=1}^{n}(TC_{Cxi} * TC_{Cyi})}{\sqrt{\sum_{i=1}^{n} TC_{Cxi}^2} * \sqrt{\sum_{i=1}^{n} TC_{Cyi}^2}}$$

Where $TC_{Cx}$ and $TC_{Cy}$ are the time-courses of two different components and n is the length of the time-courses (M. S. Cetin et al., 2014).

There is another conventional metric called functional connectivity (FC) that reports the evidence of connectivity in the brain. The main difference between FC and FNC is that FC reports the connectivity between predefined region or seeds (Cordes et al., 2002), while FNC presents the connectivity among brain networks identified by ICA.

## 2.5 Schizophrenia

Schizophrenia is a severe chronic mental disorder characterized by enduring, idiopathic psychotic symptoms (ie: delusions, hallucinations and disorganized thinking and behavior). Schizophrenia affects almost 1 percent of the population with equal probability in genders, however the symptoms of diseases usually begin to show up in women in later ages compared to the men (Bakhshi et al., 2015; Schultz et al., 2007). Schizophrenia has multiple subtypes, and can be characterized via positive and negative symptoms. Positive symptoms are hallucination, delusions like paranoid and hearing voices, while negative symptoms include social withdrawal, losing sense of pleasure, loosing of will and flattened affect, which is a severe reduction in emotional expressiveness (Schultz et al., 2007). The symptoms interrupt the patients' and their family's life. The etiology of schizophrenia has not been totally understood, however studies have confirmed existing of multiple structural differences in schizophrenia patient's brain compared to health

control (Bakhshi et al., 2015). The symptoms can be controlled with antipsychotic medicines, but these medications have severe side effects, the lifetime risk of committing suicide in schizophrenia patients is around 10 percent (Schultz et al., 2007). Early diagnosis of schizophrenia is very important like almost all diseases; diagnoses are usually based on the patient's self-reported experiences and long-term observation of the behaviors, which makes the diagnosis a challenging issue. This fact motivates researchers for finding biomarkers of schizophrenia, and there have been several fMRI studies looking for disrupted brain activities. Several studies have reported altered connectivity of brain regions in schizophrenia patients (Calhoun et al., 2009a; Lynall et al., 2010; Yu et al., 2012).

## 2.6 Lateralization

The idea that the two halves of our brain's cerebral cortex perform different functions has been known for centuries, starting with the seminal observations by Broca (1861) and Wernicke (1874), and later confirmed and extended by the work of Sperry (1974) and numerous others (see Kenneth Hugdahl et al. (2010) for an overview of research on brain laterality). In humans, the left hemisphere has been shown to be involved in functions associated with language such as grammar and vocabulary, as well as analytical and logical functions, while the right hemisphere is associated with non-verbal functions such as visuospatial, intuitive and sensory tasks (Breier et al., 1999; Cai et al., 2013; Clements et al., 2006; Gobbele et al., 2008; Gotts et al., 2013; Groen et al., 2012; Smith et al., 1996; Stephan et al., 2003; Thomason et al., 2009). Other studies have probed how lateralization of the brain effects our perception of color, the formation of language, our understanding of mathematics (Herve et al., 2013), and a whole range of other cognitive

and emotional functions (Davidson, 1998; J. B. Hellige, 1993). Furthermore, research shows that lateralization is not uniquely human; cerebral lateralization has also been shown to occur in non-human primates (Bianki, 1981; Corballis, 2014; Denenberg, 1981; Denenberg et al., 1978; Hauser et al., 1994) and songbirds (Bottjer et al., 1985; Nottebohm, 1970). Recent studies have indicated that both genetic and environmental factors can influence brain lateralization (Liu et al., 2009; Yoon et al., 2010).

The invention of modern brain imaging techniques, such as positron emission tomography (PET) and fMRI, provided new sets of tools to study cerebral lateralization (Kenneth Hugdahl, 2011). Even though there have been several studies related to cerebral lateralization using PET or fMRI, most of them are focused on lateralization in task-related data. Very few studies on lateralization of brain activity at rest have been published. For example, Liu et al. (2009) found 37 left lateralized and 47 right lateralized regions, and reported multiple separate factors contribute to lateralization of these regions and along with small sex differences. Nielsen et al. (2013) found 9 left and 11 right lateralized hubs on the resting brain and reported a small increase in lateralization with age and no gender effects. Moreover, Zhu et al. (2014) found lateralization of speech production and reception areas in a small-scale (N = 25) resting state fMRI paradigm, but this analysis was restricted to the language area, not including other networks and network nodes. Also, there has been some resting state functional connectivity studies of lateralization, Gotts et al. (2013) claimed right and left hemispheres are lateralized in two distinct ways, left hemisphere preferably interacts more itself, while right hemisphere interacts with both hemispheres. Zuo et al. (2010b) analyzed the human brain's homotopic resting-state functional connectivity globally and found regions that are

effected by aging linearly, quadratic and cubically, also observed homotopic differences on functional connectivity between genders. Zuo et al. (2012) explored the connectivity within a whole brain functional network using 4 different types of network centrality measures based on graph theory approaches on a dataset combined from 21 centers. Results in that paper show that local or direct connectivity shows a decrease with increasing age in connections with hub-like regions within the brain. Filippi et al. (2013) reported higher resting state functional connectivity (RSFC) for men in parietal and occipital regions and higher functional connectivity (FNC) in cognitive and sensory regions, and higher RSFC for women in frontal, temporal regions, and in cerebellum, and higher FNC in attentional and right working memory networks.

Lateralization has also been investigated in mental disorders, such as schizophrenia. Some studies also show evidence of an abnormal lateralization within certain brain networks in schizophrenia. Swanson et al. (2011) showed significant lateral differences between schizophrenia patients and healthy controls in the default mode network. Several other studies investigated FC in schizophrenia patients, reported abnormal asymmetries of functional connectivity in schizophrenia (See Ribolsi et al. (2014) for a detailed review). Hoptman et al. (2012) used voxel-mirrored homotopic connectivity method to show decreased homotopic connectivity at schizophrenia or schizoaffective disorder patients, particularly in the occipital lobe, the thalamus and the cerebellum. Ke et al. (2010) found increased leftward asymmetry of FC at patients with exhibiting positive symptom scores, while patients with negative symptoms had increased rightward asymmetry, in their ROI based resting fMRI study. Oertel-Knochel et al. (2013) found reduced FC asymmetries in the planum temporale in the schizophrenia patients and their

relatives. Also, Mwansisya et al. (2013) found aberrant interhemispheric resting state FC in globus pallidus, medial frontal gyrus and inferior temporal gyrus in first-episode schizophrenia patients and found positive correlation of connectivity with Wechsler Adult Intelligence Scale symbol-coding subset scores in the pallidum and medial frontal gyrus, and with duration of the illness in the pallidum, and with negative symptom scores in the inferior temporal gyrus. Gee et al. (2011) examined the connectivity of heterotopic regions in different hemispheres and compared with intra-hemisphere connectivity in their atlas based study.

# Chapter 3: Lateralization of Resting State Networks and Relationship to Age and Gender

## 3.1 Motivation

Brain lateralization is a widely studied topic; however there has been little work focused on lateralization of intrinsic networks (regions showing similar patterns of covariation among voxels) in the resting brain. While the idea that some cognitive functions are lateralized to left or right hemispheres has gained acceptance, there has been little work focusing on the lateralization of the brain's functional organization as assessed by functional connectivity, more specifically in the context of the lateralization of specific functional brain networks (rather than global measures of laterality). In addition, much of the previous brain imaging work has involved relatively small sample sizes, e.g., Zhu et al. (2014) studied only included 25 subjects and Filippi et al. (2013) studied only 48/56 men/women subjects. In this work, we focus on resting fMRI data from over 600 subjects, representing one of the largest single site studies of functional connectivity of the human brain. We re-analyze data previously presented in Allen et al. (2011) with a focus on network lateralization. Using the functional networks detailed in Allen et al. (2011), we assess gender and age effects on a local voxel-wise measure of laterality (Swanson et al., 2011) and also a more global network-level measure. Previous functional imaging studies on the effects of gender and age on lateralization of brain activation have mostly been related to active task processing though there is some work on resting state activity, they analyzed the whole brain rather than intrinsic networks (Zuo et al., 2012; Zuo et al., 2010b) and have also been confined to analysis of single brain areas, so called "blobs", e.g., (K. Hugdahl et al., 2006). In this study, we evaluate resting state network

lateralization in an age and gender-balanced functional magnetic resonance imaging (fMRI) dataset comprising over 600 healthy subjects ranging in age from 12 to 71. After establishing sample-wide network lateralization properties, we continue with an investigation of age and gender effects on network lateralization.

## 3.2 Methods and Materials

Data, preprocessing, and group ICA were identical to Allen et al. (2011), to allow comparisons of lateralization measures with previously extracted and discussed intrinsic networks. We re-summarize the methods in Sections 3.2.1-3.2.4 for clarity and later explained the lateralization framework in Sections 3.2.5-3.2.7. A graphical summary of the data processing is presented in Figure 3.1

### 3.2.1 Participants

Existing data from a total of 603 subjects combined from 34 studies and the work of 18 principal investigators at the Mind Research Network (MRN) on the same scanner with identical parameters were used for this study. In accordance with institutional guidelines at the University of New Mexico, informed consent was obtained from all subjects. The data were all obtained using the same scanner, and were made anonymous before group analysis began. At the time of the scan, none of the subjects were taking psychoactive medications, nor did any have a history of psychiatric or neurological disorders. Subjects were excluded from the study if they were consuming high levels of alcohol (2.5 or more drinks a day) or nicotine (average of 11 or more cigarettes a day). Subjects whose functional scans showed extreme motion (maximum translation > 6mm, approximately 2 voxels) were also excluded from the study. Table 3.1 shows the demographic information of the subjects, with 305 males and 298 females in the sample, gender is nearly balanced,

and the age distributions for genders are also very similar. Handedness is not considered in this study, as the sample is mostly right-handed (46 ambidextrous or left-handed individuals) and preliminary tests in Allen et al. (2011) had insufficient evidence for handedness effects.

**Table 3.1: Demographic information of the subjects. Gender and age distribution.**

| | N | % |
|---|---|---|
| **Gender** | 603 | 100 |
| Male | 305 | 49.4 |
| Female | 298 | 50.6 |

| | Mean | SD | Min | 25% | 50% | 75% | Max |
|---|---|---|---|---|---|---|---|
| **Age**(year) | 23.4 | 9.2 | 12 | 17 | 21 | 27 | 71 |
| Male | 23.8 | 9.1 | 12 | 17 | 21 | 26 | 71 |
| Female | 23.1 | 9.3 | 12 | 16 | 21 | 27 | 55 |

### 3.2.2 Data Acquisition

Images were collected using the 3-Tesla Siemens Trio scanner. High resolution T1-weighted structural images were obtained using a 5-echo MPRAGE sequence with TE = [1.64, 3.5, 5.36, 7.22, 9.08] ms, TR = 2.53 s, TI = 1.2 s, flip angle = 7º, number of excitations = 1, slice thickness = 1 mm, field of view = 256 mm, resolution = 256 × 256. T2*-weighted functional images were obtained using a gradient-echo EPI sequence with TE = 29 ms, TR = 2 s, flip angle = 75 º, slice thickness = 3.5 mm, slice gap = 1.05 mm, field of view = 240 mm, matrix size = 64×64, voxel size = 3.75×3.75×4.55 mm. Resting state scans were a minimum of 5 minutes, 4 seconds (152 volumes). In order to match

data quantity throughout participants, additional volumes, if collected, were not used. During the scan, subjects were told to stare passively at a fixation cross. They were also instructed to keep their eyes open, as it has been suggested this helps network delineation, when compared to eyes-closed conditions (Van Dijk et al., 2010).

### 3.2.3 Data Preprocessing

Functional and structural MRI data were preprocessed as in Allen et al. (2011), using an automated preprocessing pipeline based on SPM5 (http://www.fil.ion.ucl.ac.uk/spm/software/spm5/) and a neuroinformatics system (Scott et al., 2011) developed at the MRN. Scanned data were automatically copied and archived to an analysis directory, where they were then preprocessed. In the functional data pipeline, the first four volumes were excluded in order to remove T1 equilibrium effects. Images are also realigned using INRIalign (Freire et al., 2002) and slice-timing correction is performed with the middle slice used as the reference frame. Data were then spatially normalized into the standard Montreal Neurological Institute (MNI) space, resliced to 3×3×3 mm voxels, and were then smoothed using a 10 mm full-width and half-maximum (FWHM) Gaussian kernel. Following automated preprocessing, the data were intensity normalized by dividing the time series of each voxel by its average intensity, converting data to percent signal change units (Allen et al., 2011).

For the structural data, spatial normalization, bias correction, tissue classification, and image registration were automatically performed using voxel-based morphometry (VBM) in SPM5, in which the above steps were incorporated into a unified model (Ashburner et al., 2005). Unmodulated grey matter images estimating local gray matter concentration

(GMC) are then matched with the functional image dimensions by being smoothed using a Gaussian kernel with a 10 mm FWHM and resliced to 3×3×3 mm.

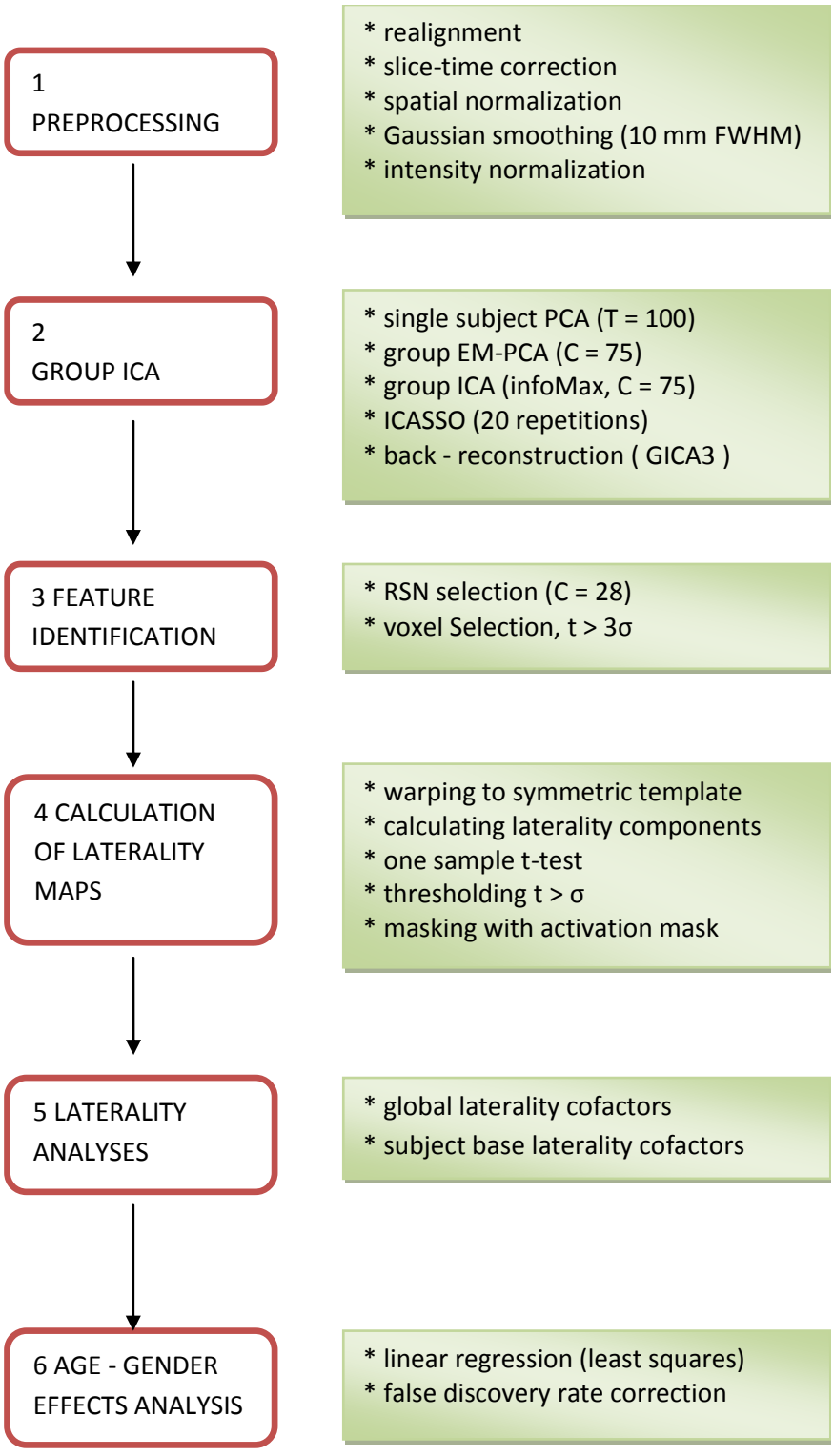


**Figure 3.1: Flowchart of the data processing, see Section 3.2 for details (Figure adapted from Allen et al. (2011)).**

### 3.2.4 Group Independent Component Analysis

Using gICA, data were decomposed into functional networks. When applied to fMRI data, gICA identifies temporally-coherent networks by estimating maximally independent spatial sources, or spatial maps, from their linearly-mixed fMRI signals, or time-courses. For a detailed discussion of the gICA analysis performed on this data, refer to Allen et al. (2011).

Out of the 75 components, a subset of 28 components, considered to be resting state networks (RSNs) are selected by inspecting the group-level spatial maps and average power spectra. We refer to Allen et al. (2011) for the detailed discussion of the RSN selection. The usage of the term "network" can be murky and Erhardt et al. (2011a) suggests that it is incumbent upon authors to provide a meaningful interpretation of networks utilized in their study. In our study, we refer to regions that have temporally-coherent time series as "networks", and thus use it interchangeably with the word component. We also calculated one sample t-tests of the spatial maps, and thresholded with the three standard deviations of the t-statistics of each of the component spatial maps, and created masks that corresponded to these thresholded regions. The most functionally active part of the components is shown in Figure 3.2 and corresponding regions in Table 3.2.

### 3.2.5 Lateralization maps

#### *3.2.5.1 Spatial normalization to symmetric templates:*

Though two hemispheres of the brains look like mirror images of each other, several known (Giedd et al., 1999; Penhune et al., 1996) asymmetries must be accounted for

before performing anatomical or functional comparisons (Stevens et al., 2005). Swanson et al. (2011) warped the data into a symmetric template in the spatial normalization process to overcome hemispheric asymmetries. We approached the problem with a different methodology. Since all subjects are already spatially normalized to the MNI template as a part of the standard pre-processing pipeline, we perform the warping to a symmetric template step as an additional step. We generated a symmetric MNI template by taking the MNI template and flipping it on the lateral axis and averaging with the original MNI template. Then, we warped the all component images for all subjects from the MNI template to the symmetrized MNI templated using SPM5 with trilinear interpolation using and with a cutoff of 25 mm of the period of the cosine basis functions. This approach facilitates comparisons with Allen et al. (2011) since, as a warping of one template to another is identical for all subjects and can be applied to component spatial maps *following* the gICA.

#### *3.2.5.2 Calculation of voxel-vise homotopic maps:*

For each subject, and for each component, we took the differences between voxel intensity values on one side of the cerebral cortex and its homotopic (geometrically corresponding) voxel and tested the difference with a one-sample t-test. For convenience, we plot voxels showing a positive difference (R>L) on the right side of the brain and voxels showing a negative difference (L>R) on the left side of the brain, that is:

$$B_v = \begin{cases} \left(R_{v_h} - L_{v_h}\right) if\ R_{v_h} > L_{v_h} \\ \left(L_{v_h} - R_{v_h}\right) if\ L_{v_h} > R_{v_h} \\ 0\ otherwise \end{cases}$$

Where $R$ represents the right hemisphere and $L$ represents the left hemisphere for each homotopic voxel $v_h$. From this point forward, we will refer to this quantity, $B$, as the laterality component.

#### *3.2.5.3 One Sample t-test*

For each of the laterality components, and for each of the voxels, we computed a one sample t-test over 603 subjects. We then apply a mask that retains voxels whose t-values exceed one standard deviation of the t-statistics. In order to count only the most functionally active part of the component, these thresholded t-models are masked with the activation masks that were calculated previously.

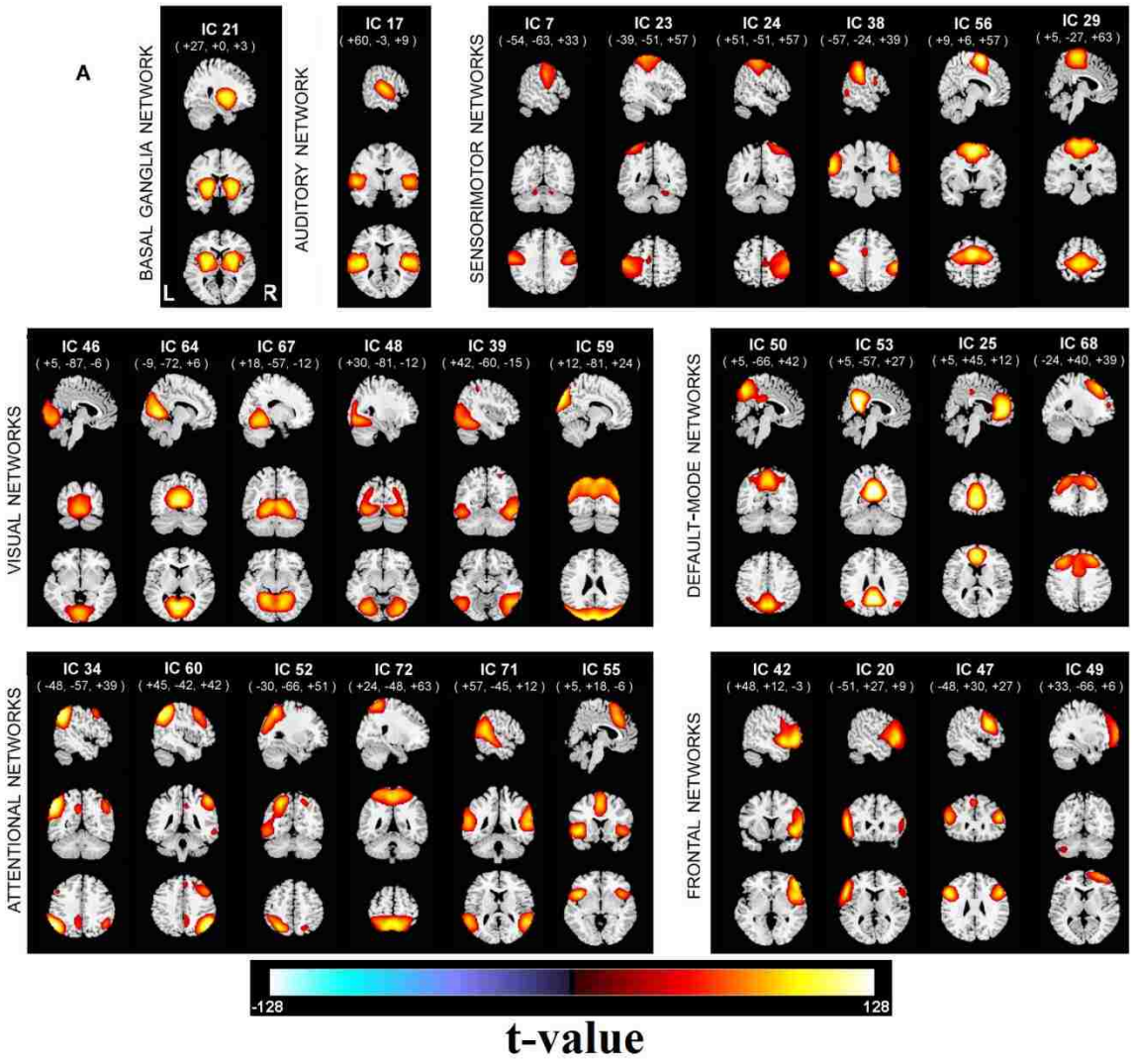


**Figure 3.2: Spatial maps of the 28 components that are identified as RSNs, plotted as one sample t-statistics, thresholded with tc>3σc, and are displayed at the three most informative slices. RSNs are divided into groups based on their anatomical and functional properties and include basal ganglia (BG), auditory (AUD), sensorimotor (MOT), visual (VIS), default-mode (DMN), attentional (ATTN), and frontal (FRONT) networks. We refer to (Allen et al., 2011) for the details of grouping.**

| Basal Ganglia Network | BA | $V_\ell$ | $t_{max}$ | Coordinate |
|---|---|---|---|---|
| **IC 21 (0.98)** | | | | |
| R Putamen | | 1454 | 108.7 | 25, - 1, 0 |
| L Putamen | | 1407 | 108.7 | -25, - 3, 0 |
| **Auditory Network** | **BA** | $V_\ell$ | $t_{max}$ | Coordinate |
| **IC 17 (0.98)** | | | | |
| L Superior Temporal gyrus | 22 | 2374 | 107.0 | -51, -18, 7 |
| R Superior Temporal gyrus | 22 | 2257 | 108.3 | 52, -15, 5 |
| R Middle Cingulate cortex | 24 | 165 | 42.8 | 2, - 4, 49 |
| **Sensorimotor Networks** | **BA** | $V_\ell$ | $t_{max}$ | Coordinate |
| **IC 07 (0.98)** | | | | |
| L Precentral gyrus | 6 | 1814 | 81.0 | -52, - 9, 31 |
| R Precentral gyrus | 6 | 1694 | 78.3 | 52, - 7, 29 |
| L Cerebellum (Declive) | | 116 | 45.5 | -16, -63, -22 |
| R Cerebellum (Declive) | | 84 | 40.9 | 17, -63, -21 |
| **IC 23 (0.98)** | | | | |
| L Precentral gyrus | 4 | 3623 | 86.8 | -35, -27, 54 |
| R Cerebellum | | 342 | 40.3 | 24, -52, -23 |
| R Postcentral gyrus | | 252 | 35.6 | 44, -28, 56 |
| R Inferior Frontal gyrus | 45 | 79 | 23.7 | 54, 29, 0 |
| R Precuneus | | 76 | 26.7 | 8, -62, 32 |
| **IC 24 (0.98)** | | | | |
| R Precentral gyrus | 4 | 3882 | 83.3 | 37, -25, 53 |
| R Middle Temporal gyrus | | 165 | 36.1 | 50, -64, - 2 |
| L Cerebellum | | 99 | 26.1 | -20, -53, -24 |
| L Middle Temporal gyrus | | 63 | 23.5 | -61, -28, - 8 |
| L Middle Temporal gyrus | | 44 | 24.5 | -51, -70, 4 |
| **IC 29 (0.98)** | | | | |
| Bi Paracentral lobule | 6 | 3199 | 100.9 | 1, -28, 61 |
| L Insula | 13 | 44 | 40.1 | -35, -24, 15 |
| **IC 38 (0.98)** | | | | |
| L Supramarginal gyrus | 2 | 1377 | 110.5 | -55, -34, 37 |
| R Supramarginal gyrus | 2 | 963 | 96.2 | 56, -32, 40 |
| L Inferior Frontal gyrus | 44 | 207 | 58.6 | -48, 5, 18 |
| Bi Middle Cingulate cortex | 24 | 189 | 51.5 | 1, 7, 38 |
| L Middle Temporal gyrus | 37 | 128 | 54.4 | -57, -60, - 2 |
| **IC 56 (0.97)** | | | | |
| Bi Supplementary Motor Area | 6 | 3770 | 122.7 | 1, - 3, 61 |
| R Superior Temporal gyrus | 22 | 193 | 48.2 | 50, 8, 4 |
| L Inferior Frontal gyrus | 44 | 149 | 42.7 | -53, 5, 14 |
| R Inferior Parietal lobule | 40 | 61 | 41.1 | 58, -29, 24 |
| L Inferior Parietal lobule | 40 | 26 | 35.9 | -58, -32, 23 |
| **Visual Networks** | **BA** | $V_\ell$ | $t_{max}$ | Coordinate |
| **IC 46 (0.96)** | | | | |
| Bi Lingual gyrus | 17,18 | 3654 | 87.3 | 1, -87, - 2 |
| Bi Middle Cingulate cortex | 31 | 230 | 34.1 | 1, -45, 32 |
| **IC 64 (0.90)** | | | | |
| Bi Calcarine gyrus | 17,18 | 3694 | 117.9 | 1, -71, 13 |
| **IC 67 (0.89)** | | | | |
| R Lingual gyrus | 18 | 1740 | 97.7 | 17, -55, - 9 |
| L Lingual gyrus | 18 | 1820 | 94.8 | -15, -56, - 8 |
| **IC 48 (0.96)** | | | | |
| R Lingual gyrus | 18,19 | 1367 | 86.5 | 29, -76, - 8 |
| L Lingual gyrus | 18,19 | 1324 | 83.6 | -29, -76, - 7 |
| L Inferior Parietal lobule | 40 | 43 | 41.0 | -49, -55, 42 |
| **IC 39 (0.97)** | | | | |
| R Inferior Temporal gyrus | 37 | 1800 | 91.9 | 48, -63, - 8 |
| L Inferior Temporal gyrus | 37 | 667 | 80.7 | -47, -63, -14 |
| R Inferior Parietal lobule | 40 | 33 | 46.2 | 42, -39, 50 |
| **IC 59 (0.92)** | | | | |
| Bi Cuneus | 19 | 3079 | 113.7 | 2, -84, 28 |

| Default-Mode Networks | BA | $V_\ell$ | $t_{max}$ | Coordinate |
|---|---|---|---|---|
| **IC 50 (0.96)** | | | | |
| Bi Precuneus | 7 | 2902 | 102.5 | 1, -64, 43 |
| **IC 53 (0.95)** | | | | |
| Bi Posterior Cingulate cortex | 23 | 2387 | 139.6 | 0, -52, 22 |
| L Angular gyrus | 39 | 332 | 71.5 | -43, -69, 33 |
| R Angular gyrus | 39 | 194 | 59.8 | 47, -66, 32 |
| Bi Medial Frontal gyrus | 10 | 61 | 50.7 | - 1, 45, - 9 |
| **IC 25 (0.98)** | | | | |
| Bi Anterior Cingulate cortex | 32 | 3126 | 114.5 | 0, 41, 4 |
| Bi Middle Cingulate cortex | 31 | 358 | 53.6 | 1, -30, 41 |
| R Inferior Frontal gyrus | | 93 | 48.2 | 32, 22, -15 |
| R Middle Frontal gyrus | 46 | 63 | 37.8 | 40, 43, 8 |
| **IC 68 (0.85)** | | | | |
| L Middle Frontal gyrus | 8 | 1490 | 95.2 | -26, 26, 42 |
| R Middle Frontal gyrus | 8 | 1210 | 87.9 | 26, 33, 41 |
| Bi Middle Cingulate cortex | 32 | 450 | 67.6 | 0, 21, 40 |
| **Attentional Networks** | **BA** | $V_\ell$ | $t_{max}$ | Coordinate |
| **IC 34 (0.98)** | | | | |
| L Inferior Parietal lobule | 40 | 1383 | 124.6 | -47, -57, 39 |
| L Middle Frontal gyrus | 8 | 1000 | 76.3 | -27, 24, 49 |
| R Inferior Parietal lobule | 40 | 482 | 75.3 | 49, -54, 39 |
| L Precuneus | 31 | 373 | 63.4 | - 6, -52, 37 |
| L Middle Temporal gyrus | 21 | 233 | 75.3 | -62, -37, -12 |
| R Superior Temporal gyrus | 22 | 124 | 44.1 | 56, 0, 2 |
| **IC 60 (0.93)** | | | | |
| R Inferior Parietal lobule | 40 | 2480 | 120.8 | 42, -56, 42 |
| R Middle Frontal gyrus | 8 | 2137 | 87.3 | 34, 24, 44 |
| L Superior Temporal gyrus | 22 | 318 | 46.9 | -61, - 2, 0 |
| R Middle Temporal gyrus | 21 | 249 | 58.7 | 64, -39, -11 |
| L Inferior Parietal lobule | 40 | 163 | 45.7 | -45, -53, 45 |
| **IC 52 (0.96)** | | | | |
| L Angular gyrus | 39 | 2841 | 100.6 | -33, -64, 31 |
| L Inferior Frontal gyrus | 45 | 295 | 54.2 | -43, 24, 21 |
| R Superior Parietal lobule | 7 | 283 | 57.8 | 27, -65, 44 |
| L Middle Frontal gyrus | 6 | 119 | 52.3 | -25, 1, 60 |
| L Superior Temporal gyrus | 22 | 24 | 40.4 | -50, - 5, - 4 |
| **IC 72 (0.93)** | | | | |
| Bi Precuneus | 7 | 3283 | 105.2 | 0, -53, 61 |
| L Superior Frontal gyrus | 9 | 111 | 35.8 | -32, 38, 39 |
| R Middle Frontal gyrus | 6 | 85 | 32.4 | 26, 0, 60 |
| L Middle Frontal gyrus | 6 | 80 | 32.4 | -23, 0, 63 |
| R Superior Frontal gyrus | 9 | 53 | 30.3 | 33, 39, 35 |
| **IC 71 (0.88)** | | | | |
| R Superior Temporal gyrus | 22 | 1775 | 95.0 | 57, -44, 11 |
| L Superior Temporal gyrus | 22 | 1337 | 89.0 | -56, -48, 18 |
| Bi Precuneus | 7 | 123 | 51.0 | 1, -51, 51 |
| R Precentral gyrus | 6 | 44 | 50.0 | 51, 2, 50 |
| **IC 55 (0.95)** | | | | |
| Bi Cingulate gyrus | 32 | 1210 | 92.8 | 0, 22, 45 |
| L Insula | 47 | 670 | 103.1 | -46, 15, - 5 |
| R Insula | 47 | 331 | 80.8 | 45, 18, - 6 |
| L Middle Frontal gyrus | 10 | 217 | 65.4 | -32, 53, 21 |
| **Frontal Networks** | **BA** | $V_\ell$ | $t_{max}$ | Coordinate |
| **IC 42 (0.98)** | | | | |
| R Inferior Frontal gyrus | 45 | 3371 | 105.7 | 50, 23, 2 |
| L Insula | 44 | 132 | 40.0 | -41, 10, - 2 |
| L Inferior Frontal gyrus | 45 | 70 | 35.3 | -42, 39, 5 |
| R Supramarginal gyrus | 2 | 65 | 35.5 | 58, -36, 36 |
| R Middle Temporal gyrus | | 56 | 33.0 | 63, -45, 0 |
| L Inferior Parietal lobule | 40 | 37 | 31.9 | -58, -40, 49 |
| R Caudate Nucleus | | 31 | 33.5 | 12, 8, 5 |
| **IC 20 (0.98)** | | | | |
| L Inferior Frontal gyrus | 44,45 | 1781 | 103.2 | -55, 22, 7 |
| R Inferior Frontal gyrus | 45 | 252 | 50.7 | 56, 26, 4 |
| **IC 47 (0.95)** | | | | |
| L Middle Frontal gyrus | 9 | 1020 | 110.8 | -48, 17, 29 |
| R Middle Frontal gyrus | 9,46 | 885 | 97.1 | 49, 22, 25 |
| Bi Superior Medial gyrus | 8 | 259 | 64.1 | - 1, 32, 46 |
| R Superior Parietal lobule | 7 | 38 | 49.3 | 33, -60, 49 |
| **IC 49 (0.97)** | | | | |
| R Middle Frontal gyrus | 10 | 1661 | 84.3 | 31, 55, 7 |
| L Pyramis | | 144 | 42.2 | -39, -66, -44 |
| L Middle Frontal gyrus | 10 | 64 | 33.4 | -31, 52, 8 |

**Table 3.2: The talairach table associated with the each selected RSN shown on Figure 3.2, BA = Brodmann area; Vl = number of voxels in each cluster; tmax = maximum t-statistic in each cluster; Coordinate = coordinate (in mm) of tmax in MNI space, following LPI convention.**

### 3.2.6 Global Effects: Laterality cofactor

In addition to the laterality cofactors, we also summarize the amount of laterality for a given functional component by computing a global laterality metric (called a laterality cofactor). This metric was applied to both our average models, as well as each of our subjects individually. The laterality cofactor was calculated by taking the differences between the sum of all intensities on the right and left hemispheres with respect to the sum of all intensities across the brain.

### 3.2.7 Local Effects: Voxel-vise Modeling of Age and Gender Effects

In addition to evaluating the laterality of the brain networks based on average intensity across subjects, we also tested the relationship of lateralization to age and gender on each voxel by a linear regression of laterality on gender and age: $B_v = \beta_0 + \beta_{gender}X_{gender} + \beta_{age}X_{age} + \varepsilon$. Where $X_{age}$ is age of the subject, $X_{gender}$ is a number indicating the gender of subject with 1 for females and -1 for males. All β's are the parameter of the regression model with ε being the error parameter for the model. This analysis gives us the voxels that are significantly ($p<0.05$, following false discovery rate (FDR) correction for multiple comparisons) affected by age and gender (Genovese et al., 2002). Surviving voxels in the most informative slices are displayed on Figure 3.6 and Figure 3.7. A similar analysis was performed to determine age and gender effects on the global laterality measure described above, and in the Appendix we present results of these analyses performed separately on subsets of the overall age distribution.

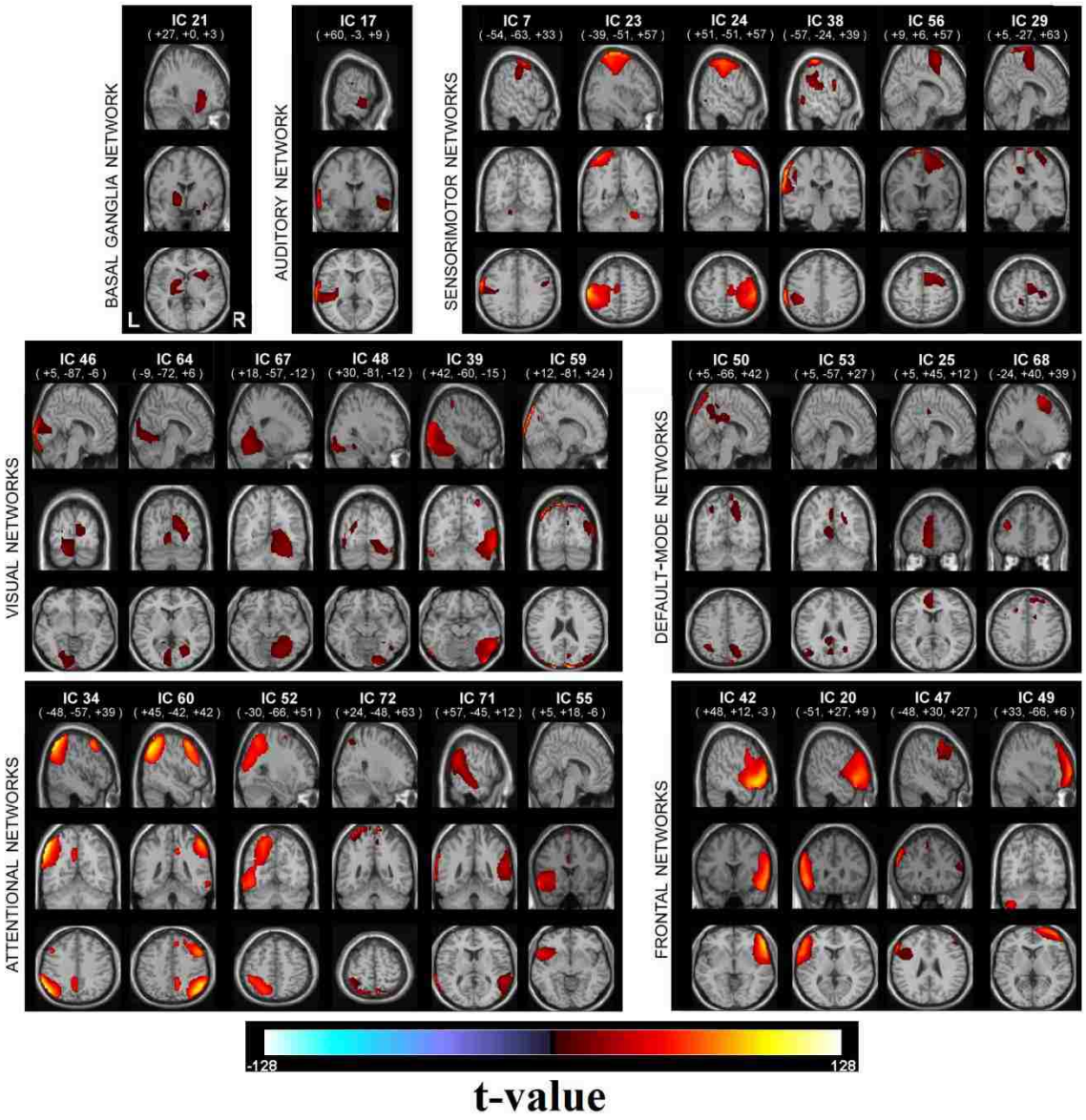


**Figure 3.3: One sample t-statistics of the laterality component masked with the RSN activation mask, and thresholded with tb> σb. RSNs are displayed at the same coordinates with the spatial maps and grouped with a similar matter with Figure 3.2 RSNs are divided into groups based on their anatomical and functional properties and include basal ganglia (BG), auditory (AUD), sensorimotor (MOT), visual (VIS), default-mode (DMN), attentional (ATTN), and frontal (FRONT) networks. We refer to Allen et al. (2011) for the details of grouping.**

| BASAL GANGLIA NETWORKS | BA | Vl | tmax | Coords. |
|---|---|---|---|---|
| **IC 21** | | | | |
| L Pallidum | | 534 | 18 | -22 -3 0 |
| R Putamen | 47 | 446 | 24 | 24 18 -9 |
| **AUDITORY NETWORKS** | **BA** | **Vl** | **tmax** | **Coords.** |
| **IC 17** | | | | |
| L Superior Temporal Gyrus | 42 | 902 | 71 | -72 -21 9 |
| **SENSORIMOTOR NETWORKS** | **BA** | **Vl** | **tmax** | **Coords.** |
| **IC 07** | | | | |
| L Postcentral Gyrus | 6 | 777 | 75 | -66 -9 36 |
| **IC 23** | | | | |
| L Postcentral Gyrus | 1 | 2460 | 85 | -48 -33 66 |
| **IC 24** | | | | |
| R Postcentral Gyrus | 2 | 2669 | 68 | 54 -24 54 |
| **IC 38** | | | | |
| L SupraMarginal Gyrus | 40 | 1128 | 97 | -69 -27 33 |
| **IC 56** | | | | |
| R Supplementary Motor Area | 6 | 725 | 75 | 3 3 78 |
| L Supplementary Motor Area | 6 | 118 | 69 | -9 6 78 |
| **IC 29** | | | | |
| R Paracentral Lobule | | 575 | 64 | 6 -27 81 |
| **VISUAL NETWORKS** | **BA** | **Vl** | **tmax** | **Coords.** |
| **IC 46** | | | | |
| L Lingual Gyrus | 17 | 554 | 25 | -18 -93 -18 |
| L Calcarine Gyrus | 18 | 425 | 66 | 3 -105 3 |
| **IC 64** | | | | |
| R Calcarine Gyrus | 31 | 626 | 17 | 12 -69 18 |
| **IC 67** | | | | |
| R Cerebellum (VI) | 19 | 1598 | 20 | 24, -66, -24 |
| **IC 48** | | | | |
| R Lingual Gyrus | 18 | 524 | 39 | 39 -90 -21 |
| **IC 39** | | | | |
| R Inferior Temporal Gyrus | 19 | 2021 | 76 | 48 -84 -9 |
| L Inferior Temporal Gyrus | 37 | 36 | 63 | -57 -66 -21 |
| **IC 59** | | | | |
| R Superior Occipital Gyrus | 19 | 374 | 112 | 18 -96 33 |

| DEFAULT-MODE NETWORKS | BA | Vl | tmax | Coords. |
|---|---|---|---|---|
| **IC 50** | | | | |
| R Precuneus | 7 | 645 | 74 | 3 -84 48 |
| **IC 53** | | | | |
| L Middle Occipital Gyrus | 39 | 231 | 56 | -6 -39 15 |
| **IC 25** | | | | |
| L Mid Orbital Gyrus | 10 | 933 | 47 | -3 63 -9 |
| **IC 68** | | | | |
| L Middle Frontal Gyrus | 6 | 428 | 35 | -21 9 60 |
| **ATTENTIONAL NETWORKS** | **BA** | **Vl** | **tmax** | **Coords.** |
| **IC 34** | | | | |
| L Angular Gyrus | 40 | 1414 | 118 | -60, -63, 33 |
| Left Middle Frontal Gyrus | 8 | 543 | 69 | -45 15 54 |
| **IC 60** | | | | |
| R Inferior Parietal Lobule | 40 | 1497 | 90 | 51 -57 45 |
| R Middle Frontal Gyrus | 8 | 1197 | 77 | 36 15 57 |
| **IC 52** | | | | |
| L Inferior Temporal Gyrus | 37 | 2387 | 62 | -60 66 -12 |
| **IC 72** | | | | |
| R Precuneus | 7 | 265 | 92 | 3 -57 72 |
| L Superior Parietal Lobule | 7 | 297 | 79 | -18 -63 72 |
| **IC 71** | | | | |
| R Angular Gyrus | 40 | 1299 | 36 | 60 -54 24 |
| **IC 55** | | | | |
| L Temporal Pole | 47 | 699 | 63 | -57 21 -12 |
| L Middle Frontal Gyrus | 10 | 333 | 57 | -39 63 18 |
| **FRONTAL-NETWORKS** | **BA** | **Vl** | **tmax** | **Coords.** |
| **IC 42** | | | | |
| R Inferior Frontal Gyrus | 47 | 2351 | 88 | 51 33 -9 |
| **IC 20** | | | | |
| L Inferior Frontal Gyrus | 47 | 2012 | 75 | -57 27 -9 |
| **IC 47** | | | | |
| L Inferior Frontal Gyrus | 9 | 745 | 74 | -60 21 33 |
| **IC 49** | | | | |
| R Middle Frontal Gyrus | 10 | 1796 | 66 | 39 57 3 |

**Table 3.3: The talairach table associated with the each t-model of RSN (shown on Figure 3.3), BA = Brodmann area; Vl = number of voxels in each cluster; tmax = maximum t-statistic in each cluster; Coordinate = coordinate (in mm) of tmax in MNI space, following LPI convention.**

## 3.3 Results

The global laterality results were useful to summarize the overall laterality of the networks, but were much less sensitive to age and gender. In contrast, the voxel-vise results were more sensitive and showed significant laterality effects with both age and gender. In the following we briefly summarize the global results and provide more details for the voxel-vise results for age and gender.

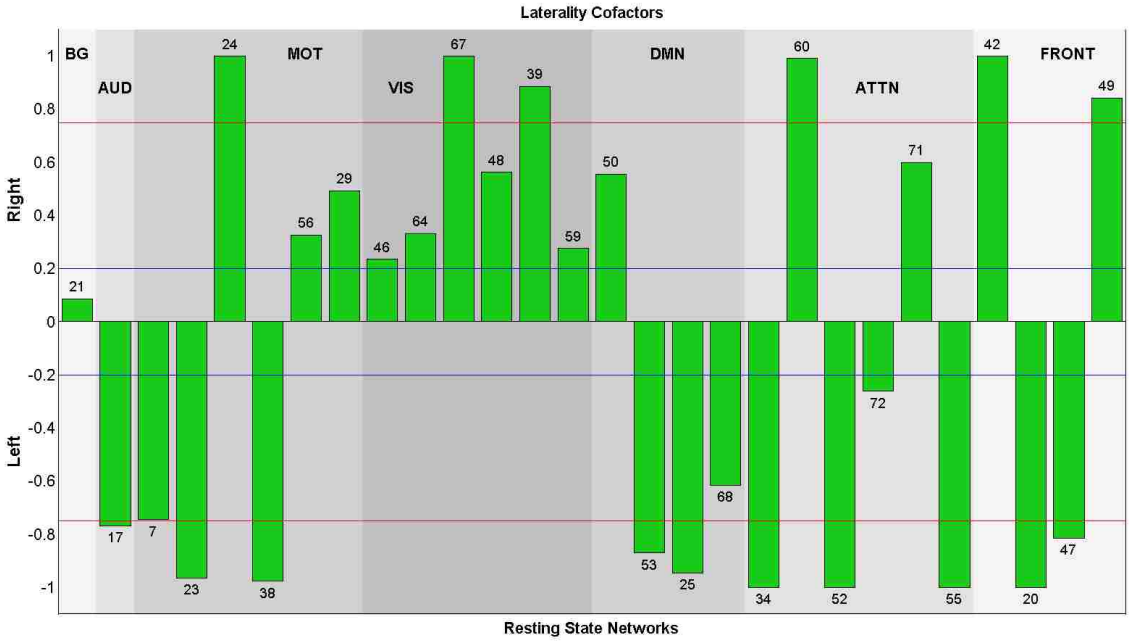


**Figure 3.4: Laterality cofactors for each component over 600 subjects that are ranging from age 12 to 71. The cofactors that have absolute value above the 0.75 (red line) are called highly lateralized and the cofactors that have absolute value above 0.2 are called lateralized.**

### 3.3.1 Global laterality effects (laterality cofactors

The laterality cofactors for each component are displayed in Figure 3.4 and indicating regions summarized on Table 3.3. We designate a component as "lateralized" if the absolute value of the laterality cofactor is greater than 0.2 and "highly lateralized" if it is above 0.75. Most of the networks are lateralized. The laterality cofactors indicate that the basal-ganglia network (IC 21) is symmetric; the auditory network (IC 17) is highly left lateralized.

The sensorimotor networks has both left lateralized and right lateralized components. The lateralized regions are mostly occurring in L/R pairs, (postcentral gyrus, and supplementary motor) which is consistent with the right hemisphere control left part of the body, left hemisphere controls right part of the body phenomena (Janssen et al., 2011). Even though we have equally distributed (3 left and 3 right), the magnitude of

lateralization is greater for the left lateralized component, which is also consistent with the left hemisphere dominant phenomena in the literature (Janssen et al., 2011).

The visual network is the most dominantly right lateralized functional network. All six components of the visual network are right lateralized, on regions lingual gyrus, calcarine gyrus (Right BA 18), cerebellum, inferior temporal gyrus and superior occipital gyrus. Liu et al. (2009) also indicated the visual cortex as one of the most strongly right lateralized regions.

The default mode network components are mostly left lateralized on regions middle occipital gyrus, mid orbital gyrus and middle temporal gyrus (ICs 53, 25, 68) with one right lateralized exception IC 50 on region of precuneus. Our results are parallel with Nielsen et al. (2013), which reports the default networks as left lateralized, and Swanson et al. (2011) that also indicates left dominancy in the default mode networks while indicating lateral differences between healthy control and schizophrenia patients.

The attentional network components are highly lateralized with the exception on ICs 72 and 71. Angular gyrus and middle frontal gyrus (IC 34); inferior temporal gyrus (IC 52); temporal pole and middle frontal gyrus (IC 55); are highly left lateralized regions while IC 60 (inferior parietal lobule, middle frontal gyrus) is highly right lateralized. The right-sided parietal lobule lateralization fit nicely with previous work on asymmetry of spatial attention, including both healthy individuals, e.g., (K. Hugdahl et al., 2006) and brain-damaged patients showing signs of visuo-spatial attentional neglect (Berger et al., 2000).

According to laterality cofactors, the frontal networks are the most sharply lateralized network, with two left (inferior frontal gyrus) and two right (inferior frontal and middle frontal gyrus) lateralized components.

#### *3.3.1.1 Assessment of component lateralization null distribution*

A possible question that might arise is how lateralized would the gICA results be by chance. To investigate this, we simulated group ICA on some synthetic data to observe the laterality on random data. We generated, for 20 trials, 2D random components according to logistic distribution with 120 random time series for 40 subjects and combined them, later we applied group ICA on these simulated data (implemented using GIFT with model order 120 using Infomax algorithm and back-reconstruction to generate subject specific spatial maps and time-courses) and calculate the laterality cofactors on these components, the results are presented in Table 3.4 and Figure 3.5. The results show the probability of finding a lateralized component, above 0.2, is almost zero and absolute mean of laterality is 0.052 indicating overall the components are not lateralized (leftward or rightward) provide additional support for the results reported in this paper.

| Absolute Maximum | Absolute Minimum | Absolute Mean | Absolute Variance |
|---|---|---|---|
| 0.234 | 0 | 0.052 | 0.0015 |

**Table 3.4: Statistics of the simulated laterality cofactors.**

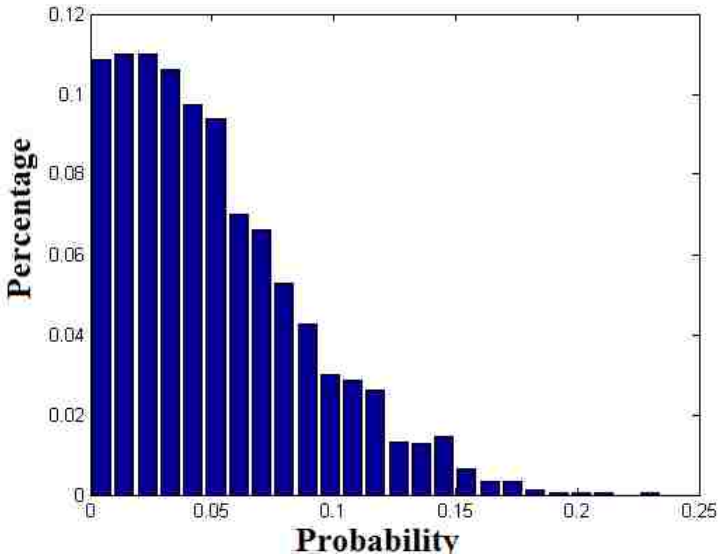


**Figure 3.5: Probability distribution of the absolute laterality cofactors on synthetic dataset**

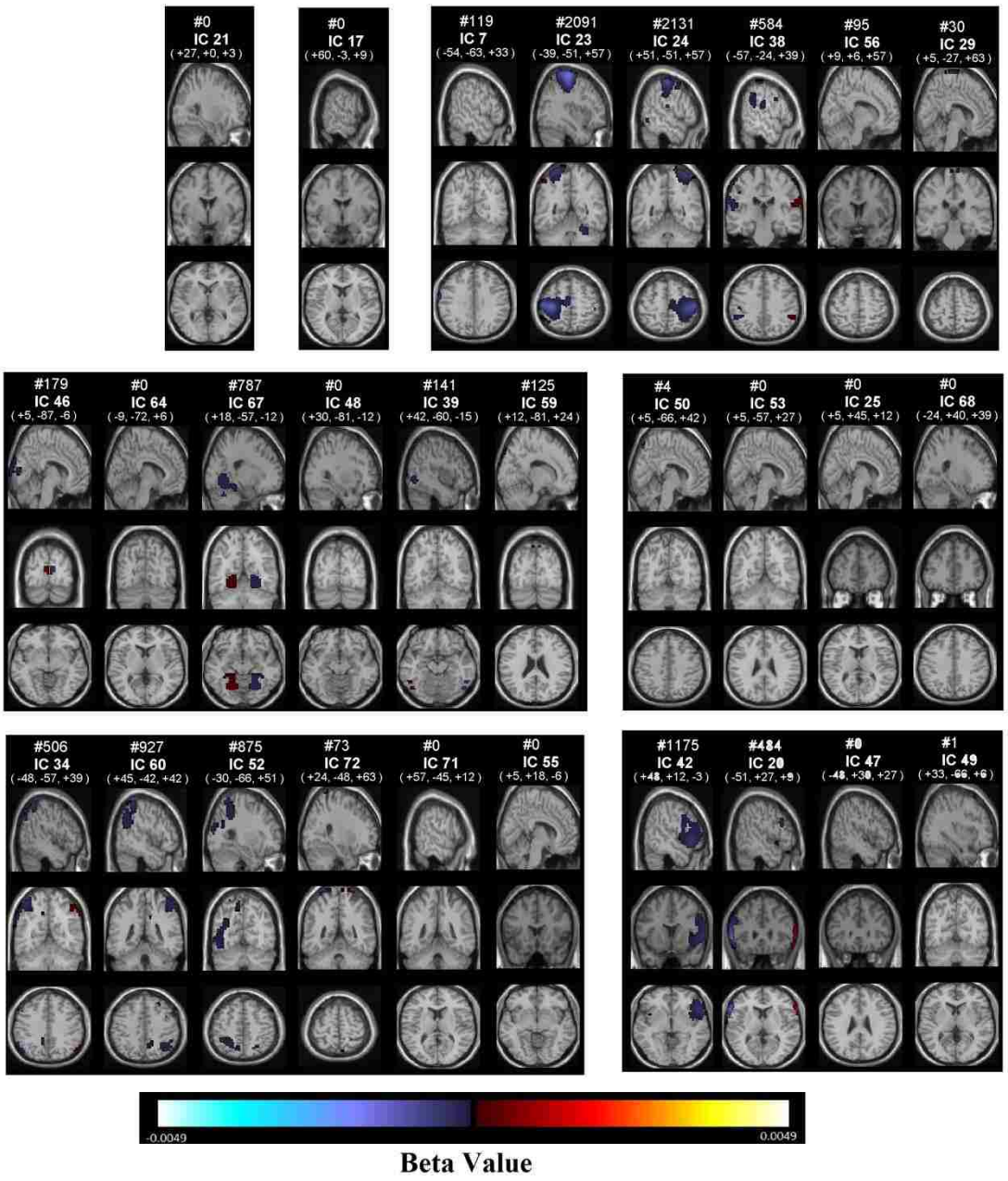


**Figure 3.6: Age effects on each voxel and each component, voxels that survives FDR correction shown in color, are displayed at the same coordinates with the spatial maps and grouped with a similar matter with Figure 3.2. RSNs are divided into groups based on their anatomical and functional properties and include basal ganglia (BG), auditory (AUD), sensorimotor (MOT), visual (VIS), default-mode (DMN), attentional (ATTN), and frontal (FRONT) networks. We refer to Allen et al. (2011) for the details of grouping.**

| SENSORIMOTOR NETWORKS | BA | Vl | Coords |
|---|---|---|---|
| IC 07 | | | |
| L Postcentral Gyrus | 6 | 130 | -66 -6 33 |
| IC 23 | | | |
| L Precentral Gyrus | 6 | 1912 | -36 -24 69 |
| IC 24 | | | |
| R Precentral Gyrus | 4 | 2088 | 36 -27 69 |
| IC 38 | | | |
| L Postcentral Gyrus | 2 | 182 | -66 -21 24 |
| L SupraMarginal Gyrus | 40 | 181 | -63 -48 24 |

| VISUAL NETWORKS | BA | Vl | Coords |
|---|---|---|---|
| IC 67 | | | |
| R Lingual Gyrus | 19 | 416 | 21 -63 -6 |

| ATTENTIONAL NETWORKS | BA | Vl | Coords |
|---|---|---|---|
| IC 34 | | | |
| L Inferior Parietal Lobule | 40 | 345 | -42 -57 60 |
| IC 60 | | | |
| R Superior Parietal Lobule | 40 | 747 | 45 -48 60 |
| IC 52 | | | |
| L Superior Parietal Lobule | 7 | 428 | -27 -60 66 |
| L Middle Temporal Gyrus | 37 | 421 | -57 -66 -3 |

| FRONTAL-NETWORKS | BA | Vl | Coords |
|---|---|---|---|
| IC 42 | | | |
| R Inferior Frontal Gyrus | 47 | 1154 | 54 21 -6 |
| IC 20 | | | |
| L Inferior Frontal Gyrus | 45 | 364 | -63 21 3 |

**Table 3.5: The talairach table associated with the FDR surviving regions on age effects, that are becoming less lateralized as age goes from 12 to 71, each (shown on Figure 3.6) , BA = Brodmann area; Vl = number of voxels in each cluster; Coords = coordinate (in mm) of tmax in MNI space, following LPI convention.**

### 3.3.2 Voxel-wise effects of age

Figure 3.6 shows the significant ($p<0.05$, following FDR correction for multiple comparisons) age effects on voxel-wise laterality, Table 3.5 shows the corresponding regions that are becoming less lateralized with aging. Sensorimotor networks contain the largest volume whose lateralization decreases (with respect to their mirror images) along with the visual, attentional and frontal networks that are also presenting many lateralized voxels. The left lateralized sensorimotor network components, 7, 23 and 38 have regions that are becoming more symmetric in postcentral gyrus, precentral gyrus and supramarginal gyrus. Right lateralized sensorimotor network, IC 24, is also becoming more symmetric in precentral gyrus.

The visual network component 67 (lingual gyrus), show decreased right lateralization with age. The attentional network components 34 and 52, show less left lateralization with age in inferior parietal lobule, superior parietal lobule and middle temporal gyrus.

The right lateralized component 60 becomes more symmetric due to the changes in superior parietal lobule.

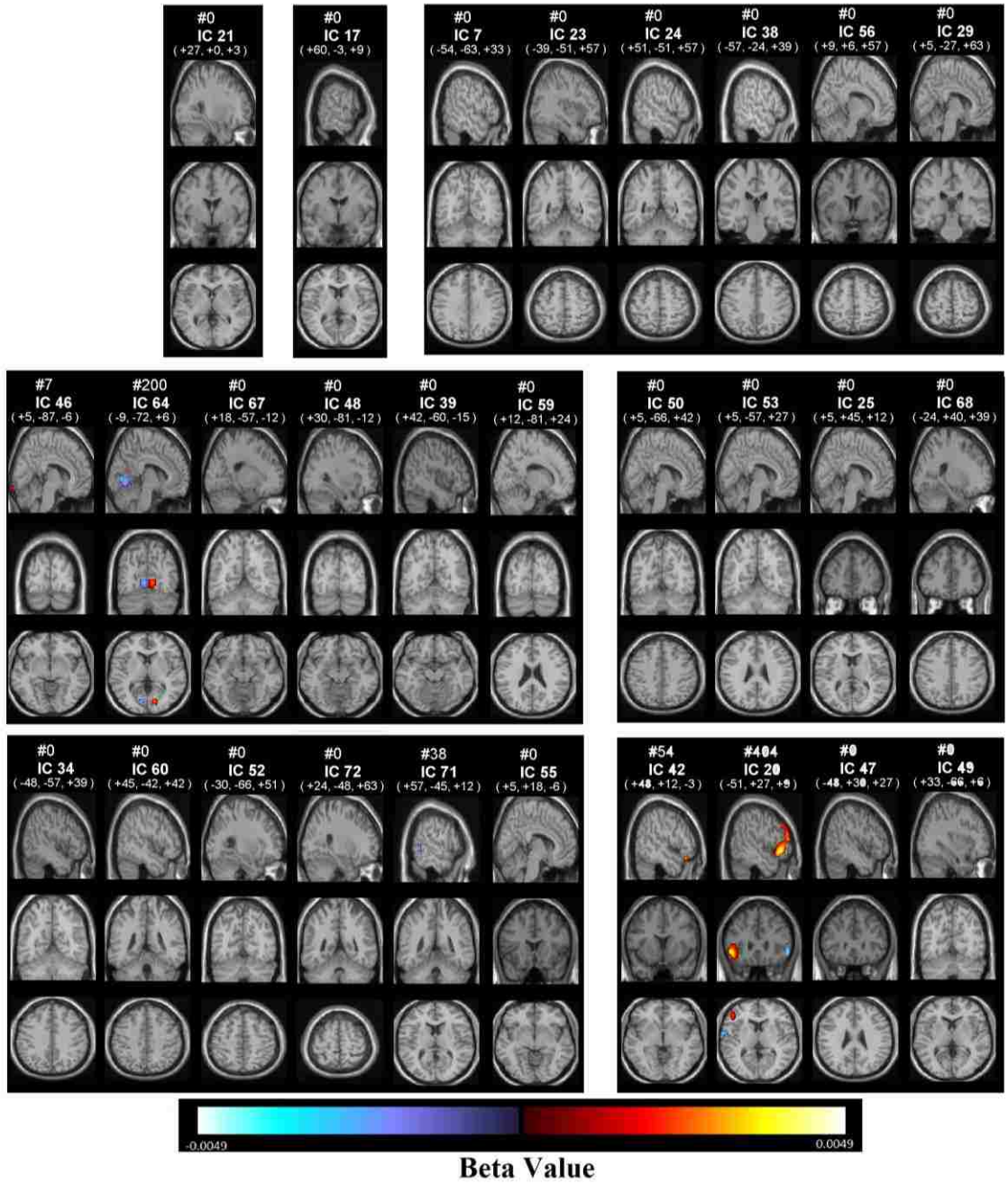


**Figure 3.7: Gender effects on each voxel and each component, voxels that survives FDR correction shown in color, are displayed at the same coordinates with the spatial maps and grouped with a similar matter with Figure 3.2. RSNs are divided into groups based on their anatomical and functional properties and include basal ganglia (BG), auditory (AUD), sensorimotor (MOT), visual (VIS), default-mode (DMN), attentional (ATTN), and frontal (FRONT) networks. We refer to Allen et al. (2011) for the details of grouping.**

*a-)*

| VISUAL NETWORKS | BA | Vl | Coords. |
|---|---|---|---|
| IC 64 | | | |
| L Lingual Gyrus | 18 | 93 | -9 -78 3 |

*b-)*

| FRONTAL-NETWORKS | BA | Vl | Coords. |
|---|---|---|---|
| IC 20 | | | |
| L Inferior Frontal Gyrus | 47 | 285 | -51 27 -6 |

**Table 3.6: a-) The Talairach table associated with the FDR surviving regions on gender effects, that are more lateralized at males, each (shown on Figure 3.7) , BA = Brodmann area; Vl = number of voxels in each cluster; Coords = coordinate (in mm) of tmax in MNI space, following LPI convention. b-) The Talairach table associated with the FDR surviving regions on gender effects, that are more lateralized at females, each (shown on Figure 3.7) , BA = Brodmann area; Vl = number of voxels in each cluster; Coords = coordinate (in mm) of tmax in MNI space, following LPI convention.**

The right lateralized frontal network component 42, shows age-related changes in inferior frontal gyrus, becoming less right lateralized as age goes from 12 to 71. The left lateralized component, 20, has regions on the inferior frontal gyrus that are becoming less left lateralized.

### 3.3.3 Voxel-wise effects of gender

We display the significant ($p<0.05$, following FDR correction for multiple comparisons) gender effects on voxel-wise laterality in Figure 3.7. Corresponding regions that are more lateralized in males are shown at Table 3.6a, and regions that are more lateralized in females listed at Table 3.6b. In general, females showed more lateralization than did males. Right lateralized visual component 64 has left lingual gyrus being more active in males, indicating more right lateralization of this region in females. Frontal network component 20 shows more left lateralization in females in the inferior frontal gyrus.

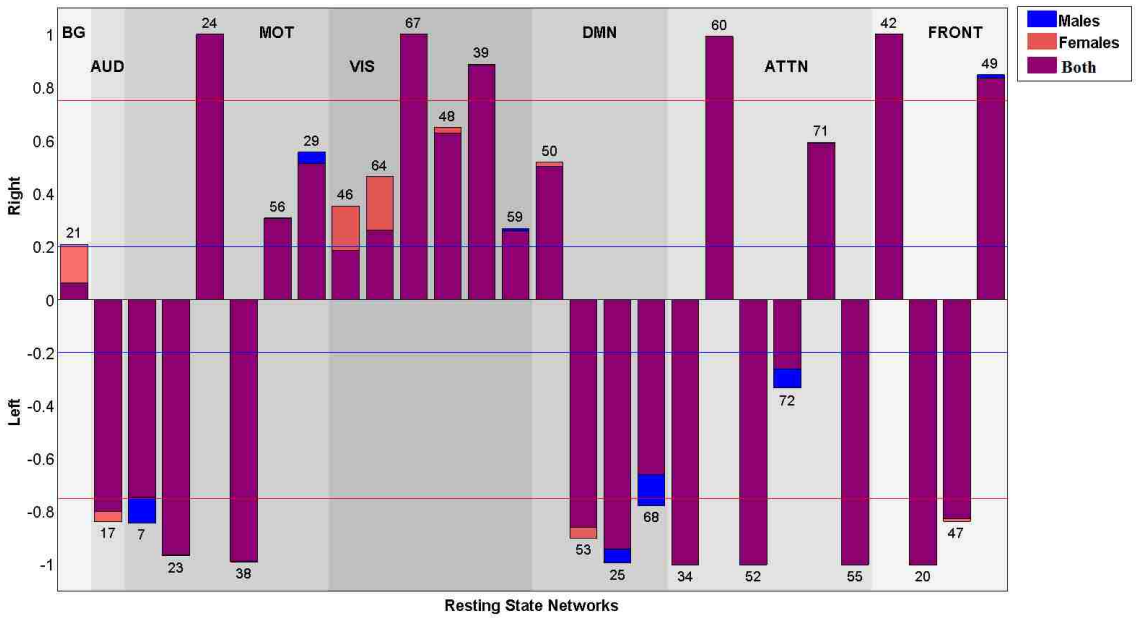


**Figure 3.8: Laterality Cofactors for gender subgroups. Visible blue bars shows the components that are more lateralized for males, visible red bars shows the components that are more lateralized for females.**

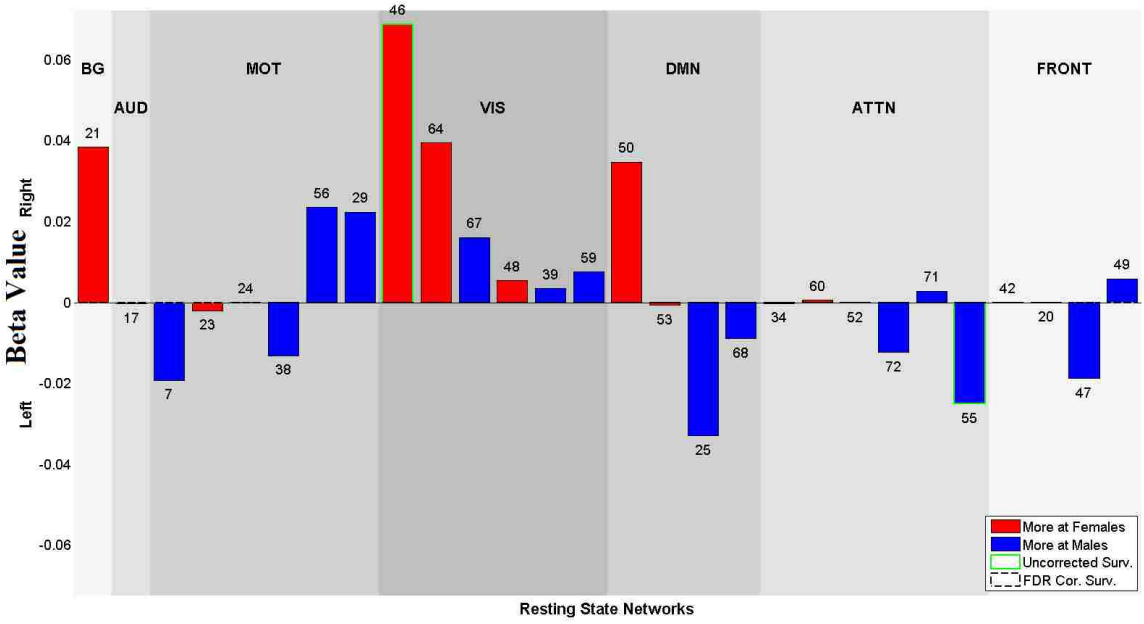


**Figure 3.9: Beta values for Gender effects on laterality cofactors. Blue bars show the components that are more lateralized for males, Red bars shows the components that are more lateralized for females. No components survive from 0.05 levels FDR correction. Component 46 is more lateralized for females (P<0.05) and component 55 is more lateralized for males (P<0.05).**

### 3.3.4 Gender laterality cofactor effects

Laterality cofactors that are calculated for the male and female subgroups are shown at Figure 3.8. The two groups show differences mostly on the visual networks, which are more right lateralized for females. Several other networks also show slight differences between genders. Though the basal-ganglia (IC 21) is predominantly symmetric, it is right lateralized in females compared to the males. The visual network components 46 (lingual and calcarine gyrus) and 64 (calcarine gyrus) are more right lateralized in females. The default mode network component 68 is more lateralized in males.

Figure 3.9 shows the beta values of regression analysis for gender effects on laterality cofactors. The effects are mild, with some uncorrected p-values less than 0.05, but none remain significant following FDR correction. The visual network component 46 (left lingual gyrus, left cingulate gyrus), ($p<0.05$, uncorrected) is more right lateralized in females, and the attentional network component 55 (temporal pole and middle temporal gyrus), ($p<0.05$, uncorrected) is more left lateralized in males.

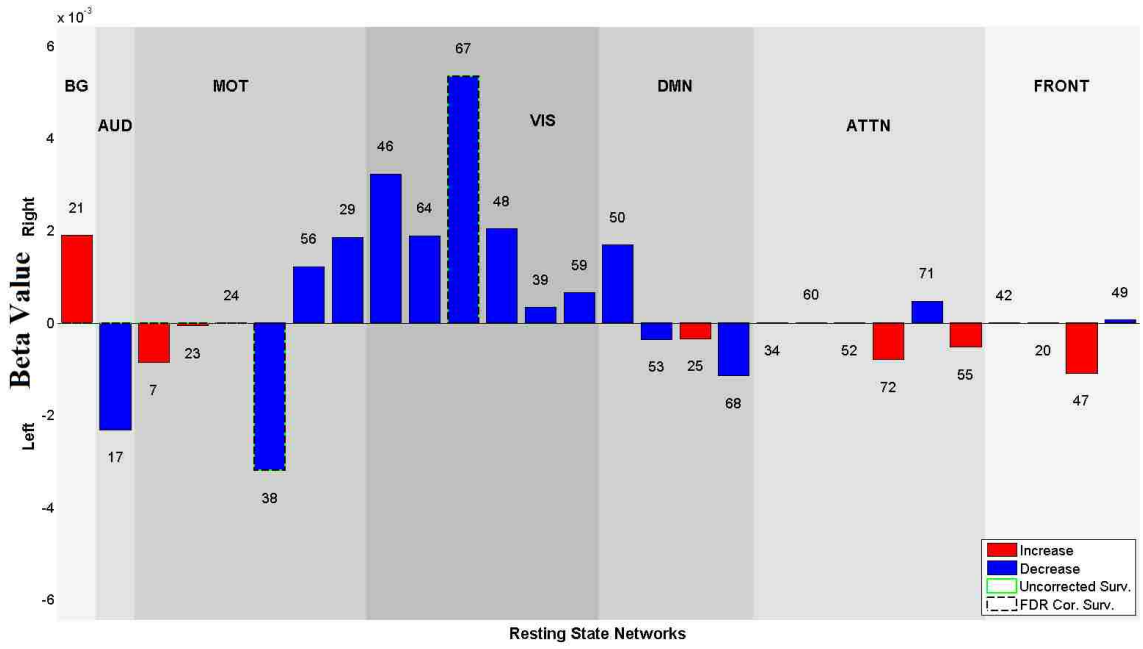


**Figure 3.10: Beta values for Age effects on laterality cofactors. Blue bars show the components that are more lateralized as age goes from 12 to 71. Red bars show the components that are less lateralized as age goes from 12 to 71. Components 38 and 67 (dashed circulated) survive 0.05 levels FDR correction, and are getting less lateralized as age goes from 12 to 71. No other component has p-value smaller than 0.05, besides the ones that also survive FDR correction.**

### 3.3.5 Age laterality cofactor effects

The beta values of regression analysis of age effects on laterality cofactors are displayed in Figure 3.10. Significant age effects are reported for sensorimotor and visual networks, both showing a decrease in lateralization as subjects are getting older. The sensorimotor network component 38 (supramarginal gyrus) and visual network component 67 (cerebellum), survived 0.05 levels FDR correction, components 38 and 67 becomes less left lateralized and less right lateralized respectively as age increases from 12 to 71. No other networks exhibit age effects with p-values less than 0.05.

### 3.3.6 Effects of the sample size on the laterality

As a further analysis, we randomly sub grouped samples into groups of 10, 25, 50 and 100 for 50 trials and calculated the lateralization cofactors and present the results in Table

3.7. For each component, we calculated the variance among 50 trials and calculate the maximum value. The second column represents the error which is the absolute difference from of the full-sample laterality cofactors from the mean of the 50 trials with the corresponding number of samples used. The last column represents the mean of the absolute error among all 28 components.

| #samples | Maximum Variance | Maximum Error | Mean of Absolute Error |
|---|---|---|---|
| 10 | 0.1 | 0.25 | 0.06 |
| 25 | 0.067 | 0.076 | 0.025 |
| 50 | 0.046 | 0.075 | 0.016 |
| 100 | 0.017 | 0.045 | 0.011 |

**Table 3.7: Robustness test on the laterality cofactor.**

The table indicates that component lateralization is quiet robust. Even with a sample size of just 10, we get very reliable and stable results.

We performed two analyses to determine the required number of samples to observe gender effects. For the first analysis, we calculated how much we can reduce the number of samples in t-statistic formula before it no longer passes the FDR threshold. Results are presented in Table 3.8:

| Component | #20 | #64 |
|---|---|---|
| Required Number of Samples | 172 | 294 |

**Table 3.8: Required number of samples to observe gender effects for each component**

In addition, we replicated the analysis on subgroups; we find that gender effects are consistent in gender balanced samples of 250 subjects.

In a similar manner, we investigated the required number of samples for stable age effects. Analysis results are shown at the Table 3.9. The required number of samples varies across components from as low as 34 for one component to as high as 235 for another. This reflects the complexity and diversity of the age effects.

| Component | #7 | #20 | #23 | #24 | #34 | #38 | #42 | #52 | #60 | #67 |
|---|---|---|---|---|---|---|---|---|---|---|
| Required Number of Samples | 235 | 149 | 34 | 44 | 93 | 159 | 82 | 155 | 92 | 138 |

**Table 3.9: Required number of samples to observe age effects for each component**

It is not straightforward to generate a well-matched age distribution in sub-samples due to the non-uniform age distribution of the dataset. This makes it difficult to determine a precise number of required number of samples by replicating the analysis on subgroups as the required sample will be sensitive to the age distribution of the randomly chosen subgroups. This is further compounded by the fact that some of the age effects exhibit non-linear properties. In order to obtain stable age effect results given these considerations, approximately 300 samples are required.

Some additional analysis can provide stronger evidence on the robustness of the lateralization; for example, using an independent dataset or repeating the analysis using a subset of matched case-control pairs (Rose et al., 2009) could be helpful.

## 3.4 Discussion

We analyzed lateralization of resting state networks in a dataset of over 600 subjects, and studied how age and gender affects brain lateralization. Most of the intrinsic networks are lateralized, and sensorimotor (postcentral, precentral supramarginal gyrus), visual (lingual gyrus), attentional (inferior parietal lobule, superior parietal lobule, middle

temporal gyrus) and frontal network (inferior frontal gyrus) have regions that are showing mostly decrease in lateralization with aging. Visual (lingual gyrus) and frontal network (inferior frontal gyrus) also have regions that are affected by gender.

Our results indicate that age is an important factor for lateralization and affecting most of the networks. We observe a decrease in lateralization in four sensorimotor network (3 left and 1 right lateralized), which suggest that left dominancy of sensorimotor networks is getting balanced with aging. Our results are consistent with Zuo et al. (2010b) who found increasing homotopic resting state connectivity on sensorimotor regions, specifically linear increase in supplementary motor area and postcentral gyrus. Zuo et al. (2010b) interpreted this change as increasing hemispheric cooperation for complex bimanual functions. We also found that attentional and frontal networks become more symmetric with aging. Though our result is conflicting with Zuo et al. (2010b) which indicates a decrease in homotopic resting state connectivity in high-order cognitive regions such as anterior cingulate, inferior parietal cortex, precuneus, it is parallel with others Reuter-Lorenz et al. (2000) who found for young adult, verbal working memory is left and spatial working memory is right lateralized in anterior working memory whereas older adults have a global pattern of anterior bilateralized working memory for both visual and verbal memory. Reuter-Lorenz et al. (2000) suggested this bilateralization can be an attempt to overcome neural decline. Cabeza et al. (2002) also found bilateral prefrontal cortex activity in older adults comparing to young adult, and compare the hemispheric asymmetries in two groups; low-performing older adults versus high performing older adults; and found a hemispheric asymmetry reduction in high performing group, supporting the compensation theory that brain cognitive networks become more bilateral

in order to compensate neural decline. If our results are supported by subsequent studies , the effects of age and gender on the components that intersect significantly with primary sensory and motor cortices, would tend to mitigate against recent findings of Mueller et al. (2013) that primary sensory and motor cortices exhibit relatively less individual variation than the association cortex.

Some studies reports that gender is a factor in brain lateralization, while some studies report no gender effect on brain lateralization. Significant gender differences in intra and inter-hemisphere connectivity were recently reported by Ingalhalikar et al. (2013) in a DTI study, Zuo et al. (2010b) presented significant differences in regions of dorsolateral prefrontal cortex (BA 9 and 47) and amygdala for homotopic functional connectivity, and some small differences are also reported (Liu et al., 2009). In our study, voxel-vise results showed gender to be a factor in lateralization of two regions, lingual gyrus (visual network) and inferior frontal gyrus (frontal network), suggesting females being more lateralized in both regions. Zuo et al. (2010b) that reports females having higher homotopic functional connectivity with in posterior cingulate cortex, medial prefrontal cortex, and the superior and middle frontal cortex, comparing to males. They also found males having stronger homotopic connectivity in cerebellum, parahippocampal gyrus, and fusiform gyrus comparing to the females. Good et al. (2001) reported several morphological asymmetries between genders, including right inferior frontal gyrus being increased in volume in females. Globally, the gender effect on lateralization cofactors are not significant which is consistent with Nielsen et al. (2013) and meaningful given our relatively large sample size.

The age effects on the laterality cofactors are varying, some components are linear, some non-linear, some are additive and some components are subtractive. For instance, lateralization of Component 47 (inferior frontal gyrus) increases significantly with age for subjects between 12 and 29 years old , decreases with age for subjects aged 30 to 71, (see Appendix). Evaluated over the whole population (ages 12 to 71) however, lateralization of the inferior frontal gyrus trends negatively with age , indicating a non-linear age effect which is consistent with the work by Zuo et al. (2010b) where linear, quadratic and cubical age related changes reported on the whole brain resting state functional connectivity. In general, there appear to be more nonlinear effects at the younger age range. In a recent large-scale study (N = 1782), Hirnstein et al. (2013) found no main-effect of sex on a dichotic listening task, which assesses auditory laterality, but that sex interacted with age. In brief, these authors found that the laterality index increased with increasing age, driven by the females. These behavioral findings however were not corroborated in an fMRI study on a selected sub-sample (N = 104) wherein males still showed greater behavioral asymmetry. Thus, the relationship between sex and age effects on brain asymmetry and lateralization is complex, and with intrinsic interactions between the two factors, future research should therefore ideally include both younger and older subjects when studying sex differences and brain function, which would also apply to analysis of cortical networks, and neuronal connectivity.

In this work, we studied the lateralization in resting state networks, rather than brain lateralization in general. Were we to ignore networks, some of the lateralized regions would appear highly symmetric. For example, ICs 23 and 24 (left and right postcentral gyrus) look like mirror images of one another. This indicates the power of our analysis

comparing to the whole brain analysis. The model order is very crucial and unfortunately, though various estimation approaches exist, there is no analytic way to determine perfect model order. We also performed an eigenvalue analysis on the ICs to evaluate the ability of the components to be well captured when using variance as the criteria. To do so, we used PCA to decompose the group average component-by-voxels matrices. Results showed that to capture 90% of the variance 50 components are needed, and 60 components are needed to capture 95% of the variance. Based on this, we conclude that there is considerable value in these higher model order approach.

### 3.4.1 Limitations

We should consider some limitation interpreting the results. Firstly, we do not have information about the education or IQ level or other domains such as the working memory of subject during the scanning process. Also, subjects have not been tested to measure their behavior abilities; they may not be balanced with verbal ability, motor skills or visuospatial attention. Though our subjects are ranging from age 12 to 71, they do not cover the most rapidly changing ages of childhood, and the distribution of age is not uniform. Moreover, for comparison purposes we focused on the resting state networks extracted from a previous study that has ICA model order of 75, but it would also be interesting to evaluate the age and gender related changes for higher and lower model orders using different criteria to determine dimensionality. Even though we used a large sample size, subjects were scanned with a minimum of 5 minutes (152 volumes), this may limit the sensitivity detection of the effects. Besides, even though, we warped the data into a symmetric template to count for well-known structural asymmetries, the possibility that additional structural asymmetries might still be present should be

considered while interpreting the results. Finally, there are many other ways to measure the amount of lateralization of a component; we choose one method, the laterality cofactor, due to its simplicity, in addition to the voxelwise homotopic effects.

## 3.5 Conclusion

In summary, we analyzed lateralization of 28 resting state networks in a large fMRI dataset consisting of over 600 healthy subjects ranging in age from 12 to 71. We found many of the intrinsic brain networks are highly lateralized, with several regions (sensorimotor, visual, attentional and frontal) showing a strong relationship with age and two networks (visual and frontal) showed voxel-wise differences between genders. On the global measure of laterality, age was found as a strong factor and gender exhibiting a trend-level effect. Our results support the theory that multiple brain networks grow more bilateral in an attempt to compensate neural decline with aging. In future work, investigating compensation effects by studying changes lateralization in subjects with injured brains or lesions, and examining age effects in more details in subgroups such as childhood, teenage, young adults etc. with more balanced numbers of subjects across the full age range, are promising research directions. Significant gender effects were also found, but showed a more complex pattern of change in which greater lateralization was observed in some regions in females and other regions in males. In summary, our approach of focusing on network-specific lateralization thus appears to be a promising and sensitive tool for studying brain organization.

# Chapter 4: Decreased Asymmetry of Intra Hemisphere and Inter Hemisphere Functional Network Connectivity at Rest in Schizophrenia

## 4.1 Motivation

Many studies have shown that schizophrenia patients have aberrant functional network connectivity (FNC) among brain regions, suggesting schizophrenia manifests with significantly diminished (in majority of the cases) connectivity. Schizophrenia is also strongly related to lack of hemispheric lateralization. Hoptman et al. (2012) found decreased in homotopic connectivity in schizophrenia patients using voxel-mirrored homotopic connectivity. In their ROI based resting fMRI study, Ke et al. (2010) reported increased leftward asymmetry of FC at patients with exhibiting positive symptom scores, and increased rightward asymmetry of FC at patients with negative symptoms.

In this study, we merge these two points of views together using a group independent component analysis (gICA)-based approach to generate hemisphere-specific time-courses and calculate intra-hemisphere and inter-hemisphere FNC on a resting state fMRI dataset consist of age and gender balanced schizophrenia patients and healthy controls. We analyze the group differences between patients and healthy controls in each type of FNC measures, and association with age and gender.

Previous lateralization studies in connectivity, used either seed/atlas based approaches or voxel-mirrored functional connectivity to investigate laterality (Gee et al., 2011; Gotts et al., 2013; Hoptman et al., 2012; Liu et al., 2009; Mwansisya et al., 2013; Nielsen et al., 2013; Oertel-Knochel et al., 2013; Stark et al., 2008; Zhu et al., 2014; Zuo et al., 2010b)

and most of these studies were only interested in connectivity within each hemisphere or connectivity of cross-hemispheric homotopic regions. In healthy population, Gee et al. (2011) examined the connectivity of heterotopic regions in different hemispheres and compared with intra-hemisphere connectivity in their atlas based study. To our best knowledge, this is the first study to use FNC measures to calculate hemispheric differences, as well as to examine connectivity differences in heterotopic regions in schizophrenia patients.

## 4.2 Methods and Materials

**Table 4.1: Demographic information of the subjects, age, gender, and diagnosis distribution.**

| | # of subject | % | | |
|---|---|---|---|---|
| **Gender** | 314 | 100 | | |
| **Male** | 231 | 73.5 | | |
| **Female** | 83 | 26.5 | | |
| **Healthy** | 163 | 52 | | |
| **Schizophrenia** | 151 | 48 | | |
| | | | | |
| | **Mean** | **SD** | **Min** | **Max** |
| **Age(year)** | 37.4 | 11.2 | 18 | 60 |
| **Male** | 37.3 | 11.2 | 18 | 60 |
| **Female** | 34.8 | 11.4 | 19 | 58 |
| **Healthy** | 36.9 | 11 | 19 | 60 |
| **Schizophrenia** | 37.8 | 11.4 | 18 | 60 |

### 4.2.1 Participants

In this study, we used a large resting state fMRI dataset containing 314 subjects, 163 healthy controls (117 males, 46 females; mean age 36.9) and 151 schizophrenia patients that are matched in age and gender to healthy control group (114 males, 37 females; mean age 37.8) combined from 7 different sites across United States and passed the data

quality control. Informed consent was received from each subject prior to scanning in accordance with the Internal Review Boards of corresponding institutions. Demographic information of the participants is displayed in Table 4.1. Using 3T scanners with a TR of 2s, a total of 162 volumes of echo planar imaging BOLD fMRI data were collected.

**Table 4.2: Distribution of Positive and Negative Syndrome Scale and mean antipsychotic dose as CPZ equivalent are presented for schizophrenia patients. 148 patients had PANSS score and 122 patients had mean antipsychotic dose data available.**

| | Mean | SD | # of subject |
|---|---|---|---|
| **Negative** | 14.3 | 5.3 | 148 |
| **Positive** | 14.8 | 4.56 | 148 |
| **CPZ** | 430.8 | 612.2 | 122 |

Cognitive and clinical measures were collected for 275 out of 314 subjects and analyzed as Computerized Multiphasic Interactive Neurocognitive System (CMINDS) composite scores. The composite scores summarize the overall cognition in six different measures: attention/vigilance, speed of processing, verbal learning, working memory, visual learning and reasoning/problem solving (van Erp et al., 2015). Distribution of the CMINDS score were shown at Table 4.2. For the schizophrenia patients, 148 patients out of 151 had Positive and Negative Syndrome Scale (PANSS) available and 129 patients have the mean antipsychotic dose as Chlorpromazine (CPZ) equivalent were available. Table 4.3 shows the distribution of the PANSS and CPZ values.

**Table 4.3: Distribution of cognitive scores, as CMINDS composite scores, for 276 subjects.**

| | Total | Schizophrenia | Healthy |
|---|---|---|---|
| **CMIND Mean** | -0.6726 | -1.4664 | 0.0550 |
| **CMIND SD** | 1.2995 | 1.1724 | 0.9346 |
| **# of subject** | 276 | 132 | 144 |

### 4.2.2 Data Acquisition

Imaging data was collected using a 3T Siemens Tim Trio System on six of the seven sites, while on a site using a 3T General Electric Discovery MR750 scanner. Resting state fMRI scans were acquired using a standard gradient-echo echo planar imaging paradigm: FOV of 220 × 220 mm (64 × 64 matrix), TR=2 s, TE=30 ms, FA=770, 162 volumes, 32 sequential ascending axial slices of 4 mm thickness and 1 mm skip. Subjects were instructed to close their eyes and stay awake during the resting state scan.

### 4.2.3 Preprocessing

Functional MRI data were preprocessed using the same pipeline as mentioned in Damaraju et al. (2014), using a combination of toolboxes, such as, AFNI (https://afni.nimh.nih.gov), SPM (http://www.fil.ion.ucl.ac.uk/spm), GIFT (http:mialab.mrn.org/software/gift) and Matlab. The INRIAlign (Freire et al., 2002) toolbox in SPM was used for rigid body motion correction for subject head motion followed by slice-timing correction to account for timing differences in slice acquisition. 3dDespike algorithm in AFNI was used to despike the fMRI data to reduce the impact of outliers. The fMRI data were subsequently warped to a Montreal Neurological Institute (MNI) template and resampled to 3 $mm^3$ isotropic voxels. Then, the fMRI data were smoothed with a 6 mm full width at half maximum (FWHM) using AFNI. Each voxel time course was variance normalized prior to the gICA. We refer to Damaraju et al. (2014) for the more details on the preprocessing.

### 4.2.4 Group Independent Component Analysis

The preprocessed data was decomposed into 100 spatially independent components using gICA that was implemented using GIFT. gICA identifies spatially distinct functionally-coherent networks by estimating maximally independent spatial sources, or spatial maps, from their linearly-mixed fMRI signals, or time-courses (Calhoun et al., 2001a; Erhardt et al., 2011b). Out of the original 100 components, 47 components were identified as resting state networks (RSNs) based upon several criteria: maximally activated voxels located in identified gray matter, minimal spatial overlap with known vascular, ventricular and head-motion susceptible edge regions, combined with large low-to-high frequency spectral power ratio in the component time-courses. We refer the readers to Damaraju et al. (2014) for a detailed discussion of the gICA analysis performed on this data and selection of RSNs.

### 4.2.5 Generating Templates and Hemisphere Specific Time-courses

We utilized spatiotemporal regression on symmetrized aggregated spatial maps of the components to generate hemisphere-specific component time-courses. Symmetrized aggregated spatial maps were generated by flipping the original aggregated spatial maps along their lateral axes, by comparing each flipped voxel value with its unflipped voxel value and retaining the maximum intensity value. Hence, the symmetrized versions of the components that are mirror images of each other, for example, components 91 (left lingual gyrus) and 76 (right lingual gyrus), those component will be collinear. We tested collinearity of the components using a variance inflation factor and removed 4 RSNs (IC 6, 91, 66 and 84) from our analyses which had high collinearity with components IC 10 (precentral and postcentral gyrus), IC 76 (lingual gyrus), IC 94 (inferior parietal lobule)

and IC 95 (angular gyrus) respectively. We also removed artifactual components (IC 17, 31 39 and 52) that have large variance inflation factor. We finalized 92 symmetrized aggregated spatial maps (43 RSNs & 49 artifacts) for our subsequent analyses. Then, we split the symmetrized spatial maps and preprocessed subject data into left and right hemispheres. Finally, we applied spatiotemporal regression on the left and right hemispheres separately to generate subject specific left and right hemisphere time-courses and spatial maps using GIFT. Generated RSNs are displayed in Figure 4.1 in terms of t-statistics and corresponding MNI regions are presented in Table 4.4.

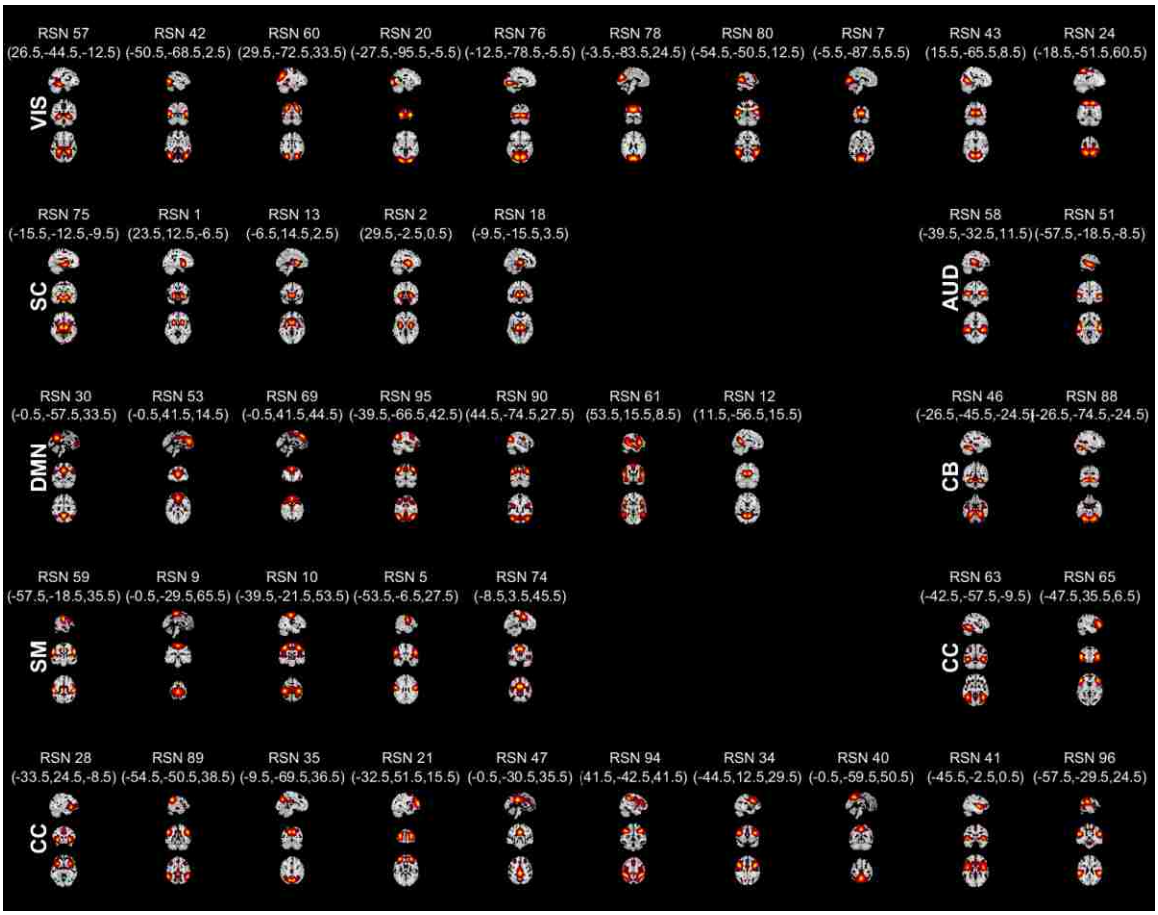


**Figure 4.1: Symmetrized aggregated spatial maps of the 43 RSNs, are displayed at the three most informative slices. RSNs are divided into groups based on their anatomical and functional properties, and include sub-cortical (SC), sensorimotor (SM), auditory (AUD), visual (VIS), attention/cognitive control (CC), default-mode (DMN), and cerebellar (CB) networks.**

### 4.2.6 Functional Network Connectivity Calculation

For each hemisphere, subject time-courses went through post-processing steps, including detrending and despiking, and band-pass filtering using a fifth-order Butterworth filter with cutoff frequencies of [0.01- 0.15 Hz]. FNC between two components is calculated by using Pearson's correlation (Jafri et al., 2008) as follow:

$$Corr_{(C_x,C_y)} = \frac{TC_{Cx} * TC_{Cy}}{\|TC_{Cx}\| * \|TC_{Cx}\|} = \frac{\sum_{i=1}^{n}(TC_{Cxi} * TC_{Cyi})}{\sqrt{\sum_{i=1}^{n} TC_{Cxi}^2} * \sqrt{\sum_{i=1}^{n} TC_{Cyi}^2}}$$

Where $TC_{Cx}$ and $TC_{Cy}$ are the time-courses of two different components and n is the length of the time-courses (M. S. Cetin et al., 2014). The FNC matrixes are calculated using the time-courses of 43 left components and 43 right components. For each subject, we have an intra left hemisphere (L_FNC) (903 pairs ($(43^2 - 43)/2$)), an intra right hemisphere (R_FNC) (903 pairs) and an inter hemisphere (Cross_FNC) (1849 pairs with 43 homotopic pairs ($43^2$)) FNC matrices. Note that, the inter-hemisphere FNC matrix is not symmetric around diagonals since one axis represents symmetrized left hemisphere-specific spatial maps and the other represents symmetrized right hemisphere-specific spatial maps.

**Table 4.4: MNI labels associated with the each symmetrized RSN show in Figure 4.1, BA = Brodmann area; Vl = number of voxels in each cluster; Tmax = maximum t-statistics in each cluster; Coordinate of Tmax in MNI space, following LPI convention.**

| | BA | Vl | Tmax | Coordinate |
|---|---|---|---|---|
| **Sub-Cortical Networks** | | | | |
| **IC75** | | | | |
| R Lingual Gyrus | | 8937 | 32.62 | 12 -21 -9 |
| L Hippocampus | L 28 | 8019 | 31.02 | -15 -15 -9 |
| **IC 1** | | | | |
| R Putamen | R 47 | 13176 | 75.38 | 24 12 -9 |
| L Putamen | L 13 | 12960 | 74.43 | -24 12 -6 |
| **IC 13** | | | | |
| R Caudate | | 15444 | 62.3 | 9 15 6 |
| L Caudate | L 25 | 15255 | 61.54 | -6 15 0 |
| **IC 2** | | | | |
| R Putamen | | 12231 | 75.42 | 30 -3 0 |
| L Putamen | | 12393 | 67.49 | -30 -6 3 |
| **IC 18** | | | | |
| R Thalamus | | 13230 | 67.43 | 12 -15 3 |
| L Thalamus | | 13284 | 68.07 | -9 -18 3 |
| **Auditory Networks** | | | | |
| **IC58** | | | | |
| R Heschls Gyrus | R 22 | 22437 | 40.88 | 48 -18 6 |
| L Superior Temporal Gyrus | L 41 | 23220 | 46.04 | -42 -30 9 |
| **IC 51** | | | | |
| R Middle Temporal Gyrus | R 21 | 21897 | 41.19 | 57 -18 -9 |
| L Middle Temporal Gyrus | L 21 | 18144 | 37.69 | -57 -12 -9 |
| **Visaul Networks** | | | | |
| **IC 57** | | | | |
| R Fusiform Gyrus | R 36 | 16092 | 45.84 | 24 -42 -12 |
| L Fusiform Gyrus | L 36 | 13392 | 49.14 | -24 -42 -12 |
| **IC 42** | | | | |
| R Middle Temporal Gyrus | R 37 | 17847 | 48.84 | 48 -66 3 |
| L Middle Temporal Gyrus | L 37 | 17469 | 47.31 | -48 -69 6 |
| **IC 60** | | | | |
| R Middle Occipital Gyrus | R 19 | 24084 | 46.19 | 30 -72 33 |
| L Middle Occipital Gyrus | L 7 | 23571 | 44.67 | -27 -69 33 |
| **IC 20** | | | | |
| R Inferior Occipital Gyrus | R 18 | 17577 | 49.94 | 30 -93 -6 |
| L Inferior Occipital Gyrus | L 18 | 20466 | 46.78 | -27 -93 -6 |
| **IC 76** | | | | |
| R Lingual Gyrus | R 18 | 21978 | 49.38 | 18 -75 -6 |
| L Lingual Gyrus | L 18 | 22410 | 49.01 | -12 -78 -6 |
| **IC 78** | | | | |
| L Cuneus | R 18 | 20871 | 51.66 | 3 -84 24 |
| L Cuneus | L 18 | 20655 | 52.49 | -3 -84 24 |
| **IC 80** | | | | |
| R Middle Temporal Gyrus | R 22 | 20790 | 46.58 | 54 -51 12 |
| L Middle Temporal Gyrus | L 22 | 21060 | 42.07 | -57 -51 12 |
| **IC 7** | | | | |
| R Calcarine Gyrus | R 18 | 20574 | 68.56 | 3 -87 6 |
| L Calcarine Gyrus | L 18 | 21627 | 69.97 | -6 -87 6 |
| **IC 43** | | | | |
| R Calcarine Gyrus | R 30 | 23895 | 58.64 | 15 -63 9 |
| L Calcarine Gyrus | L 30 | 22734 | 56.3 | -12 -66 9 |
| **IC 24** | | | | |
| R Superior Parietal Lobule | R 7 | 20628 | 40.18 | 18 -54 63 |
| L Superior Parietal Lobule | L 7 | 20277 | 41.39 | -24 -51 60 |
| **Somatomotor Networks** | | | | |
| **IC 59** | | | | |
| R Postcentral Gyrus | R 4 | 15660 | 40.46 | 60 -18 36 |
| L Postcentral Gyrus | L 3 | 14526 | 38.51 | -60 -18 33 |
| **IC 9** | | | | |
| R Paracentral Lobule | R 6 | 20250 | 56.22 | 3 -33 63 |
| L Paracentral Lobule | L 6 | 20547 | 54.44 | -3 -27 63 |
| **IC 10** | | | | |
| R Postcentral Gyrus | R 3 | 27864 | 46.41 | 42 -21 54 |
| L Postcentral Gyrus | L 3 | 27162 | 43.02 | -42 -24 60 |
| **IC 5** | | | | |
| R Postcentral Gyrus | R 6 | 17739 | 58.65 | 54 -6 27 |
| L Postcentral Gyrus | L 6 | 15147 | 56.56 | -54 -9 30 |
| **IC 74** | | | | |
| R Middle Cingulate Cortex | R 24 | 23355 | 49.52 | 3 -3 45 |
| L SMA | L 24 | 20601 | 46.79 | 0 0 48 |

| | BA | Vl | Tmax | Coordinate |
|---|---|---|---|---|
| **Cognitive Control Networks** | | | | |
| **IC 63** | | | | |
| R Fusiform Gyrus | R 37 | 12771 | 38.94 | 42 -54 -12 |
| L Fusiform Gyrus | L 37 | 12393 | 43.58 | -42 -51 -12 |
| **IC 65** | | | | |
| R Inferior Frontal Gyrus | R 46 | 18441 | 34.31 | 51 39 3 |
| L Inferior Frontal Gyrus | L 47 | 16956 | 37.4 | -45 39 -3 |
| **IC 28** | | | | |
| R Inferior Frontal Gyrus | R 47 | 18711 | 57.8 | 33 24 -9 |
| L Inferior Frontal Gyrus | L 47 | 17469 | 50.67 | -33 24 -6 |
| **IC 89** | | | | |
| R SupraMarginal Gyrus | R 40 | 17739 | 49.69 | 57 -48 36 |
| L Inferior Parietal Lobule | L 40 | 15606 | 45.36 | -54 -54 39 |
| **IC 35** | | | | |
| R Precuneus | R 7 | 16011 | 51.6 | 9 -72 39 |
| L Precuneus | L 7 | 14391 | 54.06 | -9 -69 36 |
| **IC 21** | | | | |
| R Middle Frontal Gyrus | R 10 | 22761 | 37.94 | 30 51 15 |
| L Middle Frontal Gyrus | L 10 | 21276 | 39.88 | -33 51 21 |
| **IC 47** | | | | |
| R Middle Cingulate Cortex | R 23 | 17928 | 58.74 | 3 -27 30 |
| R Middle Cingulate Cortex | L 23 | 17037 | 53.19 | 0 -27 30 |
| **IC 94** | | | | |
| R Inferior Parietal Lobule | R 40 | 27702 | 43.3 | 42 -45 48 |
| L Inferior Parietal Lobule | L 40 | 32805 | 45.09 | -45 -39 39 |
| **IC 34** | | | | |
| R Inferior Frontal Gyrus | R 9 | 17982 | 39.27 | 48 12 27 |
| L Precentral Gyrus | L 9 | 15984 | 41.63 | -45 12 30 |
| **IC 40** | | | | |
| R Precuneus | R 7 | 19170 | 57.25 | 3 -57 51 |
| L Precuneus | L 7 | 19440 | 56.52 | 0 -60 51 |
| **IC 41** | | | | |
| R Insula | R 13 | 19872 | 49.75 | 45 0 0 |
| L Insula | L 22 | 17604 | 46.92 | -45 3 -3 |
| **IC 96** | | | | |
| R SupraMarginal Gyrus | R 40 | 13446 | 41.72 | 60 -27 24 |
| L SupraMarginal Gyrus | L 13 | 12636 | 36.02 | -51 -36 24 |
| **Default-mode Networks** | | | | |
| **IC 30** | | | | |
| L Precuneus | R 7 | 19089 | 69.94 | 3 -63 36 |
| L Precuneus | L 31 | 17496 | 65.02 | -3 -57 33 |
| **IC 53** | | | | |
| Anterior Cingulate Cortex | 32 | 21870 | 50.72 | -3 42 15 |
| **IC 69** | | | | |
| Superior Medial Gyrus | 8 | 17982 | 50.48 | 0 42 45 |
| **IC 95** | | | | |
| R Angular Gyrus | R 40 | 28134 | 50.56 | 48 -63 42 |
| L Angular Gyrus | L 40 | 31212 | 49.31 | -42 -63 45 |
| **IC 90** | | | | |
| R Middle Occipital Gyrus | R 39 | 13554 | 40.7 | 45 -75 30 |
| L Middle Occipital Gyrus | L 39 | 13851 | 37.8 | -39 -75 30 |
| **IC 61** | | | | |
| R Inferior Frontal Gyrus | R 45 | 24219 | 32.99 | 51 18 6 |
| L Inferior Frontal Gyrus | L 44 | 32535 | 38.66 | -54 15 9 |
| **IC 12** | | | | |
| R Precuneus | R 30 | 17226 | 65.19 | 12 -54 15 |
| L Precuneus | L 23 | 16956 | 70.24 | -9 -57 15 |
| **Cerebellar Networks** | | | | |
| **IC 46** | | | | |
| R Cerebellum | R 37 | 14634 | 44.93 | 27 -48 -24 |
| L Cerebellum | L 37 | 14175 | 45.29 | -24 -45 -24 |
| **IC 88** | | | | |
| R Cerebellum | R 19 | 28863 | 49.02 | 33 -72 -24 |
| L Cerebellum | L 19 | 26865 | 49.35 | -30 -72 -24 |

### 4.2.7 Calculating Group Averages

Using all participants and also separately for the patient and control subgroups, we tested whether the FNC means differ from zero by using one sample t-test with 0.05 false discovery rate (FDR) correction. Figure 4.2 shows the results for all participants; Figure 4.3 shows the subgroup results. For visualization purposes, we displayed homotopic FNC results in a bar plot.

### 4.2.8 Comparing Strength of lateralized FNC types in Patients and Healthy Control

For the patient and healthy control subgroups separately, we compared the two sets of hemisphere specific connectivity strengths captured in L_FNC and R_FNC, and also the compared L_FNC and R_FNC connectivity strengths to the connectivity strengths captured in Cross_FNC. To do so, for each group and for each type of FNC, we performed a one sample t-test and thresholded with 0.05 levels FDR correction; then for each pair of FNC types, the indices of network-pairs whose connectivity had the same directionality (positive or negative) and also were significant in both FNC matrices were recorded. We were interested in connectivity strength (as long as it was the same in both FNC types), so the network-pair connectivity was then converted to absolute values. For each pair of FNC types, a paired t-test on magnitudes was then performed. Results were corrected with 0.05 levels FDR. Among the significant paired t-test network-pairs, we retained only those pairs that were previously recorded as being significant in both FNC types with same directionality. Later, for patient and control groups separately, we identified the number of significant network-pairs, and recorded which FNC type they favored.

### 4.2.9 Modeling Age, Gender, Schizophrenia and Handedness Effects in Intra FNC Differences

In order to investigate the differences between left and right hemisphere-specific FNCs, a left-right FNC difference map was calculated for each subject (L_FNC minus R_FNC). The values from this difference map were then individually employed as the dependent variable in a multiple linear regression on age, gender, schizophrenia, handedness as well as motion parameters. We prefer the regression method in order to regress out the motion and handedness effect on the differences. The model used is formulized below:

$$\sigma_{(i,j)} = \beta_{o} + \beta_{age}^{(i,j)} X_{age} + \beta_{gen}^{(i,j)} X_{gen} + \beta_{diag}^{(i,j)} X_{diag} + \beta_{hand}^{(i,j)} X_{hand} + \beta_{mot}^{(i,j)} X_{mot} + \varepsilon_{(i,j)}$$

$X_{gen}$ is a categorical variable representing the gender of subject with 1 for females and 0 for males before mean removal. The age ($X_{age}$) is the mean removed age distribution, $X_{diag}$ is 1 for schizophrenia patients and 0 for healthy control before mean removal, and handedness is subject's Edinburg handedness score ranges between -2 and 2 (positive for right handers) before mean removal, $X_{mot}$ is the mean frame displacement. All β's are the coefficients of the regression model with ε being the error parameter for the model, $\sigma_{(i,j)}$ is the difference between L_FNC and R_FNC. This analysis captures the network pairs for which the differences in left/right hemisphere-specific connectivity are significantly ($p<0.05$, following false discovery rate (FDR) correction for multiple comparisons) (Genovese et al., 2002) affected by age, gender, diagnosis, and handedness..

#### 4.2.10 Modeling Age, Gender, Schizophrenia and Handedness Effects in Intra Hemisphere and Inter Hemisphere FNC

We also checked the effects of age, gender, diagnosis and handedness on the hemisphere-specific FNCs (L_FNC and R_FNC), and also on Cross_FNC. We used a similar regression model as described above, with $\sigma_{(i,j)}$ being the intra or inter-FNC value, rather than the differences. Significance for beta values was later thresholded with 0.05 levels FDR.

#### 4.2.11 Modeling Effects of Cognitive Scores, Symptom Scores and Mean Antipsychotic Dose

We checked the effect of cognitive scores (CMINDS), symptom scores PANSS, and mean antipsychotic dose (CPZ equivalent) in separate regression analysis on hemisphere-specific FNCs and the left-right difference FNCs.

### 4.3 Results

#### 4.3.1 Results of Group Averages

The average FNC results for all subjects are displayed in Figure 5.2 in terms of FDR corrected (0.01 levels) t-statistics. Overall, the connectivity patterns show similar trends in intra left, intra right and inter hemisphere FNC. We observe high correlation in intra-subcortical, intra-visual, intra-sensorimotor, intra-default mode, and sensorimotor & visual networks in all FNC types. Intra-cognitive control also is mostly positively correlated, with the exception of one anti-correlated network, IC 63 (fusiform gyrus). General hemisphere-specific and inter-hemispheric connectivity patterns also show similar patterns as to those seen under a standard whole brain FNC analysis (Damaraju et

al., 2014). Homotopic networks are highly correlated, and their connectivity strength is much higher than heterotopic networks. Their connectivity strength also changes among themselves, and we found that the closer the homotopic pairs were to each other, the higher the connectivity strength became.

Separate FNC results for healthy control and schizophrenia patient groups are displayed in Figure 5.3 in terms of FDR corrected (0.01 levels) t-statistics. In all FNC types, patients have lower connectivity strength relative to healthy controls. However, the overall patterns of connectivity look alike for both groups.

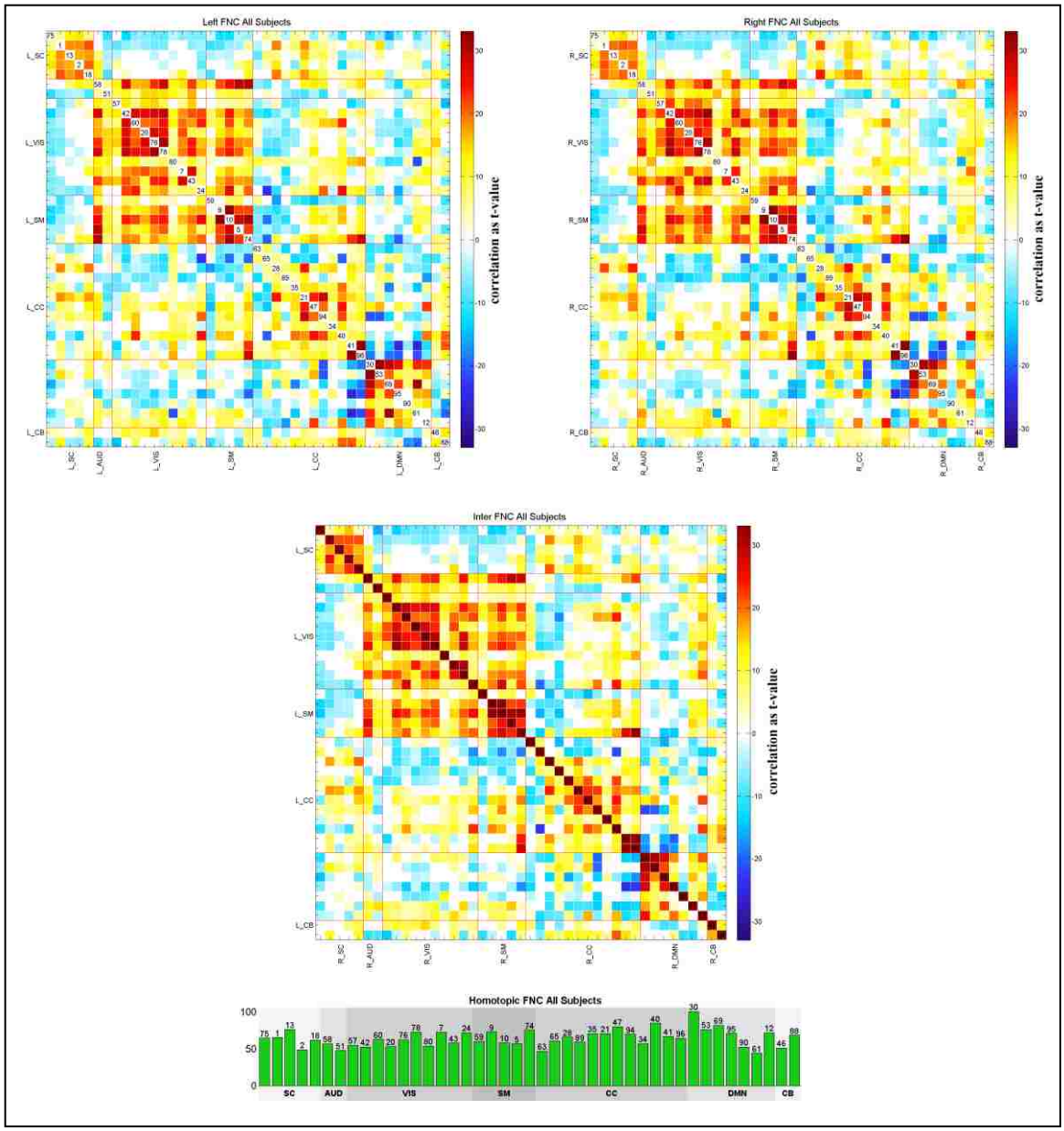


**Figure 4.2: Averages of L_FNC (top left), R_FNC matrix (top right) and Cross_FNC (bottom) are displayed as t-statistics thresholded with 0.01 levels FDR. Homotopic FNCs are also plotted as bar plot for visualization purposes. Connectivity pattern look very similar in all FNC types, indicating that in general communication in brain do not differ much in hemispheres, though the strength of communication may differ. Homotopic regions have the highest connectivity strength.**

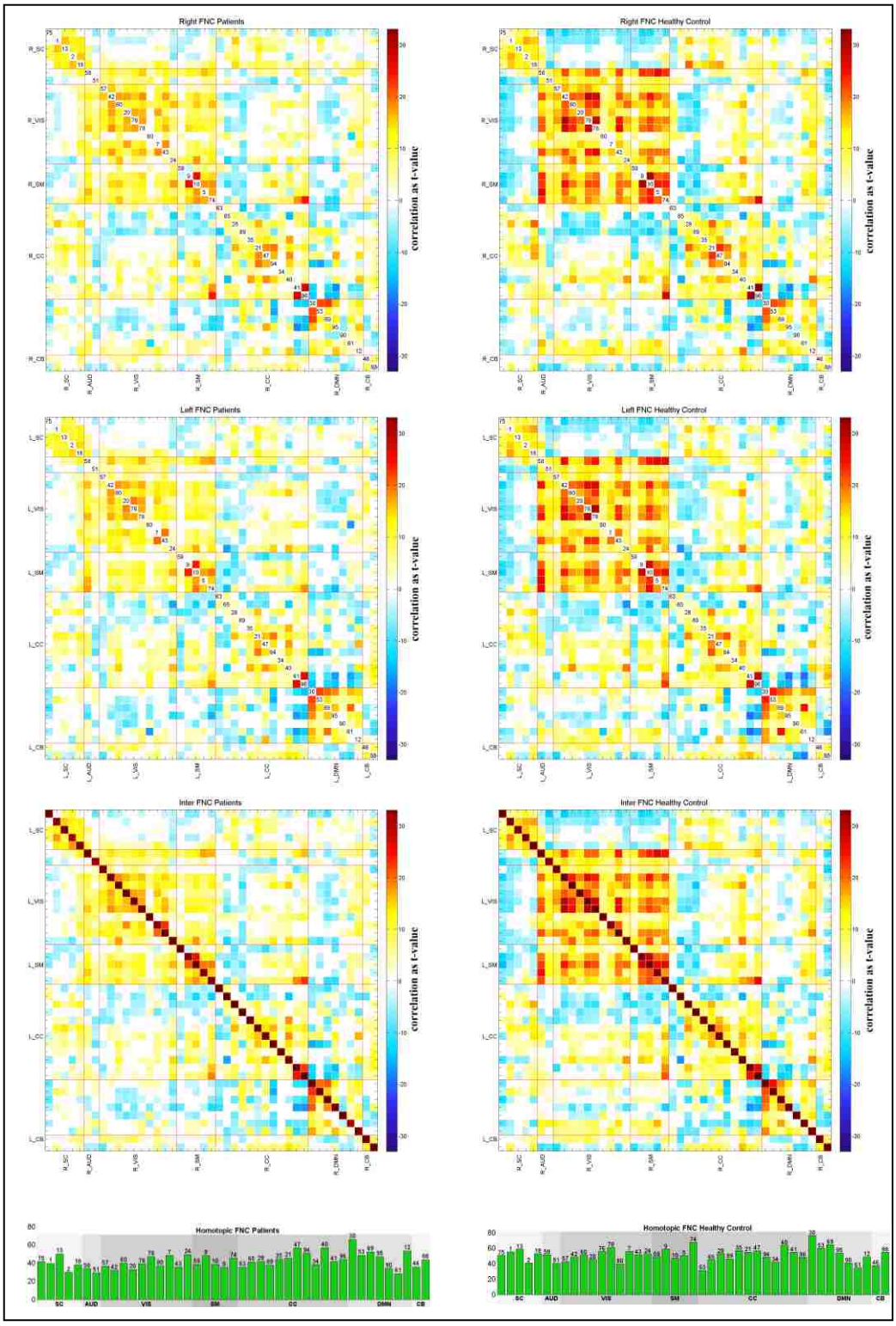


**Figure 4.3 Averages of Patients (left column) and Healthy Control (right column) subgroups for all FNC types (R_FNC, L_FNC and Cross_FNC from top to bottom respectively) are displayed as t-statistics thresholded with 0.01 levels FDR. Homotopic FNCs are also displayed in bar plots for visualization purposes and they have the highest connectivity strength. In all FNC types, we observe diminished connectivity strength in patients.**

### 4.3.2 Results of Connectivity Strength

Results of comparison of connectivity strength between different FNC types are summarized in Table 4.5 and also in Figure 4.4. While comparing L_FNC and R_FNC among healthy controls, we found 614 out of 903 network pairs that are significantly (0.05 levels FDR corrected) connected in both FNCs, and 609 of them have the same sign. By performing a paired t-test on L_FNC and R_FNC magnitudes and correcting with 0.05 levels FDR threshold, we found 135 network pairs exhibiting significant differences, and 93 of them higher in R_FNC having stronger connectivity, while 42 of them higher in L_FNC among 609 previously selected network-pairs. However, in patients, 553 network pairs were significantly connected in both L_FNC and R_FNC, and 549 pairs had same sign and paired t-test revealed 52 network pairs with significant magnitude differences, of which 39 pairs higher in R_FNC while 13 pairs higher in L_FNC.

In comparing L_FNC and Cross_FNC, we analyzed LR (lower triangular) and RL (upper triangular) of the Cross_FNC, separately. Healthy controls and lower triangular 631 pairs out of 903 showed significant connectivity in both L_FNC and Cross_FNC (LR), of which 625 had the same sign. Paired t-tests revealed that 65 regions were in favor of Cross_FNC, while 55 network-pairs were in favor of L_FNC. This number reduced to 556 significantly connected network-pairs, of which 552 had the same sign. Of these, 20 pairs favored Cross_FNC, and 24 of them favored L_FNC. In healthy controls and in upper triangular; 646 pairs out of 903 showed significant connectivity in both L_FNC and Cross_FNC (LR), and 643 of those pairs had the same sign. Paired t-tests revealed 34 network-pairs favoring Cross_FNC, while 64 network-pairs favoring L_FNC. This

number reduced to 567 significantly connected pairs, of which 566 with the same sign, among which 18 pairs favor Cross_FNC, and 36 of them favor L_FNC.

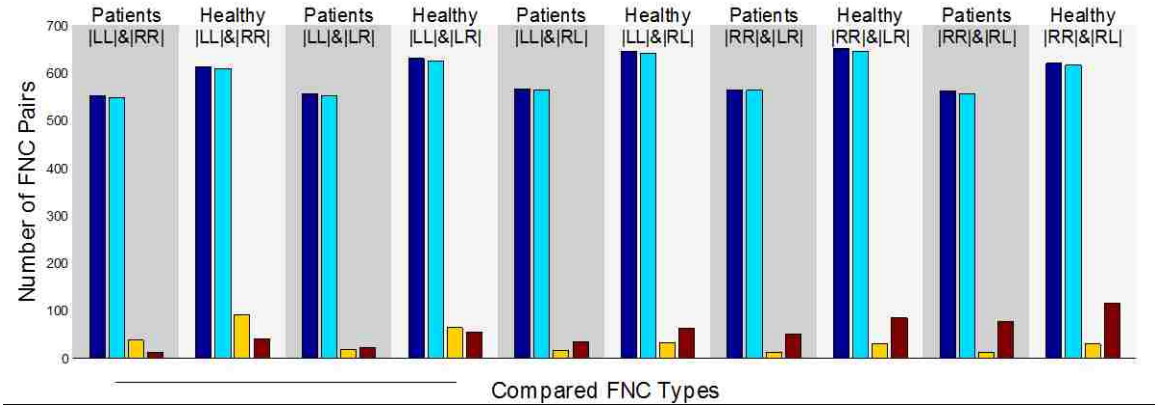


**Figure 4.4: Comparing strength of connectivity in different FNC types for patients and healthy control groups. LL is the L_FNC, RR is the R_FNC, LR is the lower triangular of Cross_FNC, and RL is the upper triangular of Cross_FNC. Dark blue shows the number of regions significant in both of the corresponding FNCs, light blue shows the significant regions with same sign, yellow shows the number of regions having greater connectivity strength in FNC written in first, while red shows the number of regions having greater connectivity strength in FNC written in the second.**

Comparison between R_FNC and Cross_FNC provided a similar pattern; in healthy controls and in lower triangular part of Cross_FNC, 651 pairs out of 903 showed significant correlation in R_FNC and Cross_FNC (LR), of which 645 had the same sign. Paired t-tests revealed 32 network-pairs favoring Cross_FNC, while 86 pairs favoring R_FNC. This number reduced to 566 significantly correlated pairs, of which 564 had the same sign. Of these, 13 pairs favored inter-hemisphere, and 52 favored R_FNC. In healthy controls and in upper triangular part of Cross_FNC, 621 pairs out of 903 showed significant correlation in R_FNC and Cross_FNC (LR), of which 616 had the same sign. Paired t-test revealed 31 pairs favoring Cross_FNC, and 118 pairs favoring R_FNC. This number reduced to 563 significantly correlated network-pairs, of which 557 had the same sign. Of these, 13 pairs favored Cross_FNC, and 78 of them favored L_FNC.

**Table 4.5: Comparing Strength of different FNC types in patients and healthy control separately. For all pairs, we see a lack of asymmetries in patients comparing to healthy control. Also, right hemisphere interact with itself more comparing to left hemisphere and, also right hemisphere has more strength in communication with itself comparing inter hemispheric interaction.**

| **Comparing Intra Left and Intra Right** | | |
|---|---|---|
| | **Patients** | **Healthy Control** |
| | **# of Region** | **# of Regions** |
| **Significant in both** | 553 | 614 |
| **Significant and same sign** | 549 | 609 |
| **Intra Left<Intra Right significant** | 39 | 93 |
| **Intra Left>Intra Right significant** | 13 | 42 |

| **Comparing Intra Left and Inter Hemisphere (LR)** | | | **Comparing Intra Left and Inter Hemisphere (RL)** | | |
|---|---|---|---|---|---|
| | **Patients** | **Healthy Control** | | **Patients** | **Healthy Control** |
| | **# of Regions** | **# of Regions** | | **# of Regions** | **# of Regions** |
| **Significant in both** | 556 | 631 | **Significant in both** | 567 | 646 |
| **Significant and same sign** | 552 | 625 | **Significant and same sign** | 566 | 643 |
| **Intra Left<Inter Hemisphere** | 20 | 65 | **Intra Left<Inter Hemisphere** | 18 | 34 |
| **Intra Left>Inter Hemisphere** | 24 | 55 | **Intra Left>Inter Hemisphere** | 36 | 64 |

| **Comparing Intra Right and Inter Hemisphere (LR)** | | | **Comparing Intra Right and Inter Hemisphere(RL)** | | |
|---|---|---|---|---|---|
| | **Patients** | **Healthy Control** | | **Patients** | **Healthy Control** |
| | **# of Regions** | **# of Regions** | | **# of Regions** | **# of Regions** |
| **Significant in both** | 566 | 651 | **Significant in both** | 563 | 621 |
| **Significant and same sign** | 564 | 645 | **Significant and same sign** | 557 | 616 |
| **Intra Right<Inter Hemisphere** | 13 | 32 | **Intra Right<Inter Hemisphere** | 13 | 31 |
| **Intra Right>Inter Hemisphere** | 52 | 86 | **Intra Right>Inter Hemisphere** | 78 | 118 |

Overall, in both patients and healthy controls, we observe the right hemisphere to be more connected with itself than the left hemisphere is with itself, and the right

hemisphere is also more connected with itself than it is connected with the left hemisphere. The left hemisphere seems to be connected with the other hemisphere and itself in a balanced way, although slightly more connected with itself. However, we observe a decrease in asymmetry in schizophrenia patients, suggesting that patients have lack of hemispheric connectivity dominance that may be associated with healthy mental functioning.

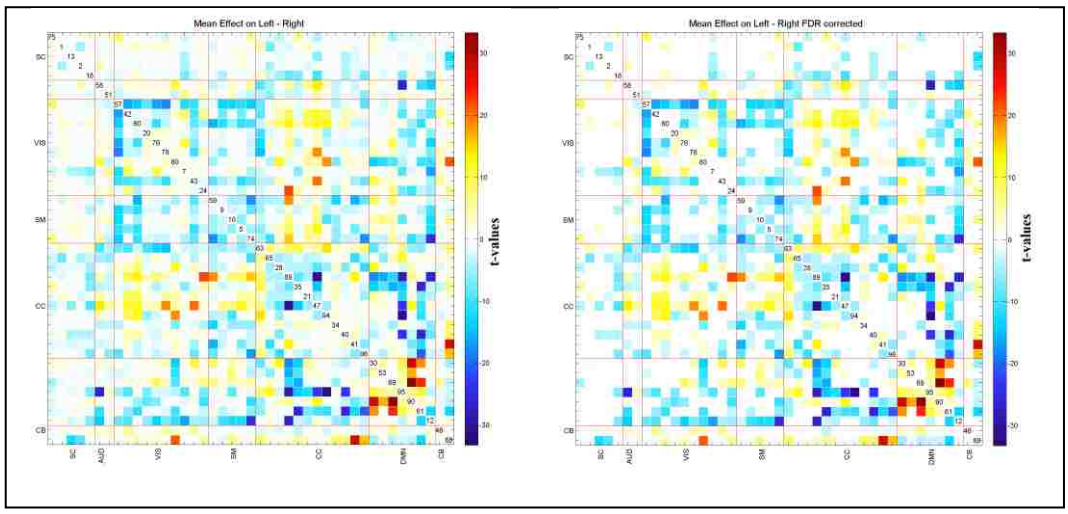


**Figure 4.5: Paired t-test (L_FNC minus R_FNC) results in – *log10(p-value)*sign(beta)* format to compare left and right FNC, corrected with 0.05 levels FDR. A lot of networks pairs exhibit significant differences, mostly suggesting right hemisphere having more connectivity strength.**

### 4.3.3 Results of Regression Analysis

The differences between intra-left and intra-right FNC matrices are presented in Figure 4.5, where a lot of network-pairs show significant differences (0.05 levels FDR corrected). In almost all network-pairs, we observe higher absolute connectivity strength in the right hemisphere (both positive and negatively correlated), besides the intra-default mode which has higher connectivity strength in L_FNC. Almost all networks in the most correlated functional domains, e.g., intra-visual, intra-sensorimotor, intra-default mode, and visual to sensorimotor networks, show higher connectivity strength in the right

hemisphere. Intra-cognitive control has higher positive correlation between most of its network pairs, and higher anti-correlation with its constituent anti-correlated network IC 63 (fusiform gyrus) in the right hemisphere relative to left hemisphere.

Regression analysis results on L_FNC and R_FNC differences for diagnosis, age and gender effects are displayed in Figure 4.6. There are significant differences between L_FNC and R_FNC, mostly suggesting diminished hemispheric differences in patients. Age and gender have significant effects on left-right differences in only two pairs, suggesting that age and gender have similar patterns of intra-hemisphere connectivity. Handedness, cognitive scores, positive and negative symptoms scores do not have any significant effects (after 0.05 levels FDR correction) on the L_FNC - R_FNC difference.

The effects of diagnosis are presented in Figure 4.7 for all FNC types. Pattern-wise, schizophrenia affects all FNC types similarly: intra-auditory, visual and sensorimotor networks are those networks that exhibit the largest connectivity decrease in patients, consistent with the conventional results (Damaraju et al., 2014).

Age effects on the three FNC types are presented in Figure 4.8, with increasing age mostly causing a decrease in correlations, particularly among visual networks and sensorimotor networks. Cognitive control networks show both increases and decreases in correlation with increasing age. Homotopic network correlation also shows decrease with increasing age in almost all networks; only one sensorimotor network exhibits increase in connectivity with aging, though the effect is not significant. This is consistent with Zuo et al. (2010b), who found a decrease in homotopic connectivity in all regions but sensorimotor in their voxel mirrored homotopic connectivity study.

We also checked the effect of gender, handedness, and cognitive scores on FNC values; our analysis indicated that gender is not a factor affecting any FNCs.

Figure 4.9 presents the results. IC 74 seems to have the widest differences on the correlations with visual, auditory and sensorimotor networks. Handedness, cognitive scores, positive and negative symptoms scores do not have any significant effects (after 0.05 levels FDR correction) on any of the FNC types.

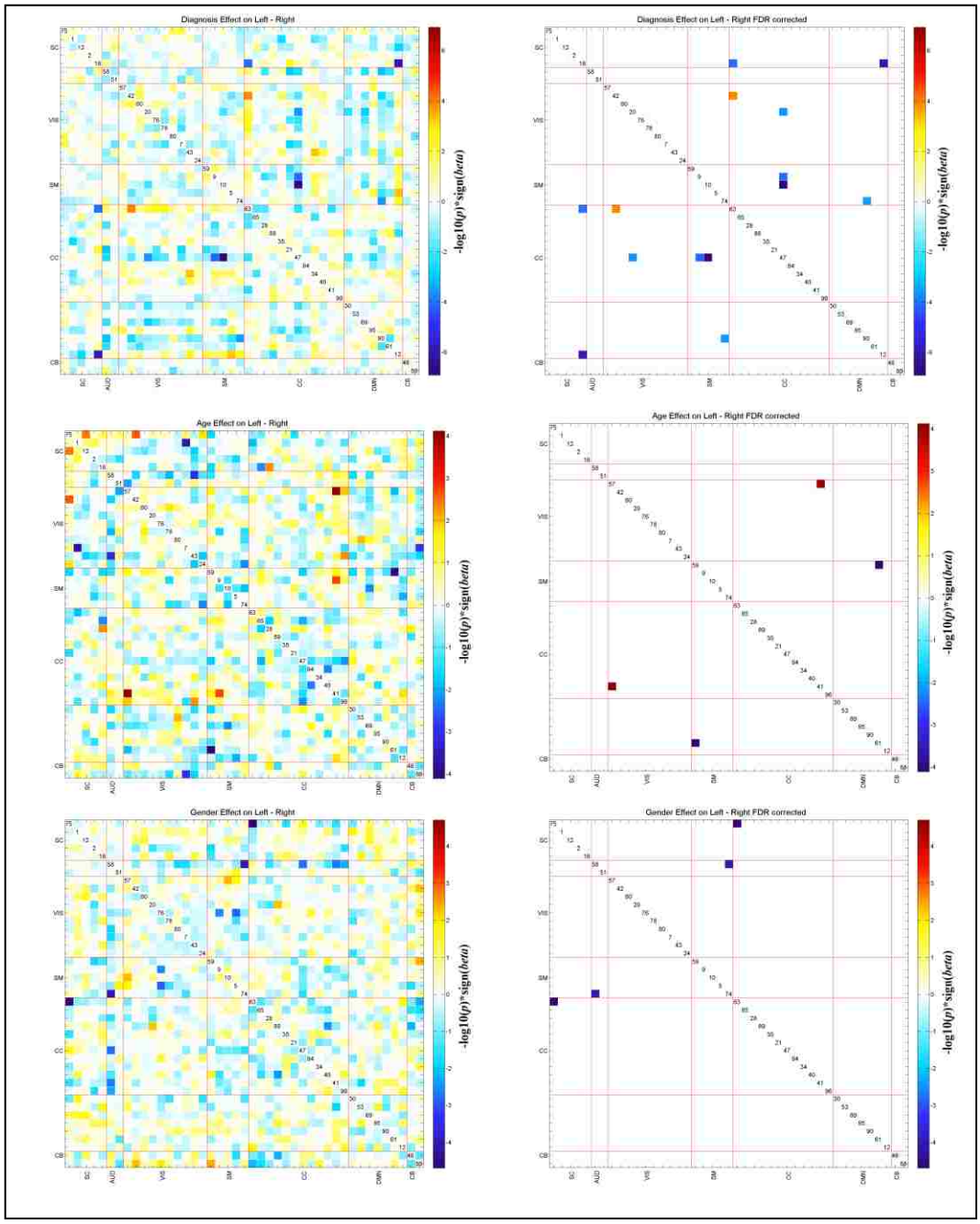


**Figure 4.6: Regression results of age, gender and diagnosis effects on L_FNC and intra R_FNC, presented in – *log10(p-value)*sign(beta)* format. With a cross check with on the mean L_FNC and R_FNC differences (Figure 4.5) lads the observation that patients have diminished left and right connectivity differences, consistent with our findings in comparing connectivity strength. Age and gender seems to affecting both FNCs in similar ways.**

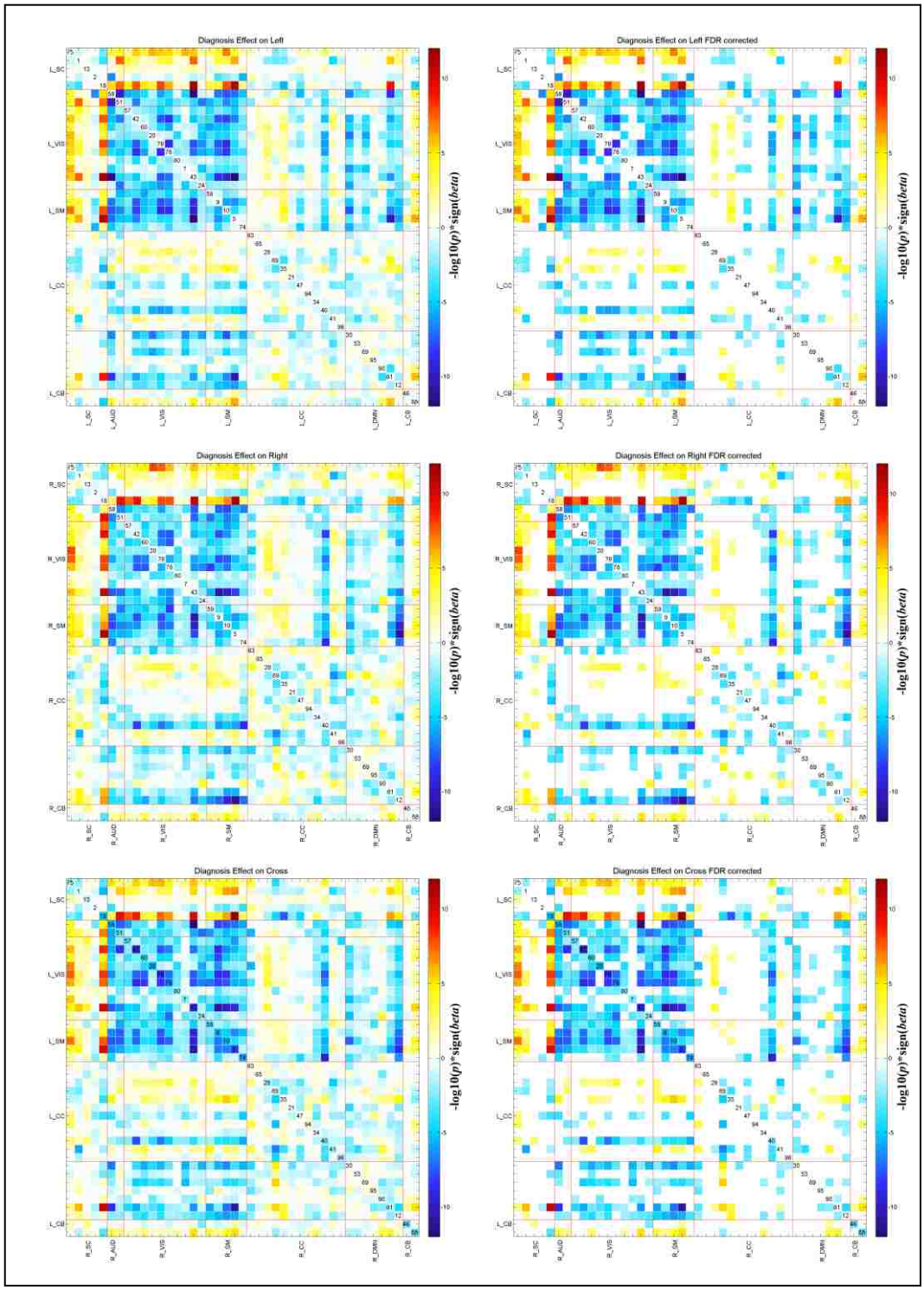


**Figure 4.7: Schizophrenia effect on all FNC types, displayed as – *log10(p-value)*sign(beta)* format (at left column); after 0.05 levels FDR correction (at right column). General patterns look similar, for almost all pairs patients have weaker connectivity. Especially, highly positively connected regions auditory, visual, sensorimotor networks show less connectivity in patients.**

#### 4.3.3.1 Effects of Cognitive Scores, Symptom Scores and Mean Antipsychotic Dose

We checked whether the cognitive scores contributed significantly to affect hemisphere-specific FNCs by using a separate regression model with parameter cognitive scores.276 subjects that the CMINDS scores available were used in this analysis. Our analysis revealed no significant effect of cognitive scores on hemisphere-specific FNCs or the left-right difference FNCs. The analysis was repeated by including age, gender, diagnosis, handedness, motion and cognitive scores to the model, and cognitive scores did not reveal any significant effect in that bigger model either.

We also checked if there exist a relationship between PANSS and hemisphere specific FNCs. We analyzed the effect of scores using a regression model including parameter PNASS (positive and negative scores in separate analysis) using 148 subjects. Results did not indicate any significant relationship between hemisphere-specific FNCs or in left-right difference FNCs. The analysis was repeated by including age, gender, handedness, cognitive scores, motion and symptoms scores to the model, but did not reveal any significant effect in the larger model either.

Finally, we checked if the mean antipsychotic dose has an effects on the hemisphere specific FNCS. 129 out of 151 patients have the mean antipsychotic dose were included. We analyzed the effects of the mean antipsychotic dose using a regression model including CPZ values as a parameter. Results did not indicate any significant relationship between hemisphere-specific FNCs or in left-right difference FNCs. The analysis was repeated by including age, gender, handedness, cognitive scores, motion and symptoms scores to the model, did not reveal any significant effect in the larger model either. The

general pattern of the results did not change; therefore we kept the analysis without CPZ values for simplicity.

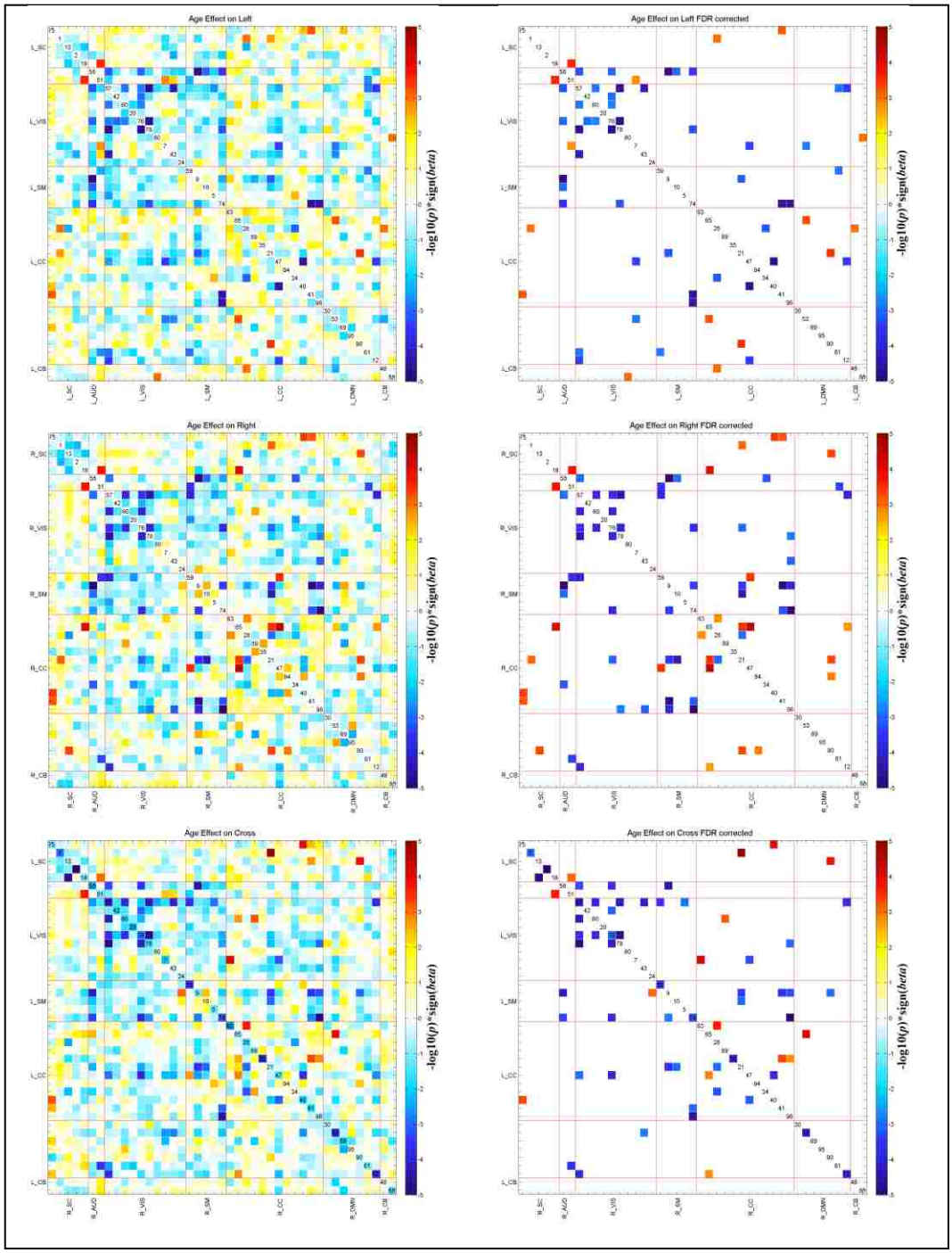


**Figure 4.8: Age effect on all FNC types, displayed as – *log10(p-value)*sign(beta)* format (at left column); after 0.05 levels FDR correction (at right column). General patterns look similar, network pairs have weaker connectivity with increasing age. Especially, visual, sensorimotor networks diminished connectivity in elders, homotopic network pairs also show a decrease with increasing age.**

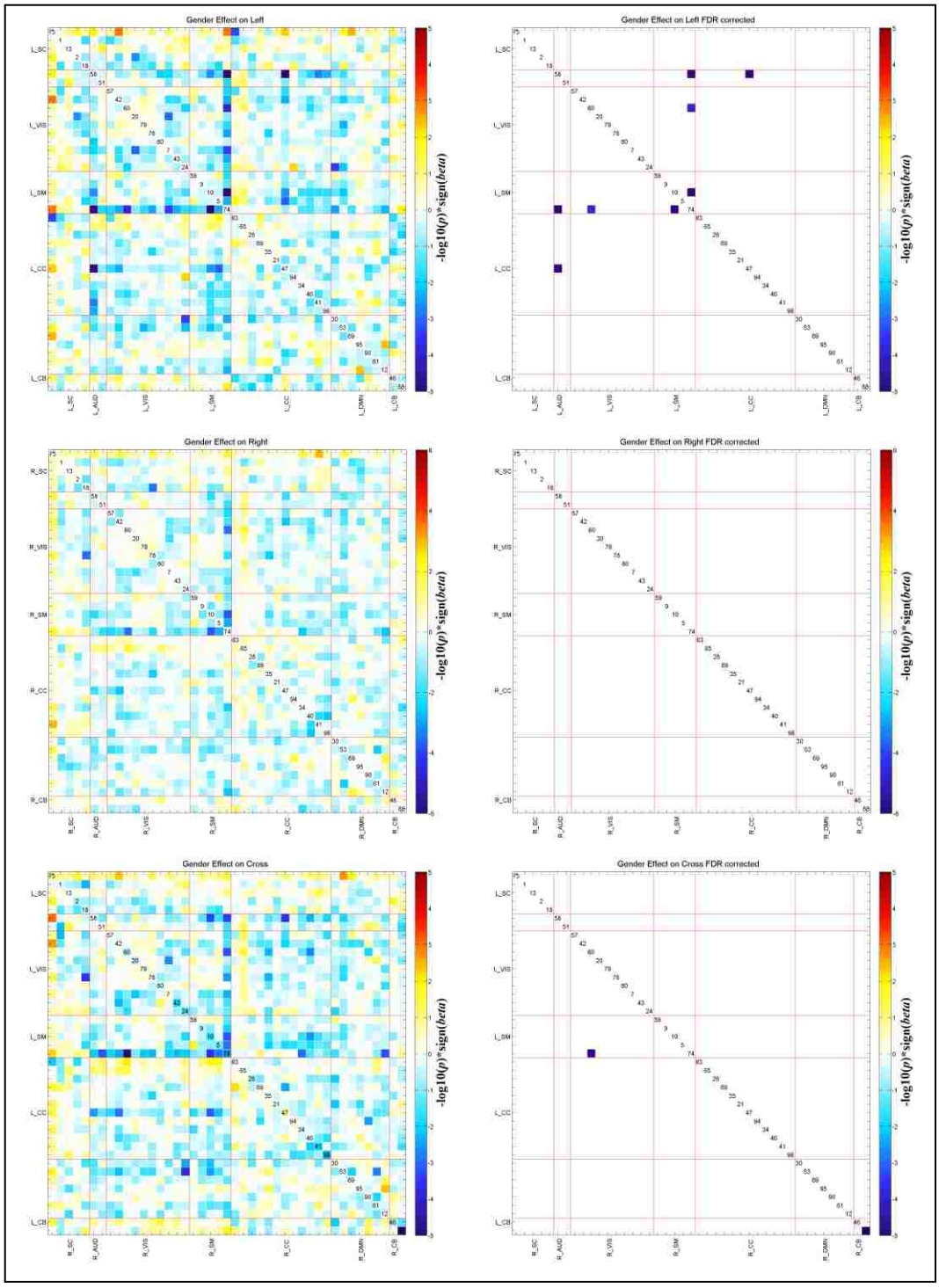


**Figure 4.9: Gender effects on all FNC types, displayed as – *log10(p-value)*sign(beta)* format (at left column); after 0.05 levels FDR correction (at right column). Gender is not a significant factor affecting FNCs, we do not have any significances besides the sensorimotor regions in.**

## 4.4 Discussion

We proposed an approach based on gICA to investigate the functional network connectivity within and between cerebral hemispheres. We also used this approach to study the hemispheric FNC differences between schizophrenia patients and healthy controls, and also investigated the effects of age, gender and handedness on hemispheric FNC. We found that in all FNC types, L_FNC, R_FNC and Cross_FNC, schizophrenia patients have diminished connectivity strength (both in positive and negative) relative to healthy controls. We also found pronounced connectivity strength differences between intra-left and intra-right FNCs, and between intra-hemisphere and inter-hemisphere, in healthy controls relative to the schizophrenia patients. So although the general pattern of schizophrenia effects in all three FNC types are mutually consistent and consistent with schizophrenia effects on conventional whole brain FNC (Damaraju et al., 2014), our analysis offers evidence of diminished connectivity strength asymmetry in schizophrenia patients. Both laterality and connectivity have been shown to be abnormal in schizophrenia (Hoptman et al., 2012; Swanson et al., 2011). Our analysis addresses the intersection between these areas of inquiry.

Our analysis of homotopic regions reveals that homotopic regions have much higher connectivity strengths than heterotopic regions. Gee et al. (2011) also found significantly higher connectivity strength in homotopic regions comparing to heterotopic regions in their atlas based study. Gee et al. (2011)ranked the homotopic regions according to connectivity strength and found an inverse relationship with the Euclidean distance of homotopic regions and their connectivity strength.

We also found significant within-hemisphere connectivity magnitude differences favoring the right hemisphere, suggesting that the right hemisphere is more tightly functionally calibrated (both in terms of phase alignment and anti-alignment) than the left hemisphere. Previous results on hemisphere-specific connectivity have been mixed: our findings are consistent with several other studies showing higher connectivity strength in the right hemisphere (Ribolsi et al., 2014), but run counter to findings of stronger intra-left connectivity (Gotts et al., 2013) and studies (Gee et al., 2011) that found no significant intra-hemispheric connectivity differences.

Regression analysis on L_FNC and R_FNC differences indicated that several functional networks including visual, sensorimotor and cognitive control showed higher connectivity strength in right hemisphere, default mode network shows higher connectivity strength in left hemisphere. Effects of diagnosis on the differences suggest that in patients, the differences are smaller, especially connectivity involving cognitive control networks, which is consistent with lack of lateralization in patients. Age and gender do not exhibit strong effects on the intra-hemisphere connectivity differences, which is consistent with our findings in Chapter 5 with the 4D domain analysis.

Separate regression analyses on whole-brain, hemisphere-specific, and cross-hemisphere-FNC types all reveal very similar patterns for age and gender. In all FNC types, a decrease in connectivity strength with increasing age is observed, which is consistent with Allen et al. (2011) that used a larger dataset consisting only of health participants, and no major differences are observed between females and males.

### 4.4.1 Limitation

We should consider some limitations regarding interpreting the results. Firstly, we do not have the information about some domains such as working memory of subjects during the scanning process. Also, schizophrenia patients were under medication with antipsychotics, which could potentially confound the results even though analysis using mean antipsychotic dose did not reveal any significant effects. Though our subjects are ranging from age 18 to 60, they do not cover the most rapidly changing ages of childhood, also subjects are not balanced in gender (83 females, 231 males). Moreover, we focused on the resting state networks extracted from a previous study that has ICA model order of 100 for comparison purposes, but it would also be interesting to evaluate hemisphere specific FNCs with higher and lower model orders. Even though we used a large sample size, the subjects were scanned for a minimum of 5 minutes 12 seconds (162 volumes); this may limit the sensitivity detection of the effects.

## 4.5 Conclusion

In summary, we propose a gICA based approach to calculate hemisphere-specific time-courses and analyzed hemisphere-specific FNC differences in a resting-state fMRI dataset balanced between schizophrenia patients and healthy controls. We found diminished connectivity strength in patients in all FNC types. A distinctive finding that has emerged from our hemispheric FNC analysis is that schizophrenia patients exhibit a significant reduction in hemispheric functional asymmetry. We also found that hemisphere-specific FNCs preserve the general connectivity patterns seen in conventional whole-brain FNC. Moreover, effects of schizophrenia distribute over intra-hemisphere and inter-hemisphere FNCs as much as they do over whole-brain FNC. Our

analysis combines two streams of resting state-fMRI research: lateralization of functional networks and functional network connectivity. This analysis has allowed us to extend and synthesize results of several previous studies tying schizophrenia to both abnormal network laterality and abnormal network connectivity. In future work, investigating hemisphere specific FNCs in a dataset containing unmedicated schizophrenia patients, and covering the full age range would help further interpret the results.

# Chapter 5 : Increased spatial granularity of left brain activation and unique age/gender signatures: A 4D Frequency Domain Approach to Cerebral Lateralization at Rest

## 5.1 Motivation

Cerebral lateralization is a well-studied topic; however most of the research to date in functional magnetic resonance imaging (fMRI) has been carried out on hemodynamic fluctuations of voxels, networks, or regions of interest (ROIs). For example, cerebral differences can be revealed by comparing the temporal activation of an ROI in one hemisphere with the corresponding homotopic region in the other hemisphere. While this approach can reveal significant information about cerebral organization, it does not provide information about the full spatiotemporal organization of the hemispheres. The cerebral differences revealed in literature suggest that hemispheres have different spatiotemporal organization in the resting state. In this study, we evaluate cerebral lateralization in the 4D spatiotemporal frequency domain to compare the hemispheres in the context of general activation patterns at different spatial and temporal scales. We use a gender-balanced resting fMRI dataset comprising over 600 healthy subjects ranging in age from 12 to 71, that have previously been studied with a network specific voxel-wise and global analysis of lateralization in Chapter 3.

## 5.2 Introduction

There has been a considerable amount of work studying the differences between cerebral hemispheres of the brain tasks (Agcaoglu et al., 2014; Breier et al., 1999; Broca, 1861; Cai et al., 2013; Clements et al., 2006; Filippi et al., 2013; Gobbele et al., 2008; Gotts et

al., 2013; Groen et al., 2012; Liu et al., 2009; Mazoyer et al., 2014; Nielsen et al., 2013; Smith et al., 1996; Sperry, 1974; Stephan et al., 2003; Swanson et al., 2011; Thomason et al., 2009; Wernicke, 1874; Zhu et al., 2014; Zuo et al., 2010b). These studies have helped us understand brain laterality and revealed interesting results; however all of these studies have approached lateralized brain function through either global measures of lateralized connectivity or comparison of hemodynamic activity in homotopic regions or voxels of the two hemispheres.

There has been some consideration of temporal frequencies in fMRI. For example, Garrity et al. (2007) showed that schizophrenia patients have significantly more spectral power at high temporal frequencies (0.08 Hz to 0.24 Hz) and significantly less spectral power at low temporal frequencies in the default mode network comparing to healthy control and indicated that temporal frequencies of the default mode network could be used to distinguish schizophrenia patients from healthy controls. Some other studies focused on amplitude of low frequency fluctuations (ALFF) (0.01- 0.08 Hz), for example Yang et al. (2007) revealed ALFF differences in resting state between eyes open and eyes close conditions, (Calhoun et al., 2011; Hoptman et al., 2010; Turner et al., 2012; Yu et al., 2013) found altered ALFF differences between schizophrenia patients and health control, consistent with Miller et al. (2015) that investigated effects of schizophrenia, age and gender in the 4D frequency domain environment. Zhang et al. (2010) investigated laterality of mesial temporal lobe (mTL), in their ALFF study that mainly focused on unilateral mTL epilepsy patients. However, to our knowledge (with the exception of Miller et al. (2015)), there have been no efforts to study spatial and temporal frequencies together in a 4D domain.

Though the brain is not organized periodically, the spatiotemporal hemodynamic patterns can, like all signals, be decomposed into additive (in this case 4-dimensional) periodic components. Our work indicates that the periodic constituents of resting state fMRI data contains interesting spatiotemporal patterns that differ between the hemispheres. Recently, we, (Miller et al., 2015) , proposed a 4D frequency domain approach that considers the whole brain fMRI scan as a single 4D signal. A 4D approach reveals the global organizational differences between hemispheres while simultaneously accounting for temporal changes. This combined spatiotemporal information provides a broader perspective relative to conventional temporal spectral analysis. Since we are working with the amplitude spectra, such an approach allows us to consider patterns of change in brain imaging data which have similar spatiotemporal frequency content but which may have different delays or spatial locations. It thus provides a rather different, yet complementary, way to view the underlying resting fMRI information in contrast to typical approaches which focus on specific networks or solely focus on spectral information in the time domain.

There are well-known hemispheric differences in measures such as complexity, interaction, connectivity, intrinsic activity (Agcaoglu et al., 2014; Gotts et al., 2013; Liu et al., 2009; Nielsen et al., 2013),therefore, we were interested in evaluating whether the frequency characteristics vary in the left versus right hemisphere. To this end, we employ a 4D frequency domain approach to study cerebral lateralization. We treat left and right hemisphere fMRI scans as 4D signals and explore group-level differences in general spatiotemporal patterning of hemodynamic activation between left and right hemispheres. Results show strong and persistent differences in spatiotemporal power in left versus

right hemisphere such that the left hemisphere is more dominant for high spatial frequencies while the right hemisphere is more dominant for low and middle spatial frequencies. These differences may indicate that the left hemisphere processes information in various small regions intensely while the right hemisphere tends to process information on a substrate of broader more diffuse spatial patterns. To the best of our knowledge, this is the first study that investigates cerebral lateralization in the 4D spatiotemporal domain.

## 5.3 Methods and Materials

A summary of the data processing is presented in Figure 5.1.

### 5.3.1 Dataset

We used the same exact dataset used in Chapter 3, with almost same preprocessing pipeline. The only difference is that in this study, no spatial smoothing was applied to the data. Please see Sections 3.2.1-3.2.3 for the details of the dataset.

### 5.3.2 Extracting Hemispheres

A common, symmetric, group-mask was used for all subjects to ensure the masking did not add subject variance to the spatiotemporal profile. Next, we divided the 4D fMRI data into left and right hemispheres. We also flipped the right hemisphere data along the left-right dimension to have an exact coordinate match with the other hemisphere, which provided data for each hemisphere for each subject.

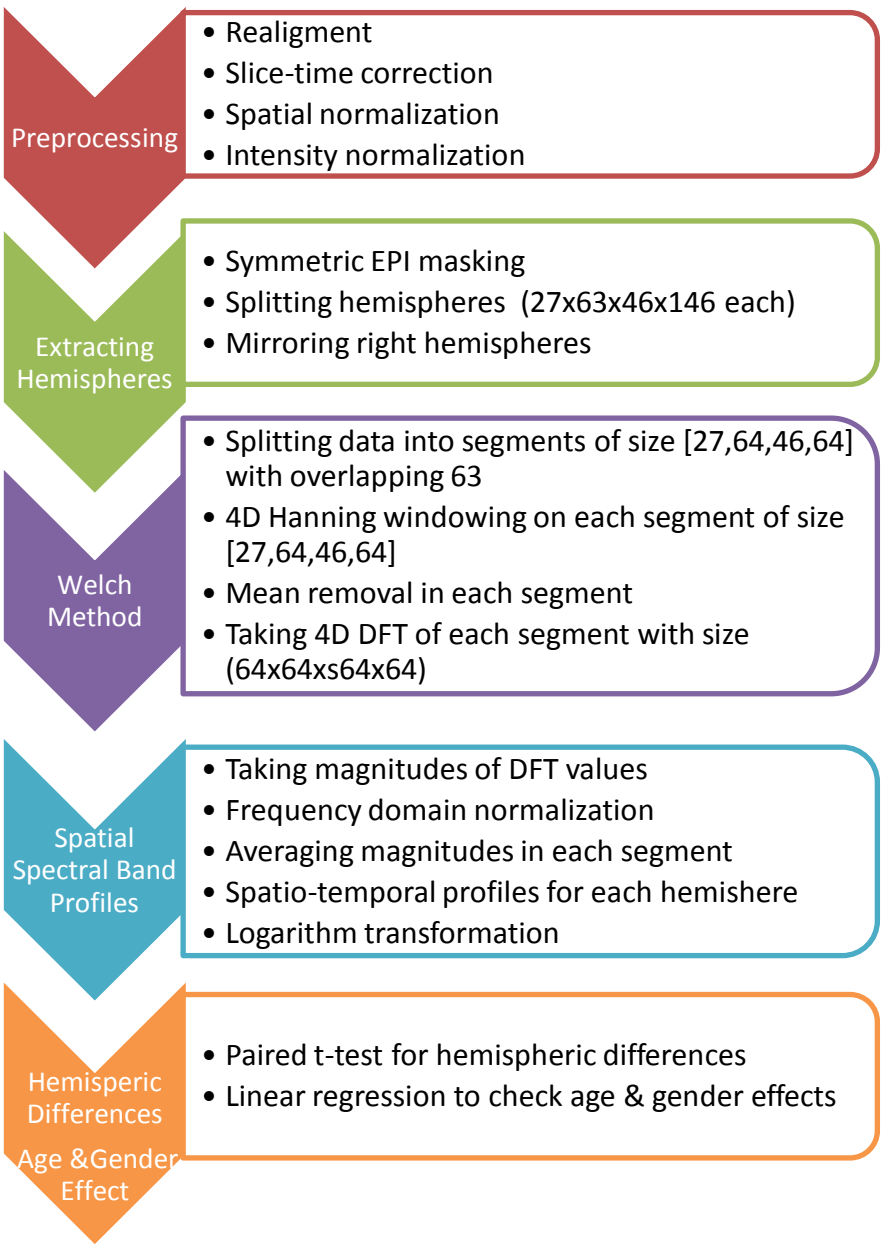


**Figure 5.1: Flowchart of data processing.**

.

### 5.3.3 Transforming to Frequency Domain

We used the Welch' method to estimate power spectral density of 4D fMRI data(Welch, 1967). To do so, we applied sliding windows on data with a 4D Hanning window of size [27, 64, 46, 64] and shifted 1 point each time. We removed the mean on each data segment and implemented an n-dimensional discrete Fourier transform using Matlab's fftn.m function. In order to maintain the same scale of spatial frequencies across x, y, and z, we used a transform size of [64, 64, 64, 64] on the [27, 63, 46, 64] sized data segments. The result is a 4 dimensional array for each segment; we used the squared magnitudes of the Fourier coefficients. The squared magnitudes are divided into (64*64*64*64) in order to equalize frequency domain power to time domain power (Perceval's theorem). Next, the magnitudes were normalized so that each subject and each hemisphere and each segment has the same total power. This normalization enables us to compare the distribution of the power in spatiotemporal frequencies among subjects. Finally, we average over each segment to estimate PSD of each subject's hemispheres.

### 5.3.4 Spatial Spherical Band Profiles (SSBPs)

In order to further reduce the dimensionality and provide an intuitive display; for each temporal frequency, we group the spatial frequencies from low to high into 32 spherical frequency bands and sum the squared magnitudes in each group. By doing so, for each subject and each hemisphere, we have a matrix of size 32 (temporal frequencies) by 32 (spatial frequencies). Finally, a logarithm transformation (log10) was applied to the SSBPs. We called this matrix the spatial spherical band profiles (SSBPs). In the equation form, the calculation of the SSBPs is given by:

$$\sigma_{(i,j)} = \log\left(\sum_{x_i,y_i,z_i \in \Phi_i} \tilde{f}\,(x_i,y_i,z_i,j)\right)$$

Where $\Phi_i$ is the $i^{th}$ spherical band $\left(i^{th}\text{spherical shell}\right)$and $x_i, y_i$, and $z_i$ are the indices that define the spherical band in 3D spatial spectrum, $\tilde{f}$ is the normalized 4D spectrum, $\sigma$ is the SSBP.We used 32 spherical shells with 1 unit thickness to cover the all 3D spatial frequencies, the mathematical definition of the spherical bands in the frequency domain are given below:

$$r_{h-32} = (h-33)^2 + (h-33)^2 + (h-33)^2 \text{ for } 33 \leq h \leq 64$$

where [33, 33, 33] represent the 0 spatial frequencies in [64x64x64] spatial frequency domain and $r_i$ represents the 32 different diameters of the spherical shells.

$$(x_i, y_j, z_k) \in \Phi_t$$

$$\text{if } \min\left\{\left|(x_i-33)^2 + \left(y_j-33\right)^2 + (z_k-33)^2 - r_t\right|\right\} \text{ is for } r_t$$

### 5.3.5 Paired t-test

We tested left and right hemisphere SSBPs differences with a paired t-test (left minus right) thresholded at $p< 0.01$ corrected for multiple comparison via a false discovery rate (FDR) correction (Genovese et al., 2002).

### 5.3.6 Modeling Age and Gender Effects

We also tested age and gender effects on the spatiotemporal organization using a linear regression model. Explanatory variables included *age* and *gender*. We also included motion covariates average scan to scan rotation, translation from INRIAlign motion estimates and also spatial normalization accuracy, which is the Spearman correlation between the warped T2*-weighted image and the EPI template, in the regression model and since results were very similar with and without motion variables, we present the results without motion covariates for the sake of simplicity.

$$\sigma_{(i,j)} = \beta_{o} + \beta^{(i,j)}_{age} X_{age} + \beta^{(i,j)}_{gen} X_{gen} + \varepsilon_{(i,j)}$$

Where $X_{gen}$ is a number indicating the gender of subject with 2 for males and 1 for females. The age ($X_{age}$) distribution ranges from 12 to 71, but it is right skewed with only 7 people older than 50 years, therefore we applied a logarithm transform to age, where $X_{age}$ represents the log transformed age of the subject. All β's are the parameter of the regression model with ε being the error parameter for the model, $\sigma_{(i,j)}$ is the combined SSBPs. This analysis gives us the regions on the SSBPs that are significantly ($p<0.01$, following FDR correction for multiple comparisons) affected by age and gender (Genovese et al., 2002).

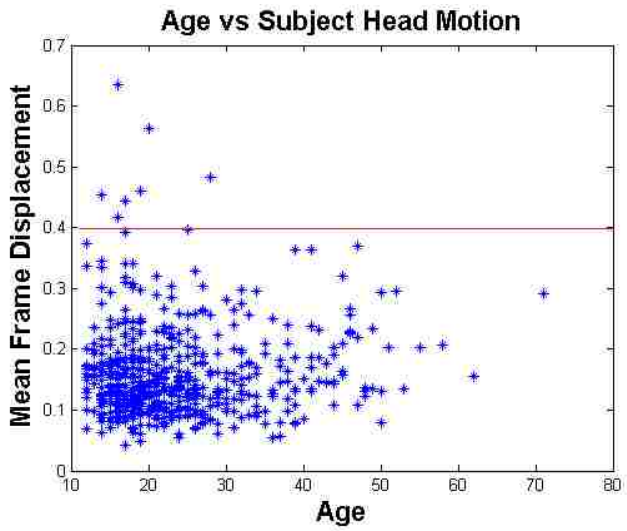


**Figure 5.2: Subject mean frame displacement versus age is presented, while there are a few more higher mean framewise displacement subjects at the younger ages, repeating the analysis with a subset of 503 subjects whose mean frame displacements less than 0.4 mm, revealed similar results with the full analysis.**

### 5.3.7 Age Effects on Subjects Movement

Generally, in fMRI, subjects with younger ages move more comparing to older adults. Figure 5.2 shows age versus mean frame displacement calculated as total absolute displacement in all dimensions. While there are a few more higher mean frame wise displacement subjects at the younger ages, repeating the analysis with a subset of 503 subjects whose mean frame displacements less than 0.4 mm, revealed similar results with the full analysis.

## 5.4 Results

Our analysis provides insight into the spatiotemporal organization of the hemispheres while revealing the differences between the hemispheres, and age and gender effects on this spatiotemporal organization. Group summaries of the spatiotemporal organization for each hemisphere are shown in Figure 5.3a and Figure 5.3b; units are decibel-Watt due to log transformation. Visual inspection indicates similar spatiotemporal trends of activation for both hemispheres, though some differences can easily be recognized. We observe the

highest power in low spatial and low temporal frequencies, though zero temporal and zero spatial frequency (index [1,1]) has no power due to the mean removal. We have sharp borders from temporal frequencies 0.008 (index 2) Hz to 0.016 (3rd index) Hz and spatial frequencies from 0 (1st index) cycles/mm to 0.005 (2nd index) cycles/mm. Overall variance is small in most of the low spatial frequencies. Generally power decreases as spatial or temporal frequencies increases. We also find significant gender and age effects in both hemispheres consistent with (Miller et al., 2015) which analyzed a different dataset but did not evaluate lateralization.

### 5.4.1 Hemispheric Differences

Paired t-test results for left hemisphere SSBPs and right hemisphere SSBPs are displayed in Figure 5.3c and Figure 5.3d. Frequencies shows significant (0.01 levels FDR corrected) differences between two hemispheres. Left hemisphere has more power in high spatial and low temporal frequencies comparing to right hemisphere. On the other hand, the frequencies favor right hemisphere occupies a larger area that covers low and middle spatial and almost all temporal frequencies.

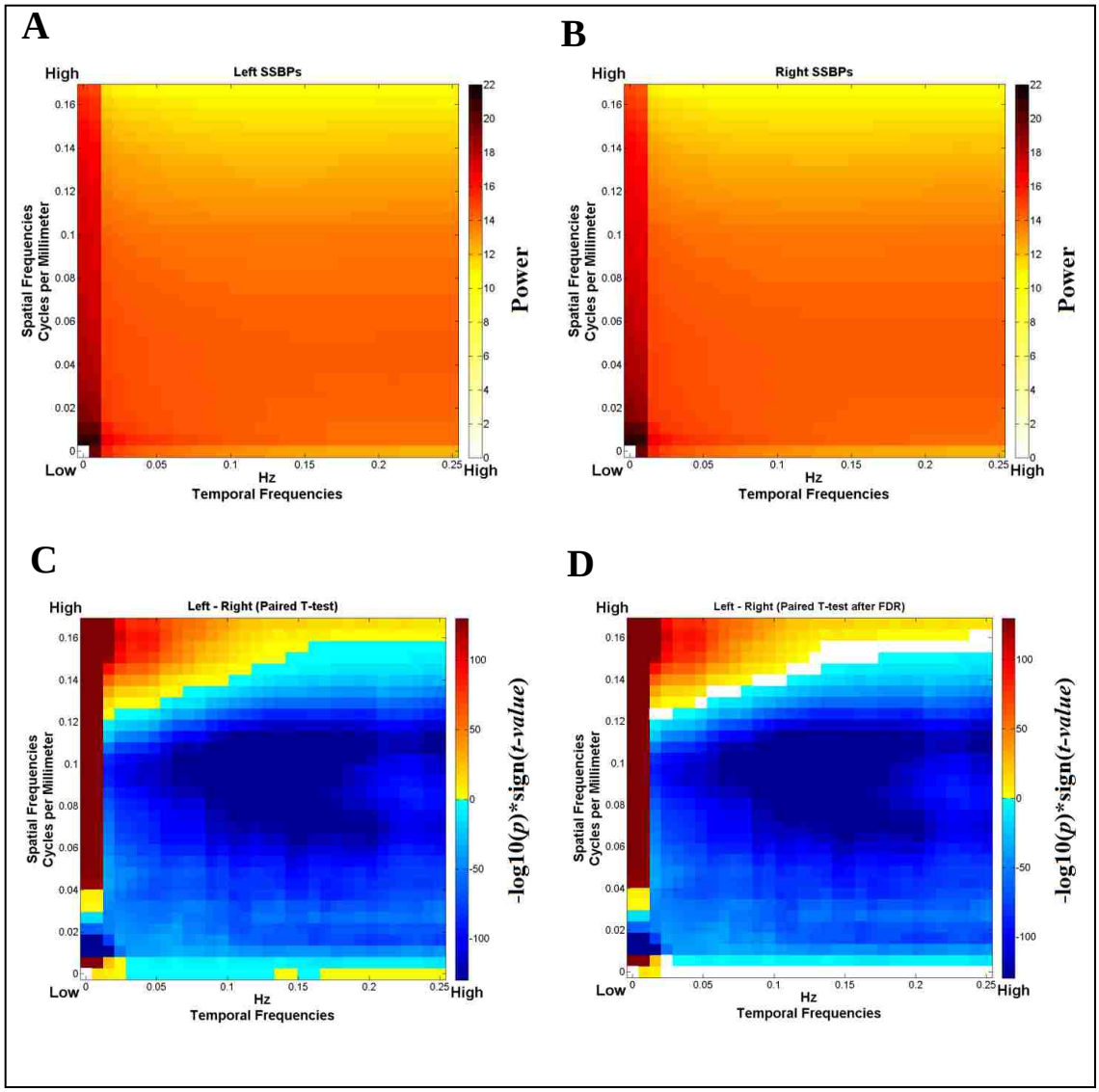


**Figure 5.3: Group averages of hemisphere SSBPs (A & B) and paired t-test result of comparison (C & D) are presented, In each image; left bottom represents the low temporal and low spatial frequencies; on the x-axis from left to right, temporal frequencies increase from 0 Hz to 0.25 Hz; on the y-axis from bottom to top, spatial frequencies increases from 0 cycles/mm to 0.17 cycles/mm. Left hemisphere (A) and Right hemisphere (B) displayed in log10 format (unit is decibel-Watt). Paired t-test results for hemisphere SSBPs, values are plotted as – *log10(p-value)*sign(t-statistic)* (C) and after 0.01 levels FDR correction (D). Red color represents the spatiotemporal frequencies bands favoring left hemisphere, while blue color represents the frequency bands favoring right hemisphere. Overall, regions favoring right hemisphere occupies a larger area and includes low and middle spatial frequencies, left hemisphere has more power in high spatial frequencies.**

### 5.4.2 Age Effects

Regression result for age effects for both left and right hemispheres are presented in Figure 5.4. Age effects are very similar for both hemisphere and a separate analysis did not reveal any significant interaction effects of hemisphere and age, indicating that

spatiotemporal organization of hemispheres is affected by aging similarly. We mainly see three regions that have reverse directional age effects and the border is mostly determined by temporal frequencies. The first region covers very low temporal frequencies (lower than 0.016 ($3^{rd}$ index) Hz) and almost all spatial frequencies (except very low and very high spatial frequencies) and shows an increase in power with aging. The second region contains almost all spatial frequencies and temporal frequencies from 0.016 ($3^{rd}$ index) Hz to 0.137 ($18^{th}$ index) Hz; showing a decrease in spectral power with increasing age. The third region also increase in power with aging and covers almost all spatial frequencies and temporal frequencies greater than 0.137 ($18^{th}$ index) Hz. Most of the region survives after FDR correction (0.01 levels). Our findings are also consistent with Miller et al. (2015) where age effects are investigated on the spatiotemporal organization of whole brain. We found significant age effects on lateralization in several regions using a network-based approach on the same data set presented in Chapter 3. Therefore, though age is an important factor affecting the lateralization of certain local features of specific functional networks, the broader difference in spatiotemporal organization of the two hemispheres does not appear to be affected by age.

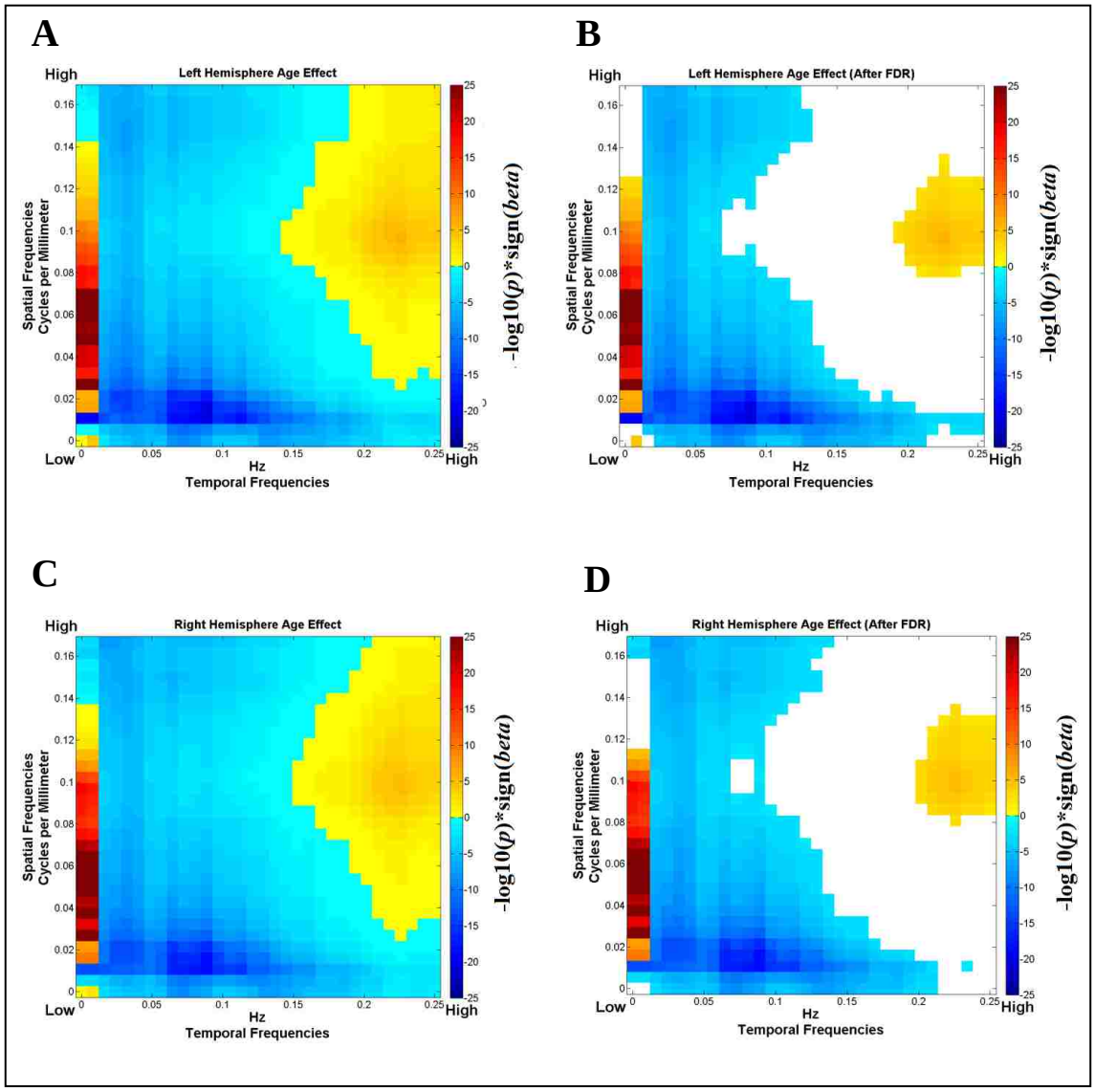


**Figure 5.4: Regression analysis result on subject SSBPs for age effects on Left and Right hemispheres. In each image; left bottom represents the low temporal and low spatial frequencies; on the x-axis from left to right, temporal frequencies increase from 0 Hz to 0.25 Hz; on the y-axis from bottom to top, spatial frequencies increases from 0 cycles/mm to 0.17 cycles/mm. Values are plotted as – *log10(p-value)*sign(beta value)* (A & C) and after 0.01 levels FDR correction (B & D). Generally, the age effects on left hemisphere (A & B) are very similar to the effect on right hemisphere (C & D). Overall, temporal frequencies determine the direction of the age effects, from 0.016 (3rd index) Hz to 0.14 (19th index) Hz and in all spatial frequencies, show a decrease in power with increasing age, while other temporal and spatial frequencies increases in power with aging.**

### 5.4.3 Gender Effects

Regression results on gender effects for left and right hemispheres are presented in Figure 5.5. Gender effects are very similar for both hemisphere and a separate analysis did not reveal any significant interaction effects of hemisphere and gender, indicating that spatiotemporal organization of hemispheres is affected by gender similarly. Gender has a more complicated pattern; males have higher power in almost all spatial and temporal frequencies except the vertical region on very low temporal and high spatial frequencies; and the horizontal region on low spatial and middle temporal frequencies. After the FDR correction (0.01 levels), these regions get smaller to the middle spatial frequencies. These middle spatial frequencies get larger in low and high temporal frequencies, and gets narrower in the middle temporal frequencies. Females have higher spectral power in spatial frequencies (greater than 0.11 ($22^{nd}$ index) cycles/mm) and low temporal frequencies (less than 0.016 ($3^{rd}$ index) Hz). Our results are generally consistent with (Miller et al., 2015) pattern-wise. The specific FDR survival areas, however, are not identical.

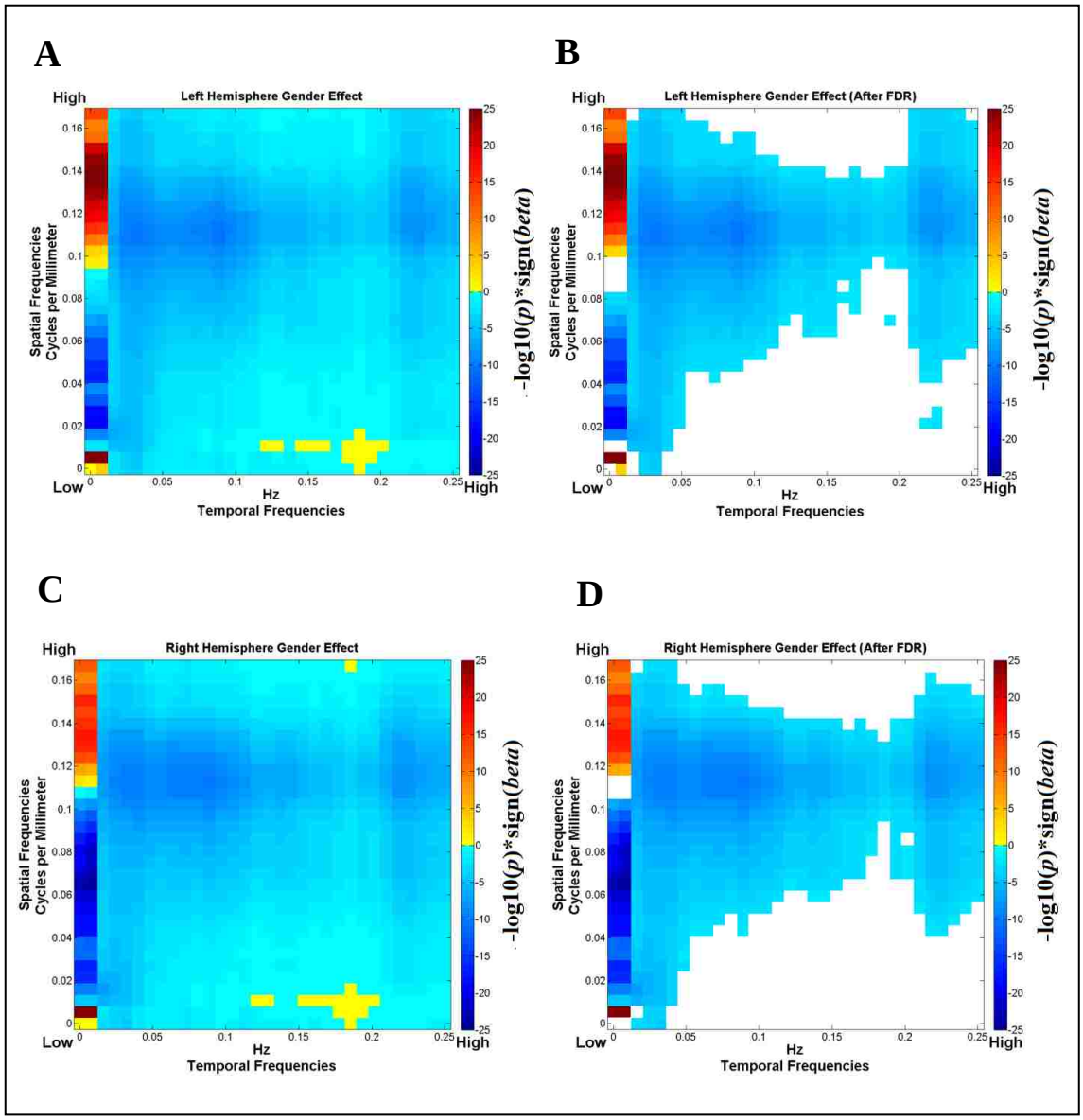


**Figure 5.5: Regression analysis result on subject SSBPs for gender effects on Left and Right hemispheres. In each image; left bottom represents the low temporal and low spatial frequencies; on the x-axis from left to right, temporal frequencies increase from 0 Hz to 0.25 Hz; on the y-axis from bottom to top, spatial frequencies increases from 0 cycles/mm to 0.17 cycles/mm. Values are plotted as *-log10(p-value)*sign(beta value)* (A & C) and after 0.01 levels FDR correction (B &D).Blue color shows the region favors males while red color shows the region favors females. Overall, the gender effects on left hemisphere (A & B) are very similar to the effect on left hemisphere (C & D). Gender patterns are complicated and dependent on both spatial and temporal frequencies.**

## 5.5 Discussion

We analyzed cerebral lateralization in the 4D frequency domain using a resting state fMRI dataset including 603 subjects, and also studied age and gender effects. Results indicate significant differences in the spatiotemporal organization of cerebral

hemispheres, while age and gender showed significant associations with the spatiotemporal organization of each hemisphere. Age and gender effects on the two hemispheres did not differ in a statistically significant way.

In general, low spatial frequencies reflect mostly the global patterns of brain spatial organization while high spatial frequencies provide more information about the differences at a more spatially granular scale. In this context, we found that the broader, more global spatial activation patterns represented by lower spatial frequencies play a relatively larger role in the right hemisphere than in the left. However the left hemisphere has more focal or distributed focal areas implicated in the spatial fluctuation. In other words the right hemisphere has smoother activation (spatially), while the left hemisphere has more of a hill-valley fluctuation pattern. This could be interpreted as that the left hemisphere processes information in various small specific regions, intensely while the right hemisphere tends to process information on a substrate of broader more diffuse spatial patterns. This is consistent with previous findings showing the left hemisphere has a more narrow function related to language processing (Kenneth Hugdahl et al., 2009), while the right hemisphere has been demonstrated to have a broader function related to visuo-spatial processing (J. B. Hellige, Laeng, B., & Michimata, C, 2010).

The left hemisphere also dominates the vertical region on very low temporal frequencies (less than 0.016 ($3^{rd}$ index) Hz) and high spatial frequencies (greater than 0.04 ($8^{th}$ index) cycles/mm).These very low temporal frequencies (<0.01 Hz) contains most of the spectral power and are usually excluded in frequency domain approaches that take averages within certain temporal bands (Baria et al., 2011; Zuo et al., 2010a). In our approach we do not average only certain bands, and thus are able to evaluate these all

frequencies in both space and time. These low temporal frequency regions are also significantly related to gender where directionality of the effect differs for different spatial frequencies, from 0.04 to 0.08 cycles/mm favoring males and frequencies greater than 0.1 cycles/mm favor female, suggesting a complex pattern. The highly overlapping female dominant region and higher power in the left hemisphere, where language processing mostly occurs, may be related to females being more successful in language related tasks (Clements et al., 2006); and the male dominant region could be related visual processing. Further studies are required to confirm such an interpretation, for instance our data is eyes open resting state data, and an analysis using an eyes closed dataset as well as task-based data would be a useful future study.

Age was found to have a strong association with the spatiotemporal organization of the brain, though no significant interaction between aging and hemisphere was found, suggesting both hemispheres are affected similarly by aging. Temporal frequencies were key determinants of the direction of the effects: we observed positive age effects in high temporal frequencies and negative age effects in low temporal frequencies covering a wider band comparing to the positively related high frequency band. A directional changing age effects were previously found in thalamus by Mather et al. (2013), who found significant age effects in fALFF (0.01-0.1 Hz) of thalamus, and further dividing the frequency range revealed that very low frequencies (0.01-0.027 Hz) has more power in older people while high frequency end (0.198-0.25 Hz). The power decrease in the low temporal frequencies may be related to the increase in reaction time with aging. Thompson et al. (2014) found that age-related slowing of the reaction time begins at the age of 24, in their task study of playing video games. Our result is also consistent with

Allen et al. (2011) which found a significant decrease in low frequency power spectra of all RSN networks with aging, and included speculation that this could be due to decrease in gray matter concentration along with the influence of other factors such as vascular compliance or decrease in neural activity. We were unable to do a more detailed comparison with Allen et al. (2011) results for higher temporal frequencies since the time series were low pass filtered in their study. There are some other age related cognitive differences in the literature, such as processing speed, reasoning, memory and executive functions (Deary et al., 2009), and also response inhibition; Hong et al. (2014) presented evidence of age-related spatiotemporal dynamics reorganization during response inhibition; and found that in older adults (18 participants ranging 50-70), brain current densities showed an increase and also more distributed comparing to younger adults (23 participants between age 18-25) during the N2d and P3d (N2 and P3 components in difference event-related potentials) periods. More distributed and increased brain currents in older adults can be related to higher temporal or lower spatial frequencies, which is consistent with our finding of increased power in higher temporal frequencies. Another factor could be related to functional consequences of age-related changes in the gyral and sulcal structure of the cortex. Kochunov et al. (2005) reported that for each ten years, the average sulci width increased about 0.7 mm , while the average sulci depth decreased at a rate of about 0.4 mm/10 years. Kochunov et al. (2005) also reported gender has significant influence on aging effect of sulcus in regions of the superior temporal, collateral, and cingulate sulci with males showing more pronounced age-related change in sulci width than females. However, in our study which was focused on function, we did not find any significant gender-age cross effects.

Gender effects show a more complex pattern than did age. Significant associations with gender were observed within each hemisphere though no significant interactions between gender-hemisphere were found. Cosgrove et al. (2007) that reported females having higher cerebral global blood flow and cognitive activity comparing to males at rest, our technique was able to relate these differences to specific spatiotemporal frequencies. Even though, due the fact that we are working with rest fMRI data, it is not possible to make a direct inversion to certain functions, these complicated patterns may be related to differences between gender on certain tasks such as verbal fluency, facial emotion recognition or emotional memory (Wang et al., 2012).

Our SSBP approach differs meaningfully from the typical brain lateralization studies, (Agcaoglu et al., 2014; Gotts et al., 2013; Liu et al., 2009; Nielsen et al., 2013; Swanson et al., 2011; Zuo et al., 2010b), with the fact that our approach reveals a global comparison of hemispheres in the frequency domain, rather than revealing specific regions. For example, the temporal activation of an ROI in one hemisphere with the corresponding homotopic region may have similar average activation value but different fluctuation rate (spatially or/and temporally), in this case, typical lateralization approaches would not reveal the differences; however our method can identify such differences. Moreover, our method can also detect significant spatiotemporal patterns regardless of when and where they actually change.

Significant hemisphere effects were quite strong and no significant interaction between hemisphere and gender or age is found. In many previous studies, the left hemisphere has been shown to facilitate functions associated with language such as grammar and vocabulary, as well as analytical and logical functions (Breier et al., 1999; Cai et al.,

2013; Clements et al., 2006; Gobbele et al., 2008; Gotts et al., 2013; Groen et al., 2012; Smith et al., 1996; Stephan et al., 2003; Thomason et al., 2009). In future work, we would like to evaluate the relationship of spatiotemporal frequencies to variables that are related to language processing.

### 5.5.1 Limitations

Some limitations should be considered while interpreting the results. No cognitive or behavior data, such as education, IQs, were available for our subjects. These factors may be important and should be investigated in future studies. In addition, as mentioned before, the ages in our dataset range from 12 to 71 with all but 7 subjects between ages 12 and 50, thus it does not fully cover the most rapidly changing ages of childhood and of old age, and though we log transformed the age to work with a more uniform distribution, age was not uniformly distributed. Age effects were strong throughout both hemispheres, but no significant changes in left versus right hemisphere were identified. Finally, our method involves a significant data reduction, though it also provides a concise and useful summary of the spatiotemporal information. Based on the significant findings we show, this approach appears to provide a new and useful way to query fMRI data which is different, but complementary, to the typical approach of creating connectivity maps. In future work we will focus on capturing additional information that may not be fully captured by the proposed approach. For example, we can also incorporate the phase information in order to identify patterns of spatiotemporal signals that shift in time-space, in order to provide some additional information about where in the brain these signals might be localized.

## 5.6 Conclusion

In summary, we analyzed hemispheric differences in the spatiotemporal domain using a large fMRI dataset. We found significant local and global spatiotemporal difference between the hemispheres, as well as age and gender effects. Age and gender were found to be affecting both hemisphere spatiotemporal organizations the same degree with no significant interaction effect. Hemisphere effects were quite robust and favored the left hemisphere for high spatial frequencies; favored right hemisphere for low and middle spatial frequencies. Age effects were mainly determined by temporal frequencies and consistent with previous studies. Gender effects were more complex and favoring males for mid-range spatial frequencies, which could be related to that male in general, perform better on visuospatial tasks. Overall, our 4D frequency domain approach appears to be a promising method to investigate brain organization in general and hemispheric specialization in particular.

# Chapter 6: Conclusion and Future Works

## 6.1 Summary

In this PhD dissertation, we discussed 3 main studies related to hemispheric lateralization using resting state fMRI data. Studies performed in Chapter 3 (Agcaoglu et al., 2014) and Chapter 4 (Agcaoglu et al., 2015a; Agcaoglu et al., 2016) are focused on revealing network level differences in the content of lateralization of activated regions and temporal covariance of these networks, Chapter 5 (Agcaoglu et al., 2015b, c) present the study that focused on global level differences between cerebral hemispheres in the content of spatiotemporal organization of hemispheres.

In Chapter 3, we analyzed lateralization of 28 resting state networks and found many of the intrinsic brain networks are highly lateralized, with several regions showing a strong association with age and gender. On the global measure of laterality, age was found as a significant factor and gender exhibiting a trend-level effect. Our results support the theory that multiple brain networks grow more bilateral in an attempt to compensate neural decline with aging.

In Chapter 4, we proposed a (gICA)-based approach to generate hemisphere-specific time-courses and calculate intra-hemisphere and inter-hemisphere FNC on a resting state fMRI dataset consist of age and gender balanced schizophrenia patients and healthy controls. Our results reveal that the FNC of schizophrenia patients does not show the hemispheric connectivity asymmetry as seen in healthy controls. We also found reduced connectivity in all FNC types, such as, intra-left (L_FNC), intra-right (R_FNC) and inter-hemisphere (Cross_FNC), in the schizophrenia patients relative to healthy controls, but

general patterns of connectivity were preserved in patients. Analyses of age and gender effects yielded results similar to those reported in whole brain FNC studies.

In Chapter 5, we evaluated cerebral lateralization in the 4D spatiotemporal frequency domain to compare the hemispheres in the context of general activation patterns at different spatial and temporal scales. Our analysis elucidates significant differences in the spatiotemporal organization of brain activity between hemispheres, and generally more spatiotemporal fluctuation in the left hemisphere especially in the high spatial frequency bands, and more power in the right hemisphere in the low and middle spatial frequencies.

Some of the studies presented in this dissertation have been published

## 6.2 Future Work

In the relevant chapters (chapter -3, 4, 5), some future research directions and suggestion were mentioned. In this section, some additional directions of future work are briefly discussed.

In the current version of 4D spatiotemporal analyses, we used the Fourier transform to estimate the power spectral density (PSD) of 4D fMRI data; however there are other methods, such as the stochastic methods that may be adapted to fMRI data to potentially improve our estimation of the PSD.

Recently, it has been shown that time-varying analysis on fMRI revealed significant information about brain (Calhoun et al., 2014) . Therefore it is reasonable to think that the differences between hemispheres of brain have dynamically characteristic. Both spatiotemporal and FNC differences between hemispheres could be changing dynamically. Time-varying characteristic can be analyzed using windowing technique on

time dimension or on time series. Another method would be generating time series each time window separately via constrained independent component analysis.

# A. Appendix

In Chapter 3, we presented the effects of age on the lateralization of the spatial maps. In order to check if the age effects are varying over age, we divide the data into two age subgroups; teenagers and young adult versus adults, and calculated laterality cofactors in each subgroup. We used the cut-off age as 29, just to match with some previous work (Nielsen et al., 2013). Later, we performed a robust regression analysis on these laterality cofactors for both groups.

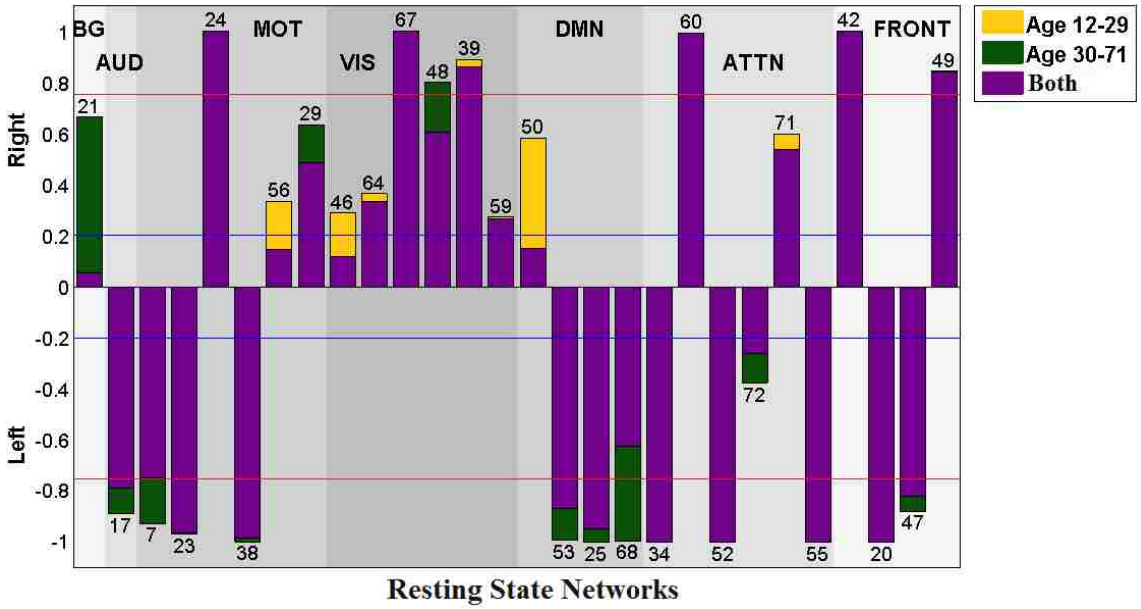


**Figure A.1: Laterality cofactors for different subgroups. Yellow bar shows components that are more lateralized for the age group 12 to 29 and green bars show the components that are more lateralized for age group 30 to 71.**

## Age and Gender Effects in Age Subgroups

We subgroup the subjects into two different age groups to look at the age effects to look for evidence of nonlinear aging effects. In general there were many more changes in lateralization at the younger (age range 12 to 29) versus the older age range (range 30 to 71). Figure A.1 shows the laterality cofactors for the two subgroups. Almost all networks have differences in laterality cofactors of two subgroups. Among them, basal ganglia,

sensorimotor and visual networks have the most remarkable differences. The basal ganglia network (IC 21) is more right lateralized for the elder age group, while it is symmetric for young age group. The sensorimotor network components 7 and 29 are more lateralized and component 56 is less lateralized in the elder age group. Components 23, 24 and 38 are almost identical for both groups. The visual network component 46 is more right lateralized and 48 are less right lateralized at elder age group. The other components 64, 67, 39 and 59 are similar. The auditory network (IC 17) is more left lateralized in the elder age group. The default mode networks are more right lateralized for the elder age group (IC 53, 25, 68), with the exception of IC 50 which is essentially symmetric in the elder age group while right lateralized in the young age group. The attentional network components 34, 60, 52 and 55 are not showing changes with age while 72 and 71 are. IC 72 is more lateralized in the elder age group while IC 71 is more lateralized at young age group. The frontal network components 55, 42, 20 are 49 same for both age groups, and with component 47 slightly more lateralized in the elder age group.

### a. Age effect in age subgroup 12 to 29

Beta values of the regression analysis on the laterality cofactors for the subjects aging from 12 to 29 are presented in Figure A.2. In general, aging from 12 to 29 makes networks less lateralized, in other words more symmetric. Three components survive 0.05 levels FDR correction, the auditory network component 17, sensorimotor network component 29 and frontal network component 47. Component 17, the auditory network including left superior temporal gyrus, is becoming less left lateralized as age increases from 12 to 29. While it is hard to make firm conclusions about the impact of learning

language and subsequent pruning of the cortex on the observed lateralization, it is consistent with the idea that lateralization at the younger ages provides a benefit for learning language (DeKeyser, 2013).

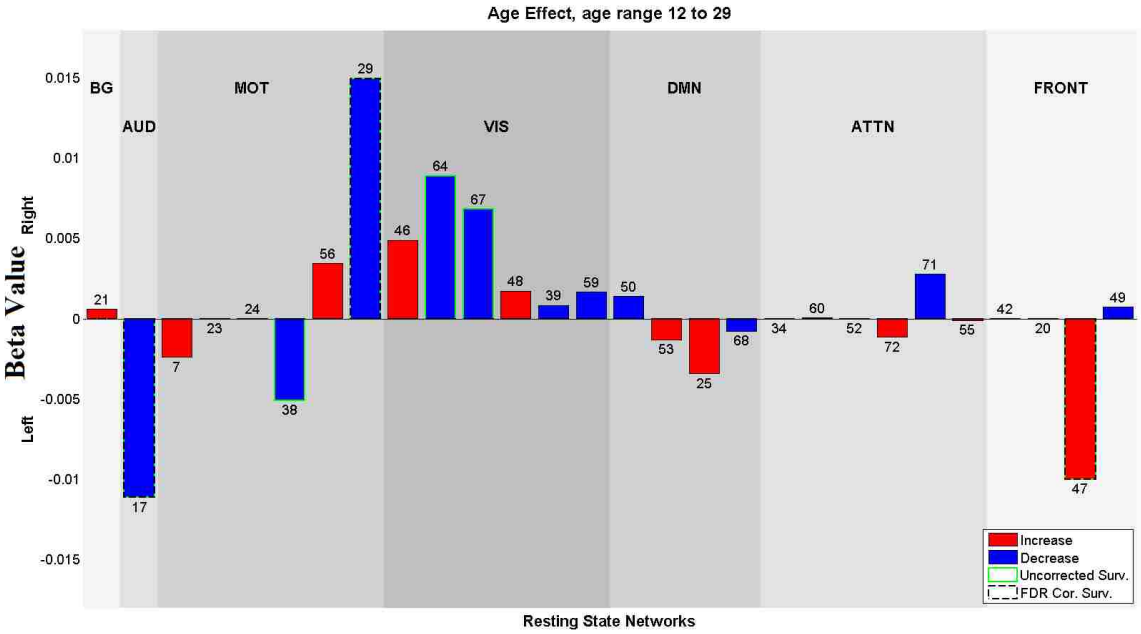


**Figure A.2: Beta values for Age effects on laterality cofactors for the subgrouped data between 12 to 29. Blue bars show the components that are more lateralized as age goes from 12 to 29, Red bars show the components that are less lateralized as age goes from 12 to 29. Component 17, 29 and 47 (dashed circulated) survive 0.05 FDR correction, components 17 and 29 are getting less lateralized and component 47 is getting more lateralized as age goes from 12 to 29. Component 38, 64, 67 (green circulated) do not survive FDR correction, but they have p-values smaller than 0.05, and are getting less lateralized as age goes from 12 to 29.**

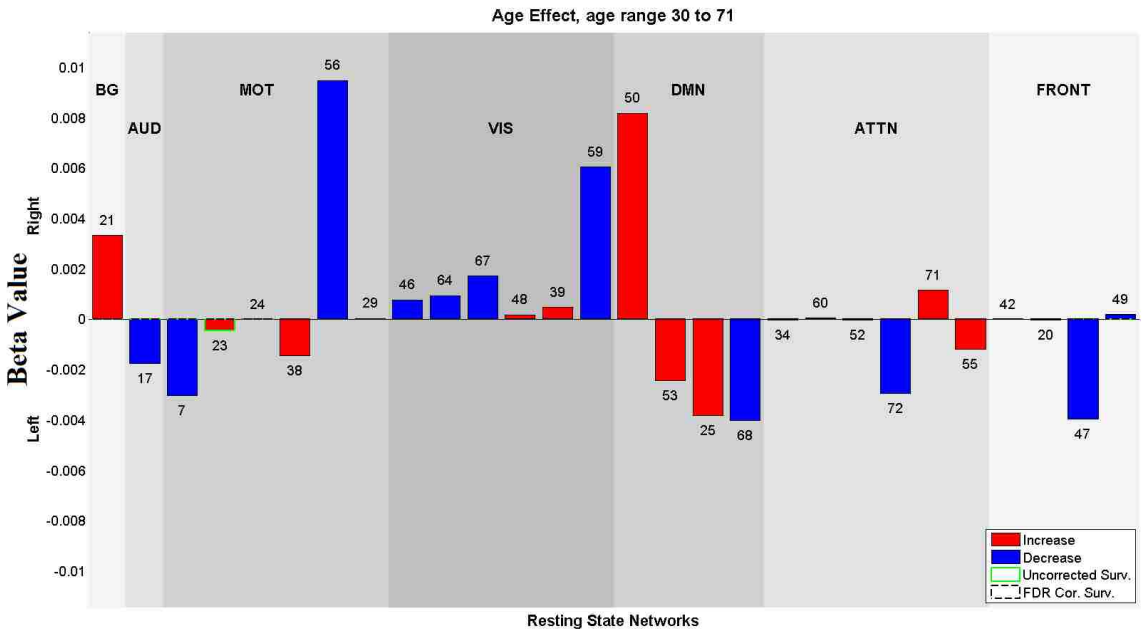


**Figure A.3: Beta values for Age effects on laterality cofactors for the subgrouped data between 30 to 71. Blue bars show the components that are more lateralized as age goes from 30 to 71, Red bars show the components that are less lateralized as age goes from 30 to 71. No component survives 0.05 FDR correction. Component 23 (outlined in green ) does not survive FDR correction, but it has a p-value smaller than 0.05, and is getting more lateralized as age goes from 30 to 71.**

Component 29, part of visual network including the paracentral lobule, is growing less right lateralized with age. Component 47, a part of the frontal network including left inferior frontal gyrus and left middle frontal gyrus, and it is growing more left lateralized as age goes from 12 to 29. Xiao (2012) reported that early developed native spoken language is processed by the left inferior frontal gyrus, while late developed written language is proceeded by the left middle frontal gyrus in a manner dependent on the age of language acquisition. Age 12 to 29 is during a phase of rapid acquisition of written language and vocabulary. As Xiao (2012) reported, the increase in the left middle frontal gyrus due to acquisition of new vocabulary is consistent with the increase in left lateralization.

Sensorimotor network component 38, regions of supramarginal and middle temporal gyrus, is decreasing in lateralization ($p<0.05$) as age goes from 12 to 29, visual network components 64 and 67, regions of calcarine and lingual gyrus respectively, and both are also growing less right lateralized ($p<0.05$) as age increases from 12 to 29.

### b. Age effect in age subgroup 30 to 71

In Figure A.2, we present the beta values of the regression analysis on the laterality cofactors data age interval 30 to 71. There is no significant age effect in this age interval surviving from 0.05 levels FDR correction, however component 23 of sensorimotor network has p-value less than 0.05, with the region of precentral gyrus and it is growing more left lateralized as age goes from 30 to 71.

### c. Gender effect in age subgroups

On two age subgroups, we also look at the gender effects to test if the gender effects vary with aging. Figure A.4 and Figure A.5 shows the beta values of regression analysis for gender effects on the laterality cofactor for the young and elder subgroup, respectively. For both groups, no component survives from FDR correction, but some components have p-values less than 0.05.

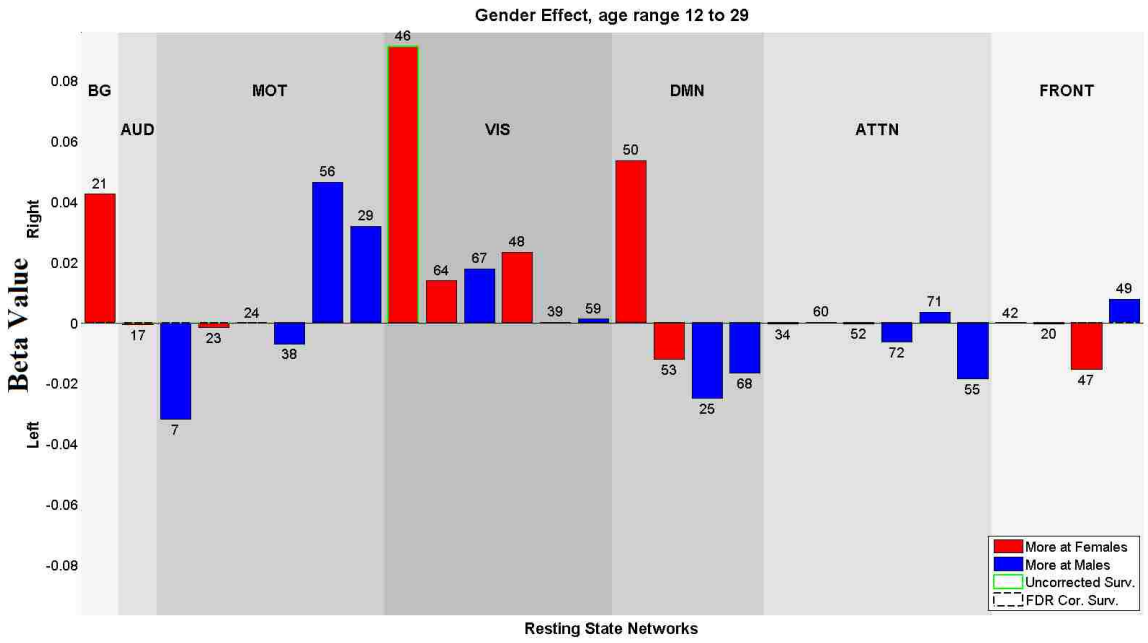


**Figure A.4: Gender effects on the data age subgroup ranging from 12 to 29. Blue bars show the components that are more lateralized for males, Red bars show the components that are more lateralized for females. No components survive 0.05 levels FDR correction. Component 46 is more lateralized for females (P<0.05).**

In the younger group, visual network component 46 is more right lateralized ($p<0.05$) on females. In the elder group, left lateralized component 55 (attentional) and component 47 (frontal) are more left lateralized on males, and right lateralized component 60 (attentional) is more lateralized at females.

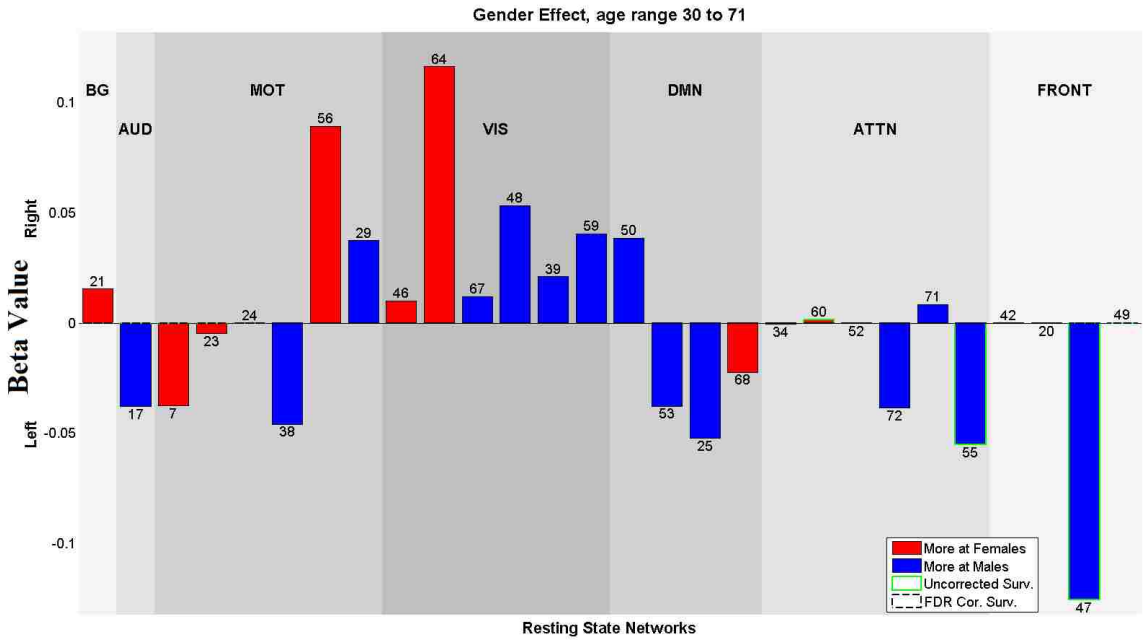


**Figure A.5: Gender effects on the data subgroup ranging from 30 to 71. Blue bars show the components that are more lateralized for males, red bars show the components that are more lateralized for females. No components survive 0.05 levels FDR correction. Components 60, 55 and 47 are more lateralized for males (P<0.05).**

# Bibliography


Agcaoglu, O., Miller, R., Cetin, M. S., & Calhoun, V. D. (2015a). Functional Network Connectivity Approach to Cerebral Lateralization at Rest. *OHBM Conference 2015, Hawaii*.

Agcaoglu, O., Miller, R., Mayer, A. R., Hugdahl, K., & Calhoun, V. D. (2014). Lateralization of resting state networks and relationship to age and gender. *Neuroimage*. doi: 10.1016/j.neuroimage.2014.09.001

Agcaoglu, O., Miller, R., Mayer, A. R., Hugdahl, K., & Calhoun, V. D. (2015b). A 4D Frequency Domain Approach to Cerebral Lateralization at Rest. *OHBM Conference 2015, Hawaii*

Agcaoglu, O., Miller, R., Mayer, A. R., Hugdahl, K., & Calhoun, V. D. (2015c). Increased spatial granularity of left brain activation and unique age/gender signatures: a 4D frequency domain approach to cerebral lateralization at rest. *Brain Imaging Behav*. doi: 10.1007/s11682-015-9463-8

Agcaoglu, O., Miller, R., Rashid, B., Bustillo, J., Cetin, M. S., & Calhoun, V. D. (2016). Decreased Asymmetry of Intra Hemisphere and Inter Hemisphere Functional Network Connectivity at Rest in Schizophrenia. *Brain Imaging Behav*(Under Review).

Allen, E. A., Erhardt, E. B., Damaraju, E., Gruner, W., Segall, J. M., Silva, R. F., . . . Calhoun, V. D. (2011). A baseline for the multivariate comparison of resting-state networks. *Front Syst Neurosci, 5*, 2. doi: 10.3389/fnsys.2011.00002

Arbabshirani, M. R., Kiehl, K. A., Pearlson, G. D., & Calhoun, V. D. (2013). Classification of schizophrenia patients based on resting-state functional network connectivity. *Front Neurosci, 7*, 133. doi: 10.3389/fnins.2013.00133

Ashburner, J., & Friston, K. J. (2005). Unified segmentation. *Neuroimage, 26*(3), 839-851. doi: 10.1016/j.neuroimage.2005.02.018

Bakhshi, K., & Chance, S. A. (2015). The neuropathology of schizophrenia: A selective review of past studies and emerging themes in brain structure and cytoarchitecture. *Neuroscience, 303*, 82-102. doi: 10.1016/j.neuroscience.2015.06.028

Bandettini, P. A. (2012). Twenty years of functional MRI: the science and the stories. *Neuroimage, 62*(2), 575-588. doi: 10.1016/j.neuroimage.2012.04.026

Bandettini, P. A., Wong, E. C., Hinks, R. S., Tikofsky, R. S., & Hyde, J. S. (1992). Time course EPI of human brain function during task activation. *Magn Reson Med, 25*(2), 390-397.

Baria, A. T., Baliki, M. N., Parrish, T., & Apkarian, A. V. (2011). Anatomical and functional assemblies of brain BOLD oscillations. *J Neurosci, 31*(21), 7910-7919. doi: 10.1523/JNEUROSCI.1296-11.2011

Beckmann, C. F., DeLuca, M., Devlin, J. T., & Smith, S. M. (2005). Investigations into resting-state connectivity using independent component analysis. *Philosophical Transactions of the Royal Society B-Biological Sciences, 360*(1457), 1001-1013. doi: 10.1098/rstb.2005.1634

Bell, A. J., & Sejnowski, T. J. (1995). An Information Maximization Approach to Blind Separation and Blind Deconvolution. *Neural Computation, 7*(6), 1129-1159. doi: DOI 10.1162/neco.1995.7.6.1129

Belliveau, J. W., Kennedy, D. N., Jr., McKinstry, R. C., Buchbinder, B. R., Weisskoff, R. M., Cohen, M. S., . . . Rosen, B. R. (1991). Functional mapping of the human visual cortex by magnetic resonance imaging. *Science, 254*(5032), 716-719.

Berger, A., & Posner, M. I. (2000). Pathologies of brain attentional networks. *Neurosci Biobehav Rev, 24*(1), 3-5.

Bianki, V. L. (1981). Lateralization of functions in the animal brain. *Int J Neurosci, 15*(1-2), 37-47.

Bottjer, S. W., Glaessner, S. L., & Arnold, A. P. (1985). Ontogeny of Brain Nuclei Controlling Song Learning and Behavior in Zebra Finches. *Journal of Neuroscience, 5*(6), 1556-1562.

Breier, J. I., Simos, P. G., Zouridakis, G., & Papanicolaou, A. C. (1999). Lateralization of cerebral activation in auditory verbal and non-verbal memory tasks using magnetoencephalography. *Brain Topogr, 12*(2), 89-97.

Broca, Paul. (1861). Sur le principe des localisations cerebrales. *Bulletin de la Societe d"Anthropologie, 2*, 190-204.

Cabeza, R., Anderson, N. D., Locantore, J. K., & McIntosh, A. R. (2002). Aging gracefully: compensatory brain activity in high-performing older adults. *Neuroimage, 17*(3), 1394-1402.

Cai, Q., Van der Haegen, L., & Brysbaert, M. (2013). Complementary hemispheric specialization for language production and visuospatial attention. *Proc Natl Acad Sci U S A, 110*(4), E322-330. doi: 10.1073/pnas.1212956110

Calhoun, V. D., Adali, T., Pearlson, G. D., & Pekar, J. J. (2001a). A method for making group inferences from functional MRI data using independent component analysis. *Hum Brain Mapp, 14*(3), 140-151.

Calhoun, V. D., Adali, T., Pearlson, G. D., & Pekar, J. J. (2001b). Spatial and temporal independent component analysis of functional MRI data containing a pair of task-related waveforms. *Hum Brain Mapp, 13*(1), 43-53.

Calhoun, V. D., Eichele, T., & Pearlson, G. (2009a). Functional brain networks in schizophrenia: a review. *Front Hum Neurosci, 3*, 17. doi: 10.3389/neuro.09.017.2009

Calhoun, V. D., Liu, J., & Adali, T. (2009b). A review of group ICA for fMRI data and ICA for joint inference of imaging, genetic, and ERP data. *Neuroimage, 45*(1 Suppl), S163-172. doi: 10.1016/j.neuroimage.2008.10.057

Calhoun, V. D., Miller, R., Pearlson, G., & Adali, T. (2014). The chronnectome: time-varying connectivity networks as the next frontier in fMRI data discovery. *Neuron, 84*(2), 262-274. doi: 10.1016/j.neuron.2014.10.015

Calhoun, V. D., Sui, J., Kiehl, K., Turner, J., Allen, E., & Pearlson, G. (2011). Exploring the psychosis functional connectome: aberrant intrinsic networks in schizophrenia and bipolar disorder. *Front Psychiatry, 2*, 75. doi: 10.3389/fpsyt.2011.00075

Cetin, M. S., Christensen, F., Abbott, C. C., Stephen, J. M., Mayer, A. R., Canive, J. M., . . . Calhoun, V. D. (2014). Thalamus and posterior temporal lobe show greater inter-network connectivity at rest and across sensory paradigms in schizophrenia. *Neuroimage, 97*, 117-126. doi: DOI 10.1016/j.neuroimage.2014.04.009

Cetin, Mustafa, Houck, Jon, Rashid, Barnaly, Agcaoglu, Oktay, Stephen, Julia, Sui, Jing, . . . Calhoun, Vince. (2016). Multimodal classification of schizophrenia patients

with MEG and fMRI data using static and dynamic connectivity measures. *Frontiers in Neuroscience, 10*(466). doi: 10.3389/fnins.2016.00466

Clements, A. M., Rimrodt, S. L., Abel, J. R., Blankner, J. G., Mostofsky, S. H., Pekar, J. J., . . . Cutting, L. E. (2006). Sex differences in cerebral laterality of language and visuospatial processing. *Brain Lang, 98*(2), 150-158. doi: 10.1016/j.bandl.2006.04.007

Comon, P. (1994). Independent Component Analysis, a New Concept. *Signal Processing, 36*(3), 287-314. doi: Doi 10.1016/0165-1684(94)90029-9

Corballis, M. C. (2014). Left brain, right brain: facts and fantasies. *PLoS Biol, 12*(1), e1001767. doi: 10.1371/journal.pbio.1001767

Cordes, D., Haughton, V., Carew, J. D., Arfanakis, K., & Maravilla, K. (2002). Hierarchical clustering to measure connectivity in fMRI resting-state data. *Magn Reson Imaging, 20*(4), 305-317.

Cosgrove, K. P., Mazure, C. M., & Staley, J. K. (2007). Evolving knowledge of sex differences in brain structure, function, and chemistry. *Biol Psychiatry, 62*(8), 847-855. doi: 10.1016/j.biopsych.2007.03.001

Damaraju, E., Allen, E. A., Belger, A., Ford, J. M., McEwen, S., Mathalon, D. H., . . . Calhoun, V. D. (2014). Dynamic functional connectivity analysis reveals transient states of dysconnectivity in schizophrenia. *Neuroimage-Clinical, 5*, 298-308. doi: 10.1016/j.nicl.2014.07.003

Davidson, R. J. (1998). Anterior electrophysiological asymmetries, emotion, and depression: conceptual and methodological conundrums. *Psychophysiology, 35*(5), 607-614.

Deary, I. J., Corley, J., Gow, A. J., Harris, S. E., Houlihan, L. M., Marioni, R. E., . . . Starr, J. M. (2009). Age-associated cognitive decline. *Br Med Bull, 92*, 135-152. doi: 10.1093/bmb/ldp033

DeKeyser, Robert M. (2013). Age Effects in Second Language Learning: Stepping Stones Toward Better Understanding. *Language Learning, 63*, 52-67. doi: 10.1111/j.1467-9922.2012.00737.x

Denenberg, V. H. (1981). Hemispheric Laterality in Animals and the Effects of Early Experience. *Behavioral and Brain Sciences, 4*(1), 1-21.

Denenberg, V. H., Garbanati, J., Sherman, G., Yutzey, D. A., & Kaplan, R. (1978). Infantile Stimulation Induces Brain Lateralization in Rats. *Science, 201*(4361), 1150-1152. doi: DOI 10.1126/science.684436

Detre, J. A., Leigh, J. S., Williams, D. S., & Koretsky, A. P. (1992). Perfusion imaging. *Magn Reson Med, 23*(1), 37-45.

Erhardt, E. B., Allen, E. A., Damaraju, E., & Calhoun, V. D. (2011a). On network derivation, classification, and visualization: a response to Habeck and Moeller. *Brain Connect, 1*(2), 1-19.

Erhardt, E. B., Rachakonda, S., Bedrick, E. J., Allen, E. A., Adali, T., & Calhoun, V. D. (2011b). Comparison of Multi-Subject ICA Methods for Analysis of fMRI Data. *Human Brain Mapping, 32*(12), 2075-2095. doi: 10.1002/hbm.21170

Filippi, M., Valsasina, P., Misci, P., Falini, A., Comi, G., & Rocca, M. A. (2013). The organization of intrinsic brain activity differs between genders: a resting-state fMRI study in a large cohort of young healthy subjects. *Hum Brain Mapp, 34*(6), 1330-1343. doi: 10.1002/hbm.21514

Freire, L., Roche, A., & Mangin, J. F. (2002). What is the best similarity measure for motion correction in fMRI time series? *IEEE Trans Med Imaging, 21*(5), 470-484. doi: 10.1109/TMI.2002.1009383

Garrity, A. G., Pearlson, G. D., McKiernan, K., Lloyd, D., Kiehl, K. A., & Calhoun, V. D. (2007). Aberrant "default mode" functional connectivity in schizophrenia. *Am J Psychiatry, 164*(3), 450-457. doi: 10.1176/appi.ajp.164.3.450

Gee, D. G., Biswal, B. B., Kelly, C., Stark, D. E., Margulies, D. S., Shehzad, Z., . . . Milham, M. P. (2011). Low frequency fluctuations reveal integrated and segregated processing among the cerebral hemispheres. *Neuroimage, 54*(1), 517-527. doi: 10.1016/j.neuroimage.2010.05.073

Genovese, C. R., Lazar, N. A., & Nichols, T. (2002). Thresholding of statistical maps in functional neuroimaging using the false discovery rate. *Neuroimage, 15*(4), 870-878. doi: 10.1006/nimg.2001.1037

Giedd, J. N., Blumenthal, J., Jeffries, N. O., Castellanos, F. X., Liu, H., Zijdenbos, A., . . . Rapoport, J. L. (1999). Brain development during childhood and adolescence: a longitudinal MRI study. *Nat Neurosci, 2*(10), 861-863. doi: 10.1038/13158

Glover, G. H. (2011). Overview of functional magnetic resonance imaging. *Neurosurg Clin N Am, 22*(2), 133-139, vii. doi: 10.1016/j.nec.2010.11.001

Gobbele, R., Lamberty, K., Stephan, K. E., Stegelmeyer, U., Buchner, H., Marshall, J. C., . . . Waberski, T. D. (2008). Temporal activation patterns of lateralized cognitive and task control processes in the human brain. *Brain Res, 1205*, 81-90. doi: 10.1016/j.brainres.2008.02.031

Good, C. D., Johnsrude, I., Ashburner, J., Henson, R. N., Friston, K. J., & Frackowiak, R. S. (2001). Cerebral asymmetry and the effects of sex and handedness on brain structure: a voxel-based morphometric analysis of 465 normal adult human brains. *Neuroimage, 14*(3), 685-700. doi: 10.1006/nimg.2001.0857

Gotts, S. J., Jo, H. J., Wallace, G. L., Saad, Z. S., Cox, R. W., & Martin, A. (2013). Two distinct forms of functional lateralization in the human brain. *Proc Natl Acad Sci U S A, 110*(36), E3435-3444. doi: 10.1073/pnas.1302581110

Groen, M. A., Whitehouse, A. J., Badcock, N. A., & Bishop, D. V. (2012). Does cerebral lateralization develop? A study using functional transcranial Doppler ultrasound assessing lateralization for language production and visuospatial memory. *Brain Behav, 2*(3), 256-269. doi: 10.1002/brb3.56

Guo, Y., & Pagnoni, G. (2008). A unified framework for group independent component analysis for multi-subject fMRI data. *Neuroimage, 42*(3), 1078-1093. doi: 10.1016/j.neuroimage.2008.05.008

Hauser, M. D., & Andersson, K. (1994). Left hemisphere dominance for processing vocalizations in adult, but not infant, rhesus monkeys: field experiments. *Proc Natl Acad Sci U S A, 91*(9), 3946-3948.

Hellige, J. B., Laeng, B., & Michimata, C. (2010). Processing asymmetries in the visual system. In K. Hugdahl (Ed.), The Two Halves of the Brain. . *Cambridge, MA: MIT Press.*, 379-416.

Hellige, Joseph B. (1993). *Hemispheric Asymmetry: What's Right and What's Left*: Harvard University Press.

Herve, P. Y., Zago, L., Petit, L., Mazoyer, B., & Tzourio-Mazoyer, N. (2013). Revisiting human hemispheric specialization with neuroimaging. *Trends Cogn Sci, 17*(2), 69-80. doi: 10.1016/j.tics.2012.12.004

Hirnstein, M., Westerhausen, R., Korsnes, M. S., & Hugdahl, K. (2013). Sex differences in language asymmetry are age-dependent and small: a large-scale, consonant-vowel dichotic listening study with behavioral and fMRI data. *Cortex, 49*(7), 1910-1921. doi: 10.1016/j.cortex.2012.08.002

Hong, X., Sun, J., Bengson, J. J., & Tong, S. (2014). Age-related spatiotemporal reorganization during response inhibition. *Int J Psychophysiol, 93*(3), 371-380. doi: 10.1016/j.ijpsycho.2014.05.013

Hoptman, M. J., Zuo, X. N., Butler, P. D., Javitt, D. C., D'Angelo, D., Mauro, C. J., & Milham, M. P. (2010). Amplitude of low-frequency oscillations in schizophrenia: a resting state fMRI study. *Schizophr Res, 117*(1), 13-20. doi: 10.1016/j.schres.2009.09.030

Hoptman, M. J., Zuo, X. N., D'Angelo, D., Mauro, C. J., Butler, P. D., Milham, M. P., & Javitt, D. C. (2012). Decreased interhemispheric coordination in schizophrenia: a resting state fMRI study. *Schizophr Res, 141*(1), 1-7. doi: 10.1016/j.schres.2012.07.027

Houck, J. M., Cetin, M. S., Mayer, A. R., Bustillo, J. R., Stephen, J., Aine, C., . . . Calhoun, V. D. (2016). Magnetoencephalographic and functional MRI connectomics in schizophrenia via intra- and inter-network connectivity. *Neuroimage*. doi: 10.1016/j.neuroimage.2016.10.011

Hugdahl, K., Thomsen, T., & Ersland, L. (2006). Sex differences in visuo-spatial processing: an fMRI study of mental rotation. *Neuropsychologia, 44*(9), 1575-1583. doi: 10.1016/j.neuropsychologia.2006.01.026

Hugdahl, Kenneth. (2011). Hemispheric asymmetry: contributions from brain imaging. *Wiley Interdisciplinary Reviews: Cognitive Science, 2*(5), 461-478. doi: 10.1002/wcs.122

Hugdahl, Kenneth, & Westerhausen, René. (2009). What Is Left Is Right: How Speech Asymmetry Shaped the Brain. *European Psychologist, 14*(1), 78-89. doi: doi:10.1027/1016-9040.14.1.78

Hugdahl, Kenneth, & Westerhausen, René. (2010). *The two halves of the brain : information processing in the cerebral hemispheres*. Cambridge, Mass.: MIT Press.

Ingalhalikar, M., Smith, A., Parker, D., Satterthwaite, T. D., Elliott, M. A., Ruparel, K., . . . Verma, R. (2013). Sex differences in the structural connectome of the human brain. *Proc Natl Acad Sci U S A*. doi: 10.1073/pnas.1316909110

Jafri, M. J., Pearlson, G. D., Stevens, M., & Calhoun, V. D. (2008). A method for functional network connectivity among spatially independent resting-state components in schizophrenia. *Neuroimage, 39*(4), 1666-1681. doi: 10.1016/j.neuroimage.2007.11.001

Janssen, L., Meulenbroek, R. G., & Steenbergen, B. (2011). Behavioral evidence for left-hemisphere specialization of motor planning. *Exp Brain Res, 209*(1), 65-72. doi: 10.1007/s00221-010-2519-5

Ke, M., Zou, R., Shen, H., Huang, X., Zhou, Z., Liu, Z., . . . Hu, D. (2010). Bilateral functional asymmetry disparity in positive and negative schizophrenia revealed by

resting-state fMRI. *Psychiatry Res, 182*(1), 30-39. doi: 10.1016/j.pscychresns.2009.11.004

Kochunov, P., Mangin, J. F., Coyle, T., Lancaster, J., Thompson, P., Riviere, D., . . . Fox, P. T. (2005). Age-related morphology trends of cortical sulci. *Hum Brain Mapp, 26*(3), 210-220. doi: 10.1002/hbm.20198

Kwong, K. K., Belliveau, J. W., Chesler, D. A., Goldberg, I. E., Weisskoff, R. M., Poncelet, B. P., . . . et al. (1992). Dynamic magnetic resonance imaging of human brain activity during primary sensory stimulation. *Proc Natl Acad Sci U S A, 89*(12), 5675-5679.

Liu, H., Stufflebeam, S. M., Sepulcre, J., Hedden, T., & Buckner, R. L. (2009). Evidence from intrinsic activity that asymmetry of the human brain is controlled by multiple factors. *Proc Natl Acad Sci U S A, 106*(48), 20499-20503. doi: 10.1073/pnas.0908073106

Lynall, M. E., Bassett, D. S., Kerwin, R., McKenna, P. J., Kitzbichler, M., Muller, U., & Bullmore, E. (2010). Functional connectivity and brain networks in schizophrenia. *J Neurosci, 30*(28), 9477-9487. doi: 10.1523/JNEUROSCI.0333-10.2010

Makeig, S., Jung, T. P., Bell, A. J., Ghahremani, D., & Sejnowski, T. J. (1997). Blind separation of auditory event-related brain responses into independent components. *Proc Natl Acad Sci U S A, 94*(20), 10979-10984.

Mather, M., & Nga, L. (2013). Age differences in thalamic low-frequency fluctuations. *Neuroreport, 24*(7), 349-353. doi: 10.1097/WNR.0b013e32835f6784

Mazoyer, B., Zago, L., Jobard, G., Crivello, F., Joliot, M., Perchey, G., . . . Tzourio-Mazoyer, N. (2014). Gaussian mixture modeling of hemispheric lateralization for language in a large sample of healthy individuals balanced for handedness. *PLoS One, 9*(6), e101165. doi: 10.1371/journal.pone.0101165

McKeown, M. J., Makeig, S., Brown, G. G., Jung, T. P., Kindermann, S. S., Bell, A. J., & Sejnowski, T. J. (1998). Analysis of fMRI data by blind separation into independent spatial components. *Hum Brain Mapp, 6*(3), 160-188.

Miller, Robyn L., Erhardt, Erik B., Allen, Elena A, Michael, Andrew M, Turner, Jessica A, Bustillo, Juan, . . . Calhoun, Vince D. (2015). Multidimensional frequency domain analysis of full-volume fMRI reveals significant effects of age, gender and mental illness on the spatiotemporal organization of resting-state brain activity. *Frontiers in Neuroscience, 9*. doi: 10.3389/fnins.2015.00203

Mueller, S., Wang, D., Fox, M. D., Yeo, B. T., Sepulcre, J., Sabuncu, M. R., . . . Liu, H. (2013). Individual variability in functional connectivity architecture of the human brain. *Neuron, 77*(3), 586-595. doi: 10.1016/j.neuron.2012.12.028

Mwansisya, T. E., Wang, Z., Tao, H., Zhang, H., Hu, A., Guo, S., & Liu, Z. (2013). The diminished interhemispheric connectivity correlates with negative symptoms and cognitive impairment in first-episode schizophrenia. *Schizophr Res, 150*(1), 144-150. doi: 10.1016/j.schres.2013.07.018

Nielsen, J. A., Zielinski, B. A., Ferguson, M. A., Lainhart, J. E., & Anderson, J. S. (2013). An evaluation of the left-brain vs. right-brain hypothesis with resting state functional connectivity magnetic resonance imaging. *PLoS One, 8*(8), e71275. doi: 10.1371/journal.pone.0071275

Nottebohm, F. (1970). Ontogeny of bird song. *Science, 167*(3920), 950-956. doi: 10.1126/science.167.3920.950

Oertel-Knochel, V., Knochel, C., Matura, S., Prvulovic, D., Linden, D. E., & van de Ven, V. (2013). Reduced functional connectivity and asymmetry of the planum temporale in patients with schizophrenia and first-degree relatives. *Schizophr Res, 147*(2-3), 331-338. doi: 10.1016/j.schres.2013.04.024

Ogawa, S., & Lee, T. M. (1990a). Magnetic resonance imaging of blood vessels at high fields: in vivo and in vitro measurements and image simulation. *Magn Reson Med, 16*(1), 9-18.

Ogawa, S., Lee, T. M., Kay, A. R., & Tank, D. W. (1990b). Brain magnetic resonance imaging with contrast dependent on blood oxygenation. *Proc Natl Acad Sci U S A, 87*(24), 9868-9872.

Ogawa, S., Lee, T. M., Nayak, A. S., & Glynn, P. (1990c). Oxygenation-sensitive contrast in magnetic resonance image of rodent brain at high magnetic fields. *Magn Reson Med, 14*(1), 68-78.

Ogawa, S., Menon, R. S., Tank, D. W., Kim, S. G., Merkle, H., Ellermann, J. M., & Ugurbil, K. (1993). Functional brain mapping by blood oxygenation level-dependent contrast magnetic resonance imaging. A comparison of signal characteristics with a biophysical model. *Biophys J, 64*(3), 803-812. doi: 10.1016/S0006-3495(93)81441-3

Penhune, V. B., Zatorre, R. J., MacDonald, J. D., & Evans, A. C. (1996). Interhemispheric anatomical differences in human primary auditory cortex: probabilistic mapping and volume measurement from magnetic resonance scans. *Cereb Cortex, 6*(5), 661-672.

Powell, J. L., Kemp, G. J., & Garcia-Finana, M. (2012). Association between language and spatial laterality and cognitive ability: an fMRI study. *Neuroimage, 59*(2), 1818-1829. doi: 10.1016/j.neuroimage.2011.08.040

Reuter-Lorenz, P. A., Jonides, J., Smith, E. E., Hartley, A., Miller, A., Marshuetz, C., & Koeppe, R. A. (2000). Age differences in the frontal lateralization of verbal and spatial working memory revealed by PET. *J Cogn Neurosci, 12*(1), 174-187.

Ribolsi, M., Daskalakis, Z. J., Siracusano, A., & Koch, G. (2014). Abnormal asymmetry of brain connectivity in schizophrenia. *Front Hum Neurosci, 8*, 1010. doi: 10.3389/fnhum.2014.01010

Rose, S., & Laan, M. J. (2009). Why match? Investigating matched case-control study designs with causal effect estimation. *Int J Biostat, 5*(1), Article 1. doi: 10.2202/1557-4679.1127

Rosen, B. R., & Savoy, R. L. (2012). fMRI at 20: has it changed the world? *Neuroimage, 62*(2), 1316-1324. doi: 10.1016/j.neuroimage.2012.03.004

Schultz, S. H., North, S. W., & Shields, C. G. (2007). Schizophrenia: a review. *Am Fam Physician, 75*(12), 1821-1829.

Scott, A., Courtney, W., Wood, D., de la Garza, R., Lane, S., King, M., . . . Calhoun, V. D. (2011). COINS: An Innovative Informatics and Neuroimaging Tool Suite Built for Large Heterogeneous Datasets. *Front Neuroinform, 5*, 33. doi: 10.3389/fninf.2011.00033

Seghier, M. L., Josse, G., Leff, A. P., & Price, C. J. (2011). Lateralization is predicted by reduced coupling from the left to right prefrontal cortex during semantic decisions on written words. *Cereb Cortex, 21*(7), 1519-1531. doi: 10.1093/cercor/bhq203

Smith, E. E., Jonides, J., & Koeppe, R. A. (1996). Dissociating verbal and spatial working memory using PET. *Cereb Cortex, 6*(1), 11-20.

Sperry, R. W. (1974). Lateral specialization in the surgically separated hemispheres. *The Neuroscience: Third Study Program Cambridge: MIT Press.*, 5-19.

Stark, D. E., Margulies, D. S., Shehzad, Z. E., Reiss, P., Kelly, A. M., Uddin, L. Q., . . . Milham, M. P. (2008). Regional variation in interhemispheric coordination of intrinsic hemodynamic fluctuations. *J Neurosci, 28*(51), 13754-13764. doi: 10.1523/JNEUROSCI.4544-08.2008

Stephan, K. E., Marshall, J. C., Friston, K. J., Rowe, J. B., Ritzl, A., Zilles, K., & Fink, G. R. (2003). Lateralized cognitive processes and lateralized task control in the human brain. *Science, 301*(5631), 384-386. doi: 10.1126/science.1086025

Stevens, M. C., Calhoun, V. D., & Kiehl, K. A. (2005). Hemispheric differences in hemodynamics elicited by auditory oddball stimuli. *Neuroimage, 26*(3), 782-792. doi: 10.1016/j.neuroimage.2005.02.044

Swanson, N., Eichele, T., Pearlson, G., Kiehl, K., Yu, Q., & Calhoun, V. D. (2011). Lateral differences in the default mode network in healthy controls and patients with schizophrenia. *Hum Brain Mapp, 32*(4), 654-664. doi: 10.1002/hbm.21055

Thomason, M. E., Race, E., Burrows, B., Whitfield-Gabrieli, S., Glover, G. H., & Gabrieli, J. D. (2009). Development of spatial and verbal working memory capacity in the human brain. *J Cogn Neurosci, 21*(2), 316-332. doi: 10.1162/jocn.2008.21028

Thompson, J. J., Blair, M. R., & Henrey, A. J. (2014). Over the hill at 24: persistent age-related cognitive-motor decline in reaction times in an ecologically valid video game task begins in early adulthood. *PLoS One, 9*(4), e94215. doi: 10.1371/journal.pone.0094215

Turner, J. A., Chen, H., Mathalon, D. H., Allen, E. A., Mayer, A. R., Abbott, C. C., . . . Bustillo, J. (2012). Reliability of the amplitude of low-frequency fluctuations in resting state fMRI in chronic schizophrenia. *Psychiatry Res, 201*(3), 253-255. doi: 10.1016/j.pscychresns.2011.09.012

Van Dijk, K. R. A., Hedden, T., Venkataraman, A., Evans, K. C., Lazar, S. W., & Buckner, R. L. (2010). Intrinsic Functional Connectivity As a Tool For Human Connectomics: Theory, Properties, and Optimization. *Journal of Neurophysiology, 103*(1), 297-321. doi: DOI 10.1152/jn.00783.2009

van Erp, T. G., Preda, A., Turner, J. A., Callahan, S., Calhoun, V. D., Bustillo, J. R., . . . Fbirn. (2015). Neuropsychological profile in adult schizophrenia measured with the CMINDS. *Psychiatry Res, 230*(3), 826-834. doi: 10.1016/j.psychres.2015.10.028

Vigario, R., Sarela, J., Jousmaki, V., Hamalainen, M., & Oja, E. (2000). Independent component approach to the analysis of EEG and MEG recordings. *IEEE Trans Biomed Eng, 47*(5), 589-593. doi: 10.1109/10.841330

Wang, L., Shen, H., Tang, F., Zang, Y., & Hu, D. (2012). Combined structural and resting-state functional MRI analysis of sexual dimorphism in the young adult

human brain: an MVPA approach. *Neuroimage, 61*(4), 931-940. doi: 10.1016/j.neuroimage.2012.03.080

Welch, Peter D. (1967). The use of Fast Fourier Transform for the estimation of power spectra: a method based on time averaging over short, modified periodograms. *IEEE Trans Audio Electroacoust 0*, 70-73.

Wernicke, Carl. (1874). Der aphasische Symptomencomplex. *Eine psychologische Studie auf anatomischer Basis; Breslau, M. Crohn und Weigert*.

Williams, D. S., Detre, J. A., Leigh, J. S., & Koretsky, A. P. (1992). Magnetic resonance imaging of perfusion using spin inversion of arterial water. *Proc Natl Acad Sci U S A, 89*(1), 212-216.

Xiao, Y. ; Hongchang, Z. ; Xu, X. (2012). Effects of Age of Acquisition and Word Frequency on the Processing Bias of the Middle/Inferior Frontal Gyrus. *International Journal of Advances in Psychology,, 1*, 26-36.

Yang, H., Long, X. Y., Yang, Y., Yan, H., Zhu, C. Z., Zhou, X. P., . . . Gong, Q. Y. (2007). Amplitude of low frequency fluctuation within visual areas revealed by resting-state functional MRI. *Neuroimage, 36*(1), 144-152. doi: 10.1016/j.neuroimage.2007.01.054

Yoon, U., Fahim, C., Perusse, D., & Evans, A. C. (2010). Lateralized genetic and environmental influences on human brain morphology of 8-year-old twins. *Neuroimage, 53*(3), 1117-1125. doi: 10.1016/j.neuroimage.2010.01.007

Yu, Q., Allen, E. A., Sui, J., Arbabshirani, M. R., Pearlson, G., & Calhoun, V. D. (2012). Brain connectivity networks in schizophrenia underlying resting state functional magnetic resonance imaging. *Curr Top Med Chem, 12*(21), 2415-2425.

Yu, Q., Sui, J., Liu, J., Plis, S. M., Kiehl, K. A., Pearlson, G., & Calhoun, V. D. (2013). Disrupted correlation between low frequency power and connectivity strength of resting state brain networks in schizophrenia. *Schizophr Res, 143*(1), 165-171. doi: 10.1016/j.schres.2012.11.001

Zhang, Z., Lu, G., Zhong, Y., Tan, Q., Chen, H., Liao, W., . . . Liu, Y. (2010). fMRI study of mesial temporal lobe epilepsy using amplitude of low-frequency fluctuation analysis. *Hum Brain Mapp, 31*(12), 1851-1861. doi: 10.1002/hbm.20982

Zhu, L., Fan, Y., Zou, Q., Wang, J., Gao, J. H., & Niu, Z. (2014). Temporal reliability and lateralization of the resting-state language network. *PLoS One, 9*(1), e85880. doi: 10.1371/journal.pone.0085880

Zuo, X. N., Di Martino, A., Kelly, C., Shehzad, Z. E., Gee, D. G., Klein, D. F., . . . Milham, M. P. (2010a). The oscillating brain: complex and reliable. *Neuroimage, 49*(2), 1432-1445. doi: 10.1016/j.neuroimage.2009.09.037

Zuo, X. N., Ehmke, R., Mennes, M., Imperati, D., Castellanos, F. X., Sporns, O., & Milham, M. P. (2012). Network centrality in the human functional connectome. *Cereb Cortex, 22*(8), 1862-1875. doi: 10.1093/cercor/bhr269

Zuo, X. N., Kelly, C., Di Martino, A., Mennes, M., Margulies, D. S., Bangaru, S., . . . Milham, M. P. (2010b). Growing together and growing apart: regional and sex differences in the lifespan developmental trajectories of functional homotopy. *J Neurosci, 30*(45), 15034-15043. doi: 10.1523/JNEUROSCI.2612-10.2010